USING MICROBIAL FUEL CELLS FOR THE REMEDIATION OF HYDROCARBON-CONTAMINATED AQUIFERS

by

Constanza Nicolau del Roure Eylerts

B.Sc., Universidad de Chile, 2011

M.Sc. (Geology), Universidad de Chile, 2013

A THESIS SUBMITTED IN PARTIAL FULFILLMENT OF

THE REQUIREMENTS FOR THE DEGREE OF

MASTER OF SCIENCE

in

THE FACULTY OF GRADUATE AND POSTDOCTORAL STUDIES

(Geological Sciences)

THE UNIVERSITY OF BRITISH COLUMBIA

(Vancouver)

August 2021

The following individuals certify that they have read, and recommend to the Faculty of Graduate and Postdoctoral Studies for acceptance, a thesis entitled:

Using Microbial Fuel Cells for the remediation of hydrocarbon-contaminated aquifers

submitted by Constanza Nicolau del Roure Eylerts in partial fulfillment of the requirements for

the degree of Master of Science

in Geological Sciences

Examining Committee:

Prof. Roger D. Beckie, The University of British Columbia, Geological Sciences
Supervisor

Prof. K. Ulrich Mayer, The University of British Columbia, Geological Sciences
Supervisory Committee Member

Prof. Sean A. Crowe, The University of British Columbia, Geological Sciences/Microbiology
Supervisory Committee Member

Prof. Kristin J. Orians, The University of British Columbia, Oceanography
Additional Examiner

Abstract

Bio-electrochemical systems (BES) have been proposed as an emerging technology for enhancing groundwater remediation and are an interesting alternative for hydrocarbon-contaminated reducing aquifers where natural attenuation may be slow. BES take advantage of the ability of exoelectrogenic bacteria to transfer electrons from organic substrates to an extracellular electron acceptor, such as the anode of a microbial fuel cell (MFC). An electrical connection between the oxidizing and reducing compartments of the MFC allows reduction of oxygen at the cathode coupled to the oxidation of the reduced contaminant in the reducing compartment, accompanied by electricity production. Electricity production has been proposed as a proxy to monitor the progress of the remediation.

The effects of additional electron donors, like ferrous iron, over the contaminant degradation efficiency and electricity production in BES have not been thoroughly studied. This research applied chemical, mineralogical, and microbiological analyses to study the degradation of naphthalene in a series of MFC experiments. The main objective was to test whether a reactor inoculated with native microorganisms from a local contaminated aquifer could successfully remediate naphthalene contamination in a reducing environment where iron was potentially an electron donor. An additional experiment was developed to address naphthalene sorption to electrodes and other reactor materials.

The sorption experiment revealed that naphthalene dynamics in the MFC were significantly affected by sorption/desorption to reactor materials, so interpretation of MFC results required the consideration of naphthalene sorption and diffusion processes.

The MFC experiments in this study did not find any advantage in providing an electrical connection between reducing and oxidizing zones of the bioreactors in terms of naphthalene degradation achieved in the system. However, the former did show the additional benefit of generating a small current. MFC experiments showed an increased electricity production when iron was available, however, the experiments with no iron achieved higher removal of

naphthalene. The results from this study suggest that measuring electricity production is no substitute for direct measurement of contaminant biodegradation, since iron, sulfur, and naphthalene metabolites were involved in electricity production.

Lay Summary

Microbial fuel cells are devices that typically aim for electricity production using organic compounds and bacteria. This technology can potentially be applied also to remediate organic contaminants from groundwater, with the additional benefit of producing small amounts of electricity. It has been proposed that instead of using expensive tools to track the extent of the groundwater remediation, the electricity produced by these devices can be monitored. This study found that dissolved iron present in the contaminated groundwater affects the contaminant removal and electricity production. Electricity production was linked to both the contaminant removal as well as the oxidation of inorganic chemicals, so monitoring electricity is not an adequate tool to track the extent of the remediation in all cases.

Preface

Research objectives and experiment design was developed by the author with guidance from Roger Beckie. All measurements and samples were collected and processed by the author. The author is responsible for data management, manipulation, and interpretation of chemical, electrochemical, mineralogical, and microbial data, with guidance from Roger Beckie, Uli Mayer, Rachel Simister and Sean Crowe.

Microbial media preparation was done by the author with guidance from Katharine Thompson. GC-MS analysis of hexane-extracted samples was done by Lina Madilao. DNA sample pooling and bioinformatics for microbial community data was done by Rachel Simister. Microbial DNA-sequencing was performed at the University of British Columbia sequencing facility. XRD analysis and mineral identification were done by Jacob Kabel, Elisabetta Pani, Edith Czech, Jenny Lai, and Lan Kato. ICP-OES analyses were done by the author with help from Maureen Soon. SEM sample preparation was done by the author with help from Derrick Horne. Sample observation under SEM was done by the author and Jacob Kabel.

All chapters were written by the author and edited by Roger Beckie.

Table of Contents

List of Tables

List of Figures

List of Abbreviations

A	Abiotic (experiment)
AMOVA	Analysis of molecular variance
BES	Bio-electrochemical system
BC	Base case (experiment)
DNA	Deoxyribonucleic acid
EDS	Energy-dispersive X-ray spectrometry
FAPROTAX	Functional Annotation of Prokaryotic Taxa
GC-MS	Gas chromatography mass spectrometry
IC	Ion chromatography
ICP-OES	Inductively coupled plasma optical-emission spectroscopy
LEfSe	Linear discriminant analysis effect size
LDA	Logarithmic discriminant analysis
MFC	Microbial fuel cell
Naph.	Naphthalene
ND	Natural degradation (experiment)
NF	No iron (experiment)
NN	No naphthalene (experiment)

OCV	Open circuit voltage
OTU	Operational taxonomic unit
PAH	Polycyclic aromatic hydrocarbon
PCR	Polymerase chain reaction
RNA	Ribonucleic acid
RSD	Relative standard deviation
SE	Standard error
SEM	Scanning electron microscopy
SD	Standard deviation
SMFC	Sediment microbial fuel cell
XRD	X-ray diffraction

Acknowledgements

I would like to thank my supervisor, Roger Beckie, for his trust, patience, and support. Thanks also to my supervisory committee members, Uli Mayer and Sean Crowe, for their guidance and support. This research was financially supported by an NSERC Discovery Grant awarded to Roger Beckie.

Thanks to Maureen Soon, Lina Madilao and Derrick Horne for sharing their expertise in specific lab methods. Special thanks to people in the Crowe lab, Katharine Thompson, Jennifer Spence, and Rachel Simister for sharing their valuable knowledge and time.

Huge thanks to the hydro group gals, Bethany Ladd, Julia Soares, Jessie Chao, Cara Manning, Elyse Sandl, Hannah Gatz-Miller, Katherine Raymond, and Laura Laurenzi.

Thanks to my family and friends for their invaluable support in the craziness of moving across the world to pursue graduate studies. Thanks to Álvaro and Javiera for being home away from home; and to Lucía for being a light in dark days. And to my partner Cristóbal for always being my effective team.

Chapter 1: Introduction

1.1 Overview

Water is a primary resource for life and for several economic and industrial activities that support economic growth and social development. Groundwater represents roughly a third of the freshwater withdrawals, however most of the major aquifers are experiencing rapid rates of depletion (Famiglietti, 2014; Konikow & Kendy, 2005). In addition to the water availability issue, the quality of groundwater is expected to decrease rapidly during the next decades, increasing risks to human health, economic development, and ecosystems (WWAP, 2016).

Several industrial and human activities contribute to groundwater pollution: leaching from agricultural fields, mine piles and landfills, wastewater mismanagement, and industrial spills. The most common groundwater contaminants include chlorinated hydrocarbons (trichloroethylene and perchloroethylene), metals, fuel hydrocarbons (benzene, toluene, ethyl-benzenes, xylene, polycyclic aromatic hydrocarbons, and methyl tertiary butyl ether), radionuclides, pesticides and nitrates (Appelo & Postma, 2004).

Polycyclic aromatic hydrocarbons (PAHs) are a global environmental issue, they constituted about 5% of volume of total environmental chemical pollutants in 1991 (Ite & Semple, 2012), however that number is expected to have increased in the last decades due to the widespread industrial use of hydrocarbons. PAH contamination is particularly important in urban areas because PAHs are potentially carcinogenic and/or mutagenic, and because of their continued emission, persistence, and mobility in the environment (Cachada et al., 2016). Groundwater PAH contamination is increasingly a concern for human health because of urban expansion into previously industrial sites in many rapidly growing cities (e.g. W. Cao et al., 2019) .

In recent years, the *in-situ* treatment of contaminated groundwater has increased worldwide, although pump-and-treat approaches are still significant (Majone et al., 2015). For example, among the US Superfund sites evaluated for remediation between 2015 and 2017, *in situ* groundwater treatment was selected as the remediation approach in over half of the sites (US

EPA, 2020). In particular, *in situ* bioremediation and chemical treatment were selected most frequently, while the use of pump-and-treat systems continues to decrease since the early 1990s (US EPA, 2020). Several advantages make bioremediation more attractive than other remediation techniques: it is relatively inexpensive, it has the potential to eliminate the contaminant in a permanent way via biochemical transformation or mineralization, and it does not require the use of chemical or physical treatments (Sturman et al., 1995).

Bioremediation techniques were proposed for the treatment of hydrocarbon-contaminated groundwater as early as 1989 (Mueller et al., 1989), and has been proved effective in laboratory experiments, reducing the contaminant to about 10% in controlled conditions (e.g. X. Lu et al., 2011). However, the success of bioremediation depends on several factors that are difficult to control: the existence of degrading microorganisms, the availability of electron acceptors and nutrients, temperature, soil properties, the carbon sources for the microbial community, and degradation kinetics (Haritash & Kaushik, 2009; Li & Yu, 2015; H. Wang, Luo, et al., 2015). A proposed way to overcome these difficulties is the use of electrodes in what have been called bio-electrochemical systems (BES).

Several types of BES have been developed with different applications: Microbial Fuel Cells (MFCs) mainly focus on electric power generation, but other BES are used to synthesize useful compounds such as hydrogen, formate, methane or to desalinate water (Santoro et al., 2017 and references therein). The development of MFCs has focused mostly on optimizing them for electricity generation but combined applications have arisen in recent decades, such as wastewater treatment accompanied by electricity production. Wastewater treatment using MFCs take advantage of their capability to convert chemical energy from organic substrates into electricity. Similarly, this capability can be used for the remediation of organic contaminants.

The potential of using BES for contaminant degradation while generating electricity and avoiding the typically high operational costs of more traditional technologies has sparked scientific research in this field. Most studies involve experiments under strictly controlled conditions and using only pure culture microbial communities (e.g. Rodrigo et al., 2014). Although there are some examples of successful field experiments (e.g. L. Lu, Yazdi, et al.,

2014), the widespread application of BES for remediation purposes on site is far from being possible yet.

The focus of this thesis is to contribute to the scientific knowledge of BES, aiming towards their application for remediation in reduced aquifers. This research was conducted via benchtop batch MFC experiments using naphthalene as a model contaminant in iron-rich water.

1.2 Background

1.2.1 Biodegradation of contaminants

Several microorganisms degrade or transform hazardous compounds by using them as an energy source or co-metabolizing them with alternative energy sources. This way, the concentration of the contaminant in the environment can be reduced naturally with time, as they are transformed to innocuous end-products by biochemical redox reactions. Typically, the extent of this natural biodegradation depends on the toxicity of the contaminant, the bioavailability of both nutrients and contaminant, and other environmental factors such as redox potential, salinity and pH (Langwaldt & Puhakka, 2000). Bioremediation consists in stimulating microbial metabolism by adding nutrients or other chemicals to enhance microbial metabolism. This approach can be used for the remediation of different types of contaminants such as heavy metals, polycyclic aromatic hydrocarbons (PAHs), petroleum-derived compounds and even plastics (Das, 2014).

There may be more than one microbial species involved in the degradation of a compound and the process sometimes involves syntrophic communities. For example, it has been reported that one group of bacteria can oxidize naphthalene anaerobically, producing hydrogen, which is in turn used by a methanogenic consortium to produce methane (Christensen et al., 2004).

The remediation of organic contaminants presents specific challenges, they often become bound by the soil particles and show reduced bioavailability, thus they become harder to degrade by microorganisms. Some microorganisms are particularly useful in these circumstances. For example, members of genus *Mycobacterium* have lipophilic cell surfaces, making them better

suited to metabolize hydrophobic hydrocarbons. (Bouchez-Naïtali et al., 1999; Haritash & Kaushik, 2009).

The environmental conditions in a contaminated aquifer can also be manipulated to enhance the microbial activity in what is designated as enhanced *in situ* bioremediation. This can involve: (1) bio-stimulation, which consists in the injection of nutrients, oxygen and/or other components to support microbial activity and growth (Scow & Hicks, 2005), (2) bio-augmentation, which is based in the addition biocatalysts, generally specific bacteria, fungi, genes or enzymes (Stroo et al., 2013); and (3) electro-bioremediation, which consists in providing an alternative electron acceptor in the form of an electrode inserted into the subsurface, thus fostering the oxidation of the pollutant in zones where oxygen or other electron acceptors are not readily available.

Bio-stimulation works relatively well for the case of limited inorganic nutrients, but it does not for oxygen, which is limited by solubility (Sturman et al., 1995). Adding oxygen peroxide appears to work in laboratory experiments, but high concentrations of oxygen peroxide inhibit microbial metabolism, and determining how much of the added peroxide will end up as available oxygen in the field is sometimes complicated (Aggarwal et al., 1991). Regarding the use of bio-augmentation techniques, it has been proven that in some cases the application of native microorganisms is more efficient than the use of extraneous ones, because native microorganisms are well adapted to their environment, so their population growth is more rapid, which guarantees better biodegradation (Zawierucha & Malina, 2006). However, bio-augmentation may also include the inoculation of genetically modified microorganisms. In this case, a series of problems can originate, such as not well-known or unpredicted side effects over the environment and potentially humans, complicated monitoring of the spatial distribution of microorganisms, and low survival of laboratory bacteria under field conditions (Zawierucha & Malina, 2006).

1.2.2 Bio-electrochemical systems and biodegradation

Concerns about cost and possible unintended effects of injecting either bacteria or chemicals into the subsurface often further complicate remediation attempts. In that sense,

electro-bioremediation is particularly appealing because it is a passive technique that can theoretically be implemented *in situ* and it does not require addition of chemicals or bacteria. Furthermore, it may have the advantage of producing electricity while the remediation of the contaminant takes place.

Bio-electrochemical remediation aims to foster the growth of microbial communities that are adapted to degrade a certain contaminant by providing an electrode that acts as an additional electron acceptor. BES take advantage of the ability of some microorganisms to transfer electrons directly or indirectly to extracellular electron acceptors, such as the anode in an MFC. They are called exoelectrogenic bacteria. A wide variety of exoelectrogenic species has been investigated, including several species in the Proteobacteria and Firmicutes phylum (Rabaey et al., 2004), several *Geobacter* species (Bond & Lovley, 2003; Reguera & Kashefi, 2019; Strycharz et al., 2008), *Shewanella* species (Marsili et al., 2008; Wu et al., 2013; Y. Yang et al., 2017), *Desulfuromonas acetoxidans* (Bond et al., 2002), *Geoalkalibacter sp* (Badalamenti et al., 2013), *Pseudomonas aeruginosa* (Venkataraman et al., 2010), *Rhodoferax ferrireducens* (Chaudhuri & Lovley, 2003), *Rhodobacter capsulatus* (Hasan et al., 2015), among others.

Exoelectrogenic bacteria that respire using an electrode as the sole electron acceptor can be used to harvest electricity from electrode-microorganism interactions in sediments (Tender et al., 2002), and their potential for remediating contaminated sites have long been recognised (Morris & Jin, 2007).

Although the electricity production using contaminated water is still far from being practically useful, there are several examples in which electro-bioremediation has been successful. Electro-enhanced techniques have been used for the removal of carbon, nitrogen and phosphorous compounds out of wastewater (Clauwaert et al., 2007; Hua et al., 2019; Pant et al., 2012; Tian & Yu, 2020), for the remediation of diesel (Mohan & Chandrasekhar, 2011; Morris et al., 2009), hydrocarbons like phenol, benzene, toluene, phenanthrene and naphthalene (Adelaja et al., 2014; Daghio et al., 2016; Hedbavna et al., 2016; S.-H. Liu et al., 2018; T. Zhang et al., 2010), azo dyes (Aulenta et al., 2010; Mu et al., 2009), and for the remediation of metals like manganese, chromium, lead and nickel (Yan Li, 2015).

Most of the studies of bio-electrochemical systems have been done on Microbial Fuel Cells (MFCs). MFCs are devices comprised of two separate compartments with different redox potential. One electrode is placed in each compartment and connected with a conductive wire. In the anode compartment, the electrons generated by oxidation reactions are transferred to the anode. Electrons are transferred from the anode to the cathode through the wire and are subsequently used to reduce the compounds, usually oxygen, in the cathodic compartment. An electrical current is generated due to the transfer of electrons through the wire from anode to cathode. The electrical connection between zones with different redox potential drives the oxidation of reduced compounds by bacteria in the anode chamber, in absence or under limited abundance of terminal electron acceptors such as oxygen, nitrate or sulfate (Logan et al., 2006; Morris & Jin, 2012).

Even though electricity generation by MFCs requires carefully controlled physico-chemical conditions, electricity can also be produced in natural systems. (Bond et al., 2002) showed that energy can be harvested from marine sediments by burying a graphite electrode into anoxic sediments and connecting it to another electrode located in overlying aerobic seawater. The study also showed that inoculating the benzoate-loaded anode compartment of the MFC with *Geobacter metallireducens* bacteria resulted in the benzoate oxidation to CO_2. In this case, the authors suggest benzoate oxidation was linked to the activity of the bacteria, which can couple the oxidation of organic compounds to the reduction of insoluble Fe(III) oxides. These results suggest that *Geobacter metallireducens* can be used for the bioremediation of organic contaminants and the generation of a current across the circuit (Bond et al., 2002).

There have been efforts to scale-up these kind of reactors for field applications (Ewing et al., 2014; Sturman et al., 1995), and it is generally believed that the use of *in situ* bio-electrical remediation treatment is possible (Sajana et al., 2016). In fact, there are examples of sediment fuel cells used *in situ* in marine sediments for energy production (Lowy et al., 2006; Tender et al., 2002). Even though some *in situ* applications of BES have been studied, there is still much to be discovered in this field.

1.2.3 Degradation of hydrocarbons

The biodegradation of hydrocarbons by bacteria can use either oxygen, nitrate, ferric iron, or sulfate as electron acceptors, although the degradation pathways are different for aerobic and anaerobic conditions (Grishchenkov et al., 2000). The biodegradation efficiency and rates depend on several factors such as the chemical structure and concentration of the contaminant, its interactions with the soil particles, its bioavailability, the acclimation of the microorganisms to the contaminated environment, and environmental conditions: temperature, pH, moisture, redox potential and nutrient availability (Ite & Semple, 2012 and references therein). Anaerobic natural degradation of hydrocarbons requires the availability of terminal electron acceptors such as nitrate or sulfate and is linked to sulfate-reducing or denitrifying bacteria. The rate of degradation is subject to the abundance of the electron acceptor, and a deficit in these compounds results in a decreased rate of biodegradation or complete absence of degradation (Boopathy, 2004)

For naphthalene, there are several kinds of bacteria that use aerobic degradation pathways including some species of *Acinetobacter*, *Alcaligenes*, *Burkholderia*, *Mycobacterium*, *Polaromonas*, *Pseudomonas*, *Ralstonia*, *Rhodococcus*, *Sphingomonas*, and *Streptomyce* (Cerniglia, 1992; Seo et al., 2009 and references therein). The anaerobic degradation pathways are less well understood and considered to be based in slower reactions than aerobic degradation (Cerniglia, 1992). Although it has been shown that aerobic and anaerobic biodegradation rates can be equal when the cell density is equal (Dou et al., 2009).

Anaerobic degradation of naphthalene can occur under nitrate (al-Bashir et al., 1990; Dou et al., 2009; McNally et al., 1998; Mihelcic & Luthy, 1988), sulfate (Meckenstock et al., 2000; Rothermich et al., 2002; Thierrin et al., 1995; X. Zhang & Young, 1997) and iron-reducing conditions (Anderson & Lovley, 1999; Kleemann & Meckenstock, 2011; Robinson et al., 2001), and is also thermodynamically favourable under methanogenic conditions in the presence of methanogens (Christensen et al., 2004). Some of the microbial species that can perform naphthalene degradation include some members of *Desulfobacteraceae* family, *Pseudomonas*

fluorescens, *Pseudomonas putida*, and *Pseudomonas stutzeri* (McNally et al., 1998; Mittal & Rockne, 2008; Wolfson et al., 2018).

The fact that there is a variety in microbial metabolisms that degrade naphthalene and other hydrocarbons suggests that bio-electro degradation of hydrocarbons is feasible. The first report on the capability to produce power using petroleum contaminants as substrate in a MFC configuration was published by Morris and Jin (2007). Since then, MFCs have been used in laboratory-scale investigations that show bio-electrochemical remediation of hydrocarbons and other petroleum derivatives (Adelaja et al., 2014; Daghio et al., 2016; Hedbavna et al., 2016; S.-H. Liu et al., 2018; L. Lu, Yazdi, et al., 2014; Morris et al., 2009; Rakoczy et al., 2013; X. Wang et al., 2012; Yan et al., 2012; T. Zhang et al., 2010).

1.3 Research gaps

Even though the use of bio-electrochemical systems for groundwater remediation have gained more attention in recent years, most of the research is still focused on power production. There are fewer examples of studies that focus purely on contaminant remediation, and more research is necessary before bio-electrochemical remediation can be practical *in situ*. It is often the case that contaminated aquifers are under reducing (anoxic) conditions, and ferrous iron or other electron donors may be available. Some studies address the influence of the inorganic chemical composition of the water over electricity generation (Q. Liu et al., 2017, 2018; Wei et al., 2013; Wu et al., 2013), however there is still a lack of knowledge regarding the effect of alternative electron donors over the electrode-driven contaminant degradation. This research project contributes to the knowledge in those specific topics to advance towards the use of bio-electrochemical processes as contaminant degradation strategies, particularly in reducing PAH-contaminated aquifers.

It has been suggested that inorganic electron donors present in the sediments may be oxidized preferentially over carbon species at the anode of a SMFC (Song et al., 2011). In a study about the effects of fuel cell operation over sediments and pore water in the sea floor the authors conclude that dissolved sulfide may be a direct source of electrons for the fuel cell (Ryckelynck

et al., 2005). Therefore, it is possible that while aiming to oxidize contaminants, the electrode instead oxidizes organic matter, or aqueous reduced species (Fe^{+2}, Mn^{+2}).

There are few studies that address the effect of the presence of alternative electron donors over MFC performance (Peng et al., 2012; H. Zhang et al., 2015; Zhou et al., 2014). One study suggests that if an iron sheet (Fe^{0}) is introduced into the reactor corrosion occurs generating ferrous iron; ferrous iron gets oxidized by the anode, and then the ferric iron ions are reduced by iron-reducing bacteria, which results in an increased power output of the MFC (H. Zhang et al., 2015). Therefore, in principle, since the presence of iron enhances the iron reducing microbial activity, which is linked to the PAH degradation, it should also enhance the degradation rate of PAHs when MFCs are used for remediation. However, this needs to be experimentally tested.

In most hydrocarbon-contaminated sites a microbial community that can degrade the contaminant develops naturally, although the biodegradation rate of these types of contaminants may be very slow. The introduction of an electrode pair into such a system would increase degradation rates as microorganisms capable of using the electrode as TEA will proliferate. However, if the microorganisms that performed the degradation using natural electron acceptors are different from those who perform the electrode reduction, then these two communities may compete for nutrients, which would be unfavourable for the PAHs degradation.

For field applications of bio-electro remediation, it is necessary to know how the naturally degrading PAH community changes when the electrode is added, because this change in the microbial community will likely produce a change in the aquifer geochemistry. Studying the changes in the microbial community composition as a response to the addition of the electrode will also give insights into the flexibility of the bacterial community to switch from their original electron acceptor, Fe(III), nitrate, or sulfate, to using the electrode as the sole electron acceptor. This is important for example to predict what the response will be for different sites with different initial microbial communities.

1.4 Motivation

This study is motivated by the increasing pressure for remediation of former industrial sites to accommodate population growth through urban land expansion, a phenomenon that is globally recurrent (WHO, 2021). In particular, creosote contamination of the reducing aquifer at the Braid Street site in Coquitlam, British Columbia presents a challenge for urban development. Would it be possible to use a bio-electrochemical system as remediation approach at this site?

According to Bieber (2003) the creosote contamination at the Braid Street site was originated from a wood preserving facility that operated at this site in the 1920s. A creosote plume extends into the aquifer sands up to a depth of approximately 22 m. The contaminants are transported by groundwater from the source area, 120 m from the shore of the Fraser River, towards a discharge area at the bottom of the river. In 1996, a pump and treat management plan was put in motion to address the contamination problem (Golder Associates Limited, 1997).

The main component of the aqueous plume in 1996 was naphthalene, although significant concentrations of fluorene, phenanthrene, acenaphthene, pyrene, fluoranthene, chrysene, benzo(a)pyrene, benzo(b)anthracene, and benzo(c)fluoranthene have also been detected (Bieber, 2003; Golder Associates Limited, 1997). A naphthalene degradation rate of 1900 µg/L per year was determined from microcosm experiments (Bieber, 2003; Lesser, 2000), which is considered a maximum degradation rate. The degradation of naphthalene was proposed to occur mainly in the off shore region of the plume by methanogenesis and iron reduction (Anthony, 1998).

The geochemistry of the groundwater in the study site is complex, as it is affected by the creosote contamination as well as the saline river water that mixes with fresh groundwater. According to the water chemistry presented by Bianchin et al. (2006) the uncontaminated groundwater is mainly Ca-HCO_3 while the contaminated groundwater would be classified as Ca-Na-HCO_3. The contaminated groundwater contains higher concentrations of methane and dissolved iron than the background clean groundwater (Table 1.1).

Table 1.1. Representative groundwater chemistry at the Braid Street site (data from Bianchin et al., 2006).

Parameter	Background groundwater chemistry			Groundwater chemistry within naphthalene plume		
	Average	Min	Max	Average	Min	Max
Ca	0.52	0.15	1.22	0.83	0.16	1.96
Fe	0.18	0	0.78	0.71	0.13	1.49
K	0.02	0	0.04	0.05	0	0.13
Mg	0.33	0.12	0.81	0.51	0.23	1.20
Mn	0.01	0	0.05	0.03	0.01	0.06
Na	0.33	0.11	0.75	1.07	0.01	10.13
Si	0.10	0.10	0.10	0.77	0.65	0.98
Sr	0	0	0.001	0.001	0	0.004
Cl^-	0.09	0.03	0.29	0.24	0.06	2.31
NO_3^-	0.02	0	0.12	0	0	0.005
SO_4^{-2}	0.03	0.00	0.10	0.00	0	0.01
HCO^-_3	2.10	0.90	4.28	3.43	0.43	10.16
CH_4	0.15	0	0.38	0.37	0.01	1.33
CO_2	0.52	0.03	0.65	4.07	0.93	6.14
O_2	0.25	0.02	0.41	0.01	0.01	0.02
pH	7.3	6.7	8	6.4	6.1	6.9

Concentration values reported as mM

The main process occurring in the uncontaminated zone of the reducing aquifer adjacent to the Fraser River is the reductive dissolution of iron and manganese oxide minerals via organic matter oxidation, whereas sulfate reduction and methanogenesis are less important but also occur (Jia, 2015). Meanwhile, in the contaminated portion of the aquifer, naphthalene is degraded anaerobically through biologically-mediated iron reduction and methanogenesis (Bieber, 2003). Therefore, the main reactions occurring at the site, as proposed by these authors are:

Iron reduction $$CH_2O + 4Fe(OH)_3 + 7H^+ \rightarrow 4Fe^{+2} + HCO_3^- + 10H_2O$$

Manganese reduction $$CH_2O + 2MnO_2 + 3H^+ \rightarrow 2Mn^{+2} + HCO_3^- + 2H_2O$$

Sulfate reduction $$CH_2O + \frac{1}{2}SO_4^{-2} \rightarrow \frac{1}{2}HS^- + HCO_3^- + \frac{1}{2}H^+$$

Methanogenesis $$2CH_2O + H_2O \rightarrow CH_4 + HCO_3^- + H^+$$

Naphthalene degradation by iron reduction

$$C_{10}H_8 + 48Fe(OH)_3 \rightarrow 48Fe^{+2} + 10CO_3^{-2} + 38H_2O + 76OH^-$$

Naphthalene degradation by methanogenesis

$$C_{10}H_8 + 12H_2O \rightarrow 6CH_4 + 4HCO_3^- + 4H^+$$

These processes occurring in the anaerobic zone of the natural aquifer affect the water composition by increasing the dissolved ferrous iron, manganese, sulphide, methane, and bicarbonate concentrations. The effect of these reactions on the water pH depends on the reaction rates. The pH will likely increase as these reactions proceed through time due to naphthalene degradation by iron reduction, and manganese and iron reduction, but this increase in pH will be buffered by sulfate reduction, especially when saline water enters the system due to the tides (Bieber, 2003).

Introducing an electrode into the anaerobic sediments will likely have the effect of favouring the oxidation of naphthalene and/or other reduced species. The reactions that occur in the system with the electrode will, however, depend on the metabolism and the composition of the microbial community that will grow using the electrode as electron acceptor. It is possible that the reactions listed above will continue to occur, however, organic carbon (naphthalene or organic matter) may also be oxidized using the electrode as electrode acceptor, and therefore Fe^{+2} and Mn^{+2} would not be produced. The reaction that will oxidize naphthalene will produce acidity as only the oxidation half reaction occurs at the anode at depth, while the reduction of oxygen will occur at the cathode, consuming acidity in the shallow part of the aquifer.

Naphthalene oxidation at the anode

$$C_{10}H_8 + 30H_2O \rightarrow 10HCO_3^- + 58H^+ + 48e^-$$

Oxygen reduction at the cathode

$$O_2 + 4H^+ + 4e^- \rightarrow 2H_2O$$

Aqueous Fe^{+2} and Mn^{+2} could potentially be oxidized directly at the anode or by microbial activity enhanced by the presence of the electrode, decreasing the concentration of these species. However, the natural Mn^{+2} oxidation rate is much lower than Fe^{+2} oxidation rate (Jia, 2015), so it is possible that Mn^{+2} plays a minor role in the geochemical evolution of the aquifer water. Whatever the case is, it is important to determine whether naphthalene or Fe^{+2}, Mn^{+2} and solid organic matter are preferentially oxidized at the anode, to predict if introducing an electrode will serve as a remediation approach for the site

Since this system is subject to groundwater flow, the reaction products will be carried away from the electrode following the groundwater direction. Naphthalene can potentially be carried away from the anode even after going through it if the oxidation rate at the anode is not sufficiently high. Therefore, it is important to determine the degradation rate that could be attained at the anode. Additionally, the groundwater flow will replenish aqueous electron acceptors and provide nutrients to the microbial community near the anode, likely enhancing the microbial activity, therefore the degradation rates may increase due to the flow.

1.5 Research objectives

The purpose of this research is to contribute to the scientific knowledge on the feasibility of enhancing microbial degradation of contaminants in anaerobic aquifers by using bio-electrochemical systems.

The main objectives are to investigate the controls and mechanisms involved in the bio-electrochemical degradation of contaminants, and test whether this approach can successfully remediate PAHs contamination in a reducing environment using native microbial communities.

The hypothesis that providing an electrical connection between the aerobic and anaerobic compartments of a batch reactor enhances the degradation rate of naphthalene, even in the presence of other reduced substances such as ferrous iron. This occurs by providing an additional electron acceptor, the anode, which is used by native anaerobic bacteria in the metabolic oxidation of naphthalene.

The research questions addressed in this thesis are:

(1) what is the effect of using electrodes to transfer electrons from reducing to oxidizing zones on the geochemical evolution of anaerobic, naphthalene-contaminated water?

(2) how is the BES affected by ferrous iron concentration?

(3) what are the dominant geochemical reactions?

(4) how is the naphthalene removal affected by the presence of electrodes and iron?

(5) how does the microbial community respond to the electrical connection between aerobic and anaerobic zones provided by the electrodes?

(6) what is the effect of the presence of ferrous iron on the final microbial community?

(7) what geochemical processes can be inferred from the final microbial community composition?

To address these questions, batch bioreactor MFC experiments were constructed mimicking the deployment of a bio-electrochemical system into a reducing aquifer. Our setup is constituted by a glass vessel with two chambers, separated horizontally by a permeable silica sand layer, and with a carbon cloth electrode in each compartment. Glass was selected for the vessel and quartz for the sand to avoid potential sorption of naphthalene. However, since the carbon cloth is likely to be a sink for naphthalene sorption, an experiment to determine the extent to which naphthalene was sorbed to glass, sand and carbon cloth was also carried out.

1.6 MFC experiment design

MFCs typically consist of two physically separated chambers, each containing an electrode, which are electrically connected (Figure 1.1). The reactor configuration varies, with the separator frequently being an ion selective membrane (Rossi et al., 2020; Rossi & Logan, 2021), although other separator materials, such as a salt bridge, have also been used (e.g. Min et al., 2005). The anode chamber is anaerobic and contains an organic substrate, such as glucose, that

microorganisms can oxidize to sustain biomass growth, releasing protons and electrons. The released electrons are collected by the anode and transferred to the cathode where they are used in the reduction reaction, while the protons migrate through the membrane to the cathode chamber. The cathodic reaction consumes protons and is usually oxygen reduction. Air-cathodes where the cathode is directly in contact with air instead of submerged in the catholyte show better power performance and solves the need to permanently oxygenating the catholyte (Rossi et al., 2020).

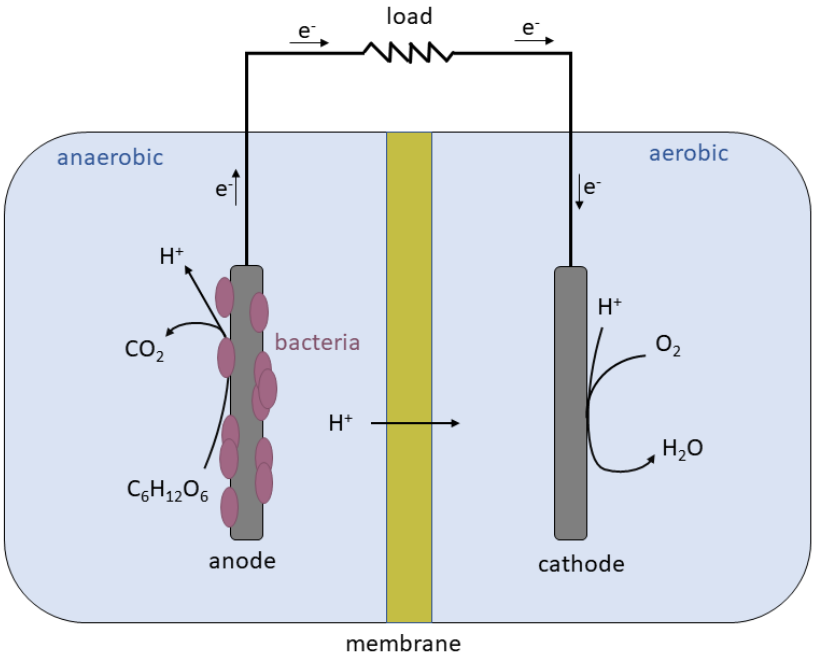

Figure 1.1. Schematic representation of the configuration and operating principles in a Microbial Fuel Cell**.**

Carbon-based materials are commonly used for the electrodes. The overall system dynamics relies on the spontaneity of the cathodic reaction; platinum is the standard catalyst used to drive the oxygen reduction reaction. Pt-coated carbon cathodes are very common in MFC research, although activated carbon and iron-nitrogen-doped carbon materials have been tested in the search for inexpensive alternatives (Cheng et al., 2006; Daniel et al., 2021; Ghasemi et al., 2011; W. Yang et al., 2020).

For the MFC experiments in this thesis, a simple and inexpensive design was chosen. It was comprised of vertically stacked anode and cathode chambers, with carbon cloth electrodes. The

separator material was fine silica sand, and the substrate was naphthalene. This reactor design aimed to mimic a naphthalene-contaminated aquifer; the anode chamber represents the lowermost anaerobic part of the aquifer. The anode was electrically connected to the cathode by a stainless-steel wire. The cathode resides in the cathode chamber, which is open to the atmosphere and constitutes the aerobic upper part of the aquifer. The reactor vessel was made of glass to minimize naphthalene sorption. A detailed description of the experimental design is presented in Chapter 3.

1.7 Organization of the thesis

This thesis has four chapters, with chapters 2 and 3 showing the results and discussion from laboratory experiments. A list of references is provided at the end of the thesis. Additional information that was not included within the body of the thesis is provided in the appendices section. It includes raw and processed data, additional plots, protocols, and details on some of the methods. The thesis is organized as follows:

- Chapter 1 introduces the research topic and delineates the rationale for this study. It gives a review the biodegradation of hydrocarbons, typical remediation technologies, and bio-electrochemical systems. Research gaps are identified, and the study objectives are articulated.
- Chapter 2 reports the results from a sorption experiment developed to test naphthalene sorption to the materials used in the MFC experiments.
- Chapter 3 reports the results from the investigation of the performance of a series of MFCs inoculated with native microbial community; naphthalene degradation, electricity production and changes in the microbial community composition are evaluated, together with the effects of ferrous iron availability in the microbial media.
- Chapter 4 highlights the key findings of this research, provides a summary of the limitations of the experimental approach used, and presents some recommendations for future work in this research topic.

Chapter 2: Naphthalene sorption experiment

Like many organic pollutants, the hydrophobic nature of naphthalene results in its tendency to become sorbed to organic matter in sediments (Appelo & Postma, 2004). Similarly, synthetic carbonaceous materials, such as carbon nanotubes, also have a tendency to sorb non-polar organic contaminants such as naphthalene (Chen et al., 2007). Carbon is also the main constituent in carbon cloth electrodes, which are typically used in MFC reactors. Carbon electrodes are common mainly because they are relatively inexpensive, and have high electrical conductivity and surface area. However, MFC experiments in the literature rarely address sorption to electrode materials, even when the objective is to enhance hydrocarbon removal.

This experiment aims to determine the degree to which naphthalene is sorbed to the different materials used in the MFC experiments (see Chapter 3:). The materials tested included glass, quartz sand (Sand, pure, 40-100 mesh, ACROS Organics), carbon cloth (CC6 Plain; Fuel Cell Earth) and the Fe precipitate that forms when adding $FeCl_2$ solution to naphthalene-spiked media used in the MFC experiments. Table 2.1 summarizes the experimental conditions tested in the sorption experiment, experiments were done in triplicate; iron was only added to the experiment testing naphthalene sorption to iron precipitates (S_Fe experiments).

Table 2.1. Experimental conditions tested in the sorption experiments.

Experiment	Experiment ID	Media composition
Glass vial (blank)	S_B1 S_B2 S_B3	Naphthalene-spiked media, no iron
Quartz sand	S_S1 S_S2 S_S3	Naphthalene-spiked media, no iron
Carbon cloth	S_C1 S_C2 S_C3	Naphthalene-spiked media, no iron
Iron precipitates	S_Fe1 S_Fe2 S_Fe3	Naphthalene-spiked media, 1.8 mM Fe

First, we obtained experimental values of the distribution coefficients for glass, sand, and carbon cloth. Then we used these experimental values to determine the mass of naphthalene to be sorbed

to each material in individual MFC experiments, based on measurements from individual reactors.

2.1 Method

2.1.1 Sampling and naphthalene measurement

Sorption experiment vessels were batch reactors consisting of 60-mL glass serum vials filled with naphthalene-spiked media and the sorbent material being tested. Vials were closed with Teflon septa and aluminum crimp seals (Figure 2.1). Since the availability of a solid surface has an influence on the sorption process, the sorption experiments aimed at replicating the solid-to-solution ratio present in the MFC experiments. In the MFC experiment (Chapter 3), the reactors contained an average of 733 g of sand, 25 cm^2 electrodes, and a total of 1400 mL of media. The ratio of sand to media was 0.52 g/mL in the MFC experiment, so 23 g of silica sand and 45 mL of media were used in the sand sorption experiment. The ratio of carbon cloth to media was 0.018 cm^2/mL in the MFC experiment, so in the sorption experiment, 1 cm^2 carbon cloth pieces and 55 mL of media were used. In the MFC experiment, 5 mL of 360 mM $FeCl_2$ solution was added to 1 L of media, so 275 µL of 360 mM $FeCl_2$ solution was added to 55 mL of media in the iron precipitate sorption experiment. The naphthalene concentration in the media was 15 mg/L, the same used in MFC experiments.

Figure 2.1. Naphthalene sorption experiment vessels.

Two experiments (for each material) were sampled 3 hours after set-up; the 3-hour time was chosen because it was the average amount of time between reactor set-up and first sampling in the MFC experiment. The third experiment (for each material) was sampled 7 days after set-up, which corresponds to the second sampling event in MFC experiment. Duplicate samples were taken at each sampling event.

Naphthalene was quantified by gas chromatography–mass spectrometry analysis. A volume of 0.5 mL unfiltered sample was poured into 2 mL Agilent amber glass vials pre-filled with hexane (1:1 by volume), and vortexed. The hexane supernatant was analyzed for naphthalene with an Agilent GC 7890A/7000A GC/MS Triple Quad equipped with an Agilent 19091S-433HP-5MS 5% Phenyl Methyl Silox column. The carrier gas was helium, and the temperature program was 40 °C (2 min isothermal), ramp of 20 °C/min to 280 °C for 1 min, 280 °C (isothermal for 15 min). The following MS conditions were used: selected ion monitoring mode (selected mass of 128), ionization energy of 70 eV, source temperature of 230 °C.

2.1.2 GC-MS calibration curve and method precision

To determine the variability of the naphthalene measurement via GC-MS, the calibration curve was constructed based on five standards and three injections per sample (Table 2.2; Figure 2.2). Precision was calculated using the relative standard deviation method (RSD), with: $\%RSD = \frac{s}{\bar{x}} \times 100$, where s is the standard deviation and $\bar{x}$ is the mean.

Table 2.2. GC-MS calibration curve data

Standard (ppm)	Area 1	Area 2	Area 3	Average area	Standard deviation	% RSD
0.1	5644	5206	5607	5486	243	4.4
1.0	77754	70135	73998	73963	3810	5.2
5.0	363327	388388	403203	384973	20156	5.2
10.0	763537	876466	892899	844301	70424	8.3
20.0	1367410	1461358	1343454	1390740	62318	4.5

The average of the calculated RSD for triplicate injections was 5.5%, the highest RSD was 8.3% for the 10-ppm standard. Overall results are deemed acceptable with good precision in triplicate samples showing RSD < 10%.

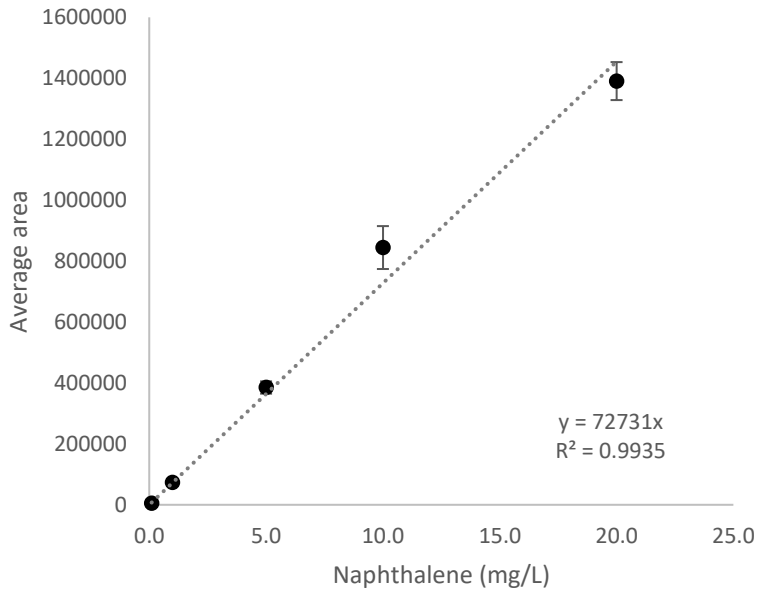

Figure 2.2. Calibration curve for GC-MS analysis of naphthalene in samples from sorption experiment.

2.1.3 Distribution coefficient determination

The amount of naphthalene sorbed per unit mass of sorbent Q_e (mg/g) was calculated using the equation:

$$Q_e = \frac{(c_i - c_e)\,V}{m} \qquad \text{(Eq. 1)}$$

Where c_i is the initial naphthalene concentration (15 mg/L), c_e (mg/L) is the equilibrium aqueous naphthalene concentration at each time point (measured), V is the volume of media (L), and m is the mass of sorbent (g).

The distribution coefficient K_d (mL/g) was calculated according to:

$$K_d = \frac{c_e}{Q_e} \qquad \text{(Eq. 2)}$$

A value of K_d was obtained for each sample. Uncertainties in the material mass measurement, volume of media measurement and naphthalene measurement were included in the calculations.

2.1.4 Variability determination

Sampling variability

Duplicate samples from each experiment replicate were analyzed to determine the naphthalene concentration variability due to sampling. For example, for experiment replicate Blank1, we used samples *s-b1-a* and *s-b1-b* for this calculation.

We used $\%RSD = \frac{s}{\bar{x}} \times 100$ where s is the standard deviation between samples of the same replicate experiment, and $\bar{x}$ the mean of the two duplicate samples.

Experiment variability

To identify the variability between replicates of the same experiment, the 3-hr experiment was run in duplicate. For example, to determine the variability in the Blank experiment, we used Blank 1 and Blank2 experiments, both sampled after 3 hours.

For each experiment, the concentration used to calculate the %RSD is the average of the two samples measured. We used $\%RSD = \frac{s}{\bar{x}} \times 100$ where s is the standard deviation between experiment averages, and $\bar{x}$ the mean of the two replicate experiments.

Combined variability

Three errors were calculated: Measurement Standard Error, Sampling Standard Error and Experiment Standard Error. Standard Errors are calculated using the formula $SE = \frac{s}{\sqrt{n}}$, where s is the standard deviation (between injections, samples, or experiments) and n is the number of replicate injections, samples, or experiments, respectively.

The combined Standard Error is $SE_c = \sqrt{SE_m^2 + SE_s^2 + SE_e^2}$, with SE_m the Measurement Standard Error, SE_s the Sampling Standard Error, and SE_e the Experiment Standard Error. Because samples were not analyzed in triplicate but only the standards used for the calibration

curve, the Measurement Standard Error for each sample was calculated as 8.3% of the measured naphthalene concentration (i.e. the %RSD obtained for the 10-ppm standard; Table 2.2).

2.1.5 Determination of naphthalene mass sorbed to MFC materials

Based on the experimental K_d obtained for each material, we calculated the expected amount of naphthalene to be sorbed on to these materials in the individual MFC reactors, Q_e. Details and parameter values used in this determination are presented in Appendix B.2. Combining (Eq. **1** and (Eq. **2**, and solving for Q_e we obtain:

$$Q_e = \frac{c_i}{\frac{m}{V} + \frac{1}{K_d}} \quad \text{(Eq. 3)}$$

With Q_e the amount of naphthalene sorbed to the sorbent (mg/g), c_i the initial naphthalene concentration (mg/L) in the MFC media, m the mass of sorbent in the MFC reactor (g), V the volume of media (L) in the MFC reactor, and K_d the distribution coefficient obtained from the sorption experiment for each material (L/g).

The mass of naphthalene sorbed by each material was determined using:

$$m_{naph\ sorbed}\ [mg] = m_{material}[g] \times Q_e \left[\frac{mg}{g}\right] \quad \text{(Eq. 4)}$$

With $m_{material}$ the mass of the material (glass, sand, electrode), and Q_e the amount of naphthalene sorbed to each material.

2.2 Results

2.2.1 Naphthalene measurements

Table 2.3 presents dissolved naphthalene measurements obtained for individual samples.

Table 2.3. Dissolved naphthalene concentration measurements for the sorption experiments.

Experiment	Sample ID	Naph (ppm)	Time (days)
Blank1	s-b1-a	11.5	0.125
Blank1	s-b1-b	14.6	0.125
Blank2	s-b2-a	13.9	0.125
Blank2	s-b2-b	12.9	0.125
Cloth1	s-c1-a	13.3	0.125
Cloth1	s-c1-b	12.7	0.125
Cloth2	s-c2-a	13.1	0.125
Cloth2	s-c2-b	11.7	0.125
Fe1	s-fe1-a	12.0	0.125
Fe1	s-fe1-b	11.9	0.125
Fe2	s-fe2-a	10.1	0.125
Fe2	s-fe2-b	13.5	0.125
Sand1	s-s1-a	12.7	0.125
Sand1	s-s1-b	13.4	0.125
Sand2	s-s2-a	12.8	0.125
Sand2	s-s2-b	13.7	0.125
Blank3	s-b3-a	14.3	7
Blank3	s-b3-b	15.2	7
Cloth3	s-c3-a	13.6	7
Cloth3	s-c3-b	12.6	7
Fe3	s-fe3-a	10.4	7
Fe3	s-fe3-b	14.0	7
Sand3	s-s3-a	11.3	7
Sand3	s-s3-b	11.1	7

2.2.1.1 Variability

Sampling variability

The RSD between duplicate samples from the same experiment was 5.5% in average for the 12 experiments (Table 2.4).

The average sampling %RSD was 9.8% for the Fe experiment, 6.1% for the Blank experiment, 3.8% for the Cloth experiment, and 2.2% for the Sand experiment. The higher variability in the Fe experiment points to inhomogeneity of the water phase and is likely related to the precipitate formed by adding $FeCl_2$ solution to the media. If naphthalene is adsorbed into this fine particulate, it is possible that a variable amount of particulate was included in the sample, then naphthalene could have been extracted into hexane and measured.

Experiment variability

The calculated RSD for replicate experiments was 2.1% or lower (1.2% in average, Table 2.4).

Combined variability

Combined sorption experiment errors are presented in Table 2.5, where SE_m is the Measurement Standard Error, SE_s the Sampling Standard Error, SE_e the Experiment Standard Error, and SE_c the Combined Standard Error.

The most important source of variability was sampling, pointing to inhomogeneity in the naphthalene dissolved in the water phase even after crystals are not visible. This is expected due to the non-polar nature of naphthalene, which inhibits its dissolution in water. The calculated combined SE fluctuated between 4.8% and 13.0%, with 5 samples having SE > 10%. The combined SE of the 16 samples for which all three errors were measured, gives an average of 0.8 ppm SE, which corresponds to 6.7% of the average measured naphthalene in each case.

Table 2.4. Sorption experiment variability.

Napthalene measurements				**Sampling variability**			**Experiment variability**		
Sample ID	**Naph (ppm)**	**RSD (ppm)**	**Time (days)**	**Sample**	**Ave. sample naph. (ppm)**	**%RSD sampling**	**Experiment**	**Ave. experiment naph. (ppm)**	**%RSD experiment**
s-b1-a	11.5	1.0	0.125	Blank1_a	13.1	11.8%	Blank1	13.1	1.3%
s-b1-b	14.6	1.2	0.125	Blank1_b					
s-b2-a	13.9	1.2	0.125	Blank2_a	13.4	3.4%	Blank2	13.4	
s-b2-b	12.9	1.1	0.125	Blank2_b					
s-c1-a	13.3	1.1	0.125	Cloth1_a	13.0	2.2%	Cloth1	13.0	2.1%
s-c1-b	12.7	1.1	0.125	Cloth1_b					
s-c2-a	13.1	1.1	0.125	Cloth2_a	12.4	5.6%	Cloth2	12.4	
s-c2-b	11.7	1.0	0.125	Cloth2_b					
s-fe1-a	12.0	1.0	0.125	Fe1_a	11.9	0.5%	Fe1	11.9	0.5%
s-fe1-b	11.9	1.0	0.125	Fe1_b					
s-fe2-a	10.1	0.8	0.125	Fe2_a	11.8	14.6%	Fe2	11.8	
s-fe2-b	13.5	1.1	0.125	Fe2_b					
s-s1-a	12.7	1.1	0.125	Sand1_a	13.0	2.6%	Sand1	13.0	0.9%
s-s1-b	13.4	1.1	0.125	Sand1_b					
s-s2-a	12.8	1.1	0.125	Sand2_a	13.3	3.3%	Sand2	13.3	
s-s2-b	13.7	1.1	0.125	Sand2_b					
s-b3-a	14.3	1.2	7	Blank3_a	14.7	3.1%			
s-b3-b	15.2	1.3	7	Blank3_b					
s-c3-a	13.6	1.1	7	Cloth3_a	13.1	3.7%			
s-c3-b	12.6	1.1	7	Cloth3_b					
s-fe3-a	10.4	0.9	7	Fe3_a	12.2	14.4%			
s-fe3-b	14.0	1.2	7	Fe3_b					
s-s3-a	11.3	0.9	7	Sand3_a	11.2	0.8%			
s-s3-b	11.1	0.9	7	Sand3_b					

Table 2.5. Sorption experiment errors.

Sample ID	Std dev sampling	Std dev experiment	SE_m (ppm)	SE_s (ppm)	SE_e (ppm)	SE_c (ppm)	SE_c (%)
s-b1-a	1.5	0.2	0.6	1.1	0.1	1.2	10.6%
s-b1-b	1.5	0.2	0.7	1.1	0.1	1.3	8.9%
s-b2-a	0.5	0.2	0.7	0.3	0.1	0.7	5.4%
s-b2-b	0.5	0.2	0.6	0.3	0.1	0.7	5.5%
s-c1-a	0.3	0.3	0.6	0.2	0.2	0.7	5.2%
s-c1-b	0.3	0.3	0.6	0.2	0.2	0.7	5.3%
s-c2-a	0.7	0.3	0.6	0.5	0.2	0.8	6.3%
s-c2-b	0.7	0.3	0.6	0.5	0.2	0.8	6.6%
s-fe1-a	0.1	0.1	0.6	0.0	0.0	0.6	4.8%
s-fe1-b	0.1	0.1	0.6	0.0	0.0	0.6	4.8%
s-fe2-a	1.7	0.1	0.5	1.2	0.0	1.3	13.0%
s-fe2-b	1.7	0.1	0.6	1.2	0.0	1.4	10.2%
s-s1-a	0.3	0.1	0.6	0.2	0.1	0.7	5.2%
s-s1-b	0.3	0.1	0.6	0.2	0.1	0.7	5.2%
s-s2-a	0.4	0.1	0.6	0.3	0.1	0.7	5.4%
s-s2-b	0.4	0.1	0.7	0.3	0.1	0.7	5.3%
s-b3-a	0.5		0.7	0.3		0.8	5.3%
s-b3-b	0.5		0.7	0.3		0.8	5.2%
s-c3-a	0.5		0.7	0.3		0.7	5.4%
s-c3-b	0.5		0.6	0.3		0.7	5.5%
s-fe3-a	1.8		0.5	1.2		1.3	12.9%
s-fe3-b	1.8		0.7	1.2		1.4	10.1%
s-s3-a	0.1		0.5	0.1		0.5	4.8%
s-s3-b	0.1		0.5	0.1		0.5	4.8%
Average =			0.6	0.5	0.1	0.8	6.7%

2.2.2 Distribution coefficients

Table 2.6 presents the experimental distribution coefficients calculated for each one of the experiments; results are summarized in Figure 2.3. The material that showed the highest naphthalene sorption per gram was the carbon cloth, followed by the iron precipitate. The quartz sand and glass vials adsorbed very little of the initial naphthalene in the media.

The experiments sampled after 3 hours and the ones sampled after 7 days showed no systematic difference in the sorption coefficient across all four experiments, suggesting that the sorption mechanism is relatively instantaneous.

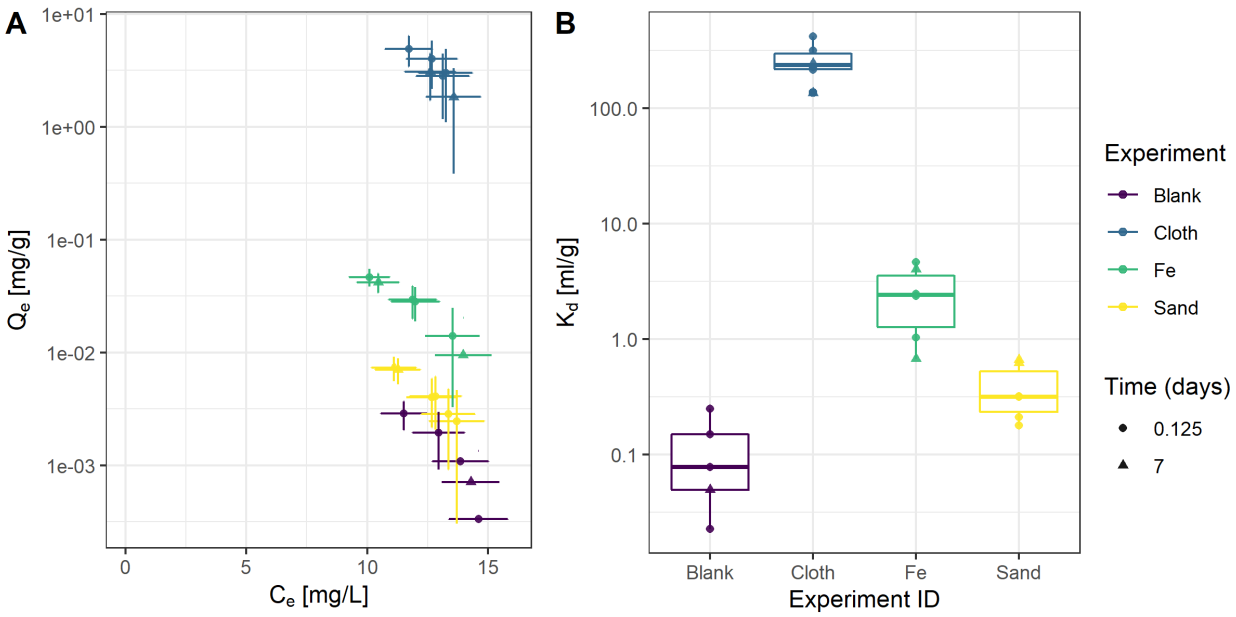

Figure 2.3. Sorption experiment results summary. (A) Calculated sorbed naphthalene (mg/g) versus measured aqueous naphthalene concentration (mg/L) for all sorption experiments. (B) Boxplot of experimental K_d values for the tested materials.

Table 2.6. Distribution coefficients calculated from sorption experiment samples.

Sample ID	Material	Material mass (g)	Media vol. (mL)	Naphthalene aq., c_e (mg/L)	Naphthalene sorbed, Q_e (mg/g)	$K_d = Q_e/c_e$ (mL/g)
s-b1-a	Blank	57.6 ± 0.58	47.44 ± 2.37	11.5 ± 1.0	0.0029 ± 0.0008	**0.25** ± 0.07
s-b1-b	Blank	57.6 ± 0.58	47.44 ± 2.37	14.6 ± 1.2	0.0003 ± 0.0010	**0.02** ± 0.07
s-b2-a	Blank	53.7 ± 0.54	50.94 ± 2.55	13.9 ± 1.2	0.0011 ± 0.0011	**0.08** ± 0.08
s-b2-b	Blank	53.7 ± 0.54	50.94 ± 2.55	12.9 ± 1.1	0.0019 ± 0.0010	**0.15** ± 0.08
s-b3-a	Blank	53.7 ± 0.54	52.54 ± 2.63	14.3 ± 1.2	0.0007 ± 0.0012	**0.05** ± 0.08
s-b3-b	Blank	53.7 ± 0.54	52.54 ± 2.63	15.2 ± 1.3	0 ± 0	**0** ± 0
s-c1-a	Cloth	0.030 ± 0.0001	51.11 ± 2.56	13.3 ± 1.1	3.0 ± 1.9015	**226.4** ± 144.74
s-c1-b	Cloth	0.030 ± 0.0001	51.11 ± 2.56	12.7 ± 1.1	4.0 ± 1.8234	**315.5** ± 146.31
s-c2-a	Cloth	0.035 ± 0.0001	51.60 ± 2.58	13.1 ± 1.1	2.8 ± 1.6429	**214.4** ± 126.49
s-c2-b	Cloth	0.035 ± 0.0001	51.60 ± 2.58	11.7 ± 1.0	4.9 ± 1.4832	**417.9** ± 131.22
s-c3-a	Cloth	0.039 ± 0.0001	49.90 ± 2.49	13.6 ± 1.1	1.8 ± 1.4583	**135.8** ± 108.08
s-c3-b	Cloth	0.039 ± 0.0001	49.90 ± 2.49	12.6 ± 1.1	3.1 ± 1.3607	**244.6** ± 109.88
s-fe1-a	Fe	5.6 ± 0.01	52.84 ± 2.64	12.0 ± 1.0	0.028 ± 0.0095	**2.4** ± 0.82
s-fe1-b	Fe	5.6 ± 0.01	52.84 ± 2.64	11.9 ± 1.0	0.029 ± 0.0094	**2.5** ± 0.82
s-fe2-a	Fe	5.6 ± 0.01	53.44 ± 2.67	10.1 ± 0.8	0.047 ± 0.0083	**4.6** ± 0.91
s-fe2-b	Fe	5.6 ± 0.01	53.44 ± 2.67	13.5 ± 1.1	0.014 ± 0.0107	**1.0** ± 0.80
s-fe3-a	Fe	5.6 ± 0.01	51.84 ± 2.59	10.4 ± 0.9	0.042 ± 0.0083	**4.0** ± 0.86
s-fe3-b	Fe	5.6 ± 0.01	51.84 ± 2.59	14.0 ± 1.2	0.009 ± 0.0107	**0.7** ± 0.77
s-s1-a	Sand	23.0 ± 0.2	39.64 ± 1.98	12.7 ± 1.1	0.0040 ± 0.0018	**0.32** ± 0.15
s-s1-b	Sand	23.0 ± 0.2	39.64 ± 1.98	13.4 ± 1.1	0.0028 ± 0.0019	**0.21** ± 0.15
s-s2-a	Sand	23.0 ± 0.2	43.49 ± 2.17	12.8 ± 1.1	0.0041 ± 0.0020	**0.32** ± 0.16
s-s2-b	Sand	23.0 ± 0.2	43.49 ± 2.17	13.7 ± 1.1	0.0025 ± 0.0022	**0.18** ± 0.16
s-s3-a	Sand	23.0 ± 0.2	43.49 ± 2.17	11.3 ± 0.9	0.0070 ± 0.0018	**0.62** ± 0.17
s-s3-b	Sand	23.0 ± 0.2	43.49 ± 2.17	11.1 ± 0.9	0.0074 ± 0.0018	**0.66** ± 0.17

2.2.3 Naphthalene sorption in MFCs

The mass of naphthalene that is expected to be removed due to sorption to reactor materials in the MFC experiments was determined based on the mass of each sorbent material in individual MFC reactors and the experimental K_d (ml/g) for each material (Table 2.7). Individual MFC reactor specifications and details are presented in Appendix B .

Table 2.7. Total naphthalene mass (mg) sorbed by each material in anode and cathode chambers of MFCs

Reactor ID	Anode chamber				Cathode chamber			
	By glass	By sand	By iron pp.	By c. cloth	By glass	By sand	By iron pp.	By c. cloth
ND_a	0.58	0	0.0039	2.73	0.43	3.90	0.0017	2.24
ND_b	0.58	0	0.0038	2.72	0.42	4.00	0.0017	2.23
NF_a	0.57	0	0.0038	2.67	0.41	3.95	0.0017	2.19
NF_b	0.57	0	0.0038	2.69	0.42	3.89	0.0017	2.20
BC_a	0.57	0	0.0038	2.70	0.42	3.88	0.0017	2.21
BC_b	0.57	0	0.0038	2.70	0.42	3.86	0.0017	2.21

In the anode chamber, the main sorbent was the carbon cloth anode, which sorbed 2.7±0.02 mg (21±0.2 μmol). In the cathode chamber, even with a small K_d, the quartz sand constituted an important sink for naphthalene, sorbing 1.1±0.5 mg (8.7±4.3 μmol) of naphthalene.

2.3 Discussion and conclusions

The results obtained for sorption of naphthalene to glass (Blank experiment average, K_d = 0.11±0.09 (ml/g) are in good agreement with the value of K_d = 0.06±0.01 (ml/g), obtained from a similar experiment testing sorption of naphthalene to borosilicate glass (Qian et al., 2011).

For the sand experiment, where sand composition is 98.8% silica, the obtained K_d = 0.39±0.21 (ml/g) is comparable to values of K_d ranging between 0.08 and 0.8 ml/g, reported on aquifer sands with low percentages of organic matter (≥98% sand and ≤0.025% organic carbon; Delle Site, 2001 and references therein). No literature values were found for pure quartz sand or for carbon cloth.

K_d estimates did not vary systematically with time, which points to a relatively fast reaction. This result is in agreement with similar sorption-desorption batch experiments performed in natural soil samples, where most of the sorption occurred the first 2 hours (Shi et al., 2020).

Difference in the sorption capacity of materials in the cathode and anode chambers will likely result in a significant concentration gradient between cathode and anode compartments of the MFC reactors, driving naphthalene diffusion between the anode and cathode chambers. Therefore, sorption and diffusion need to be addressed to adequately understand naphthalene dynamics in the MFC experiment.

Chapter 3: Naphthalene degradation in MFCs inoculated with native microbial communities

3.1 Introduction

Microbial fuel cells (MFCs) are bio-electrical devices capable of converting chemical energy into electricity through the oxidation of organic or inorganic compounds (Logan et al., 2006). Electrons are harvested by the anode via exoelectrogenic microorganisms and transferred to the cathode where an oxidized compound is reduced. Research on MFCs is mainly focused on achieving high energy generation (H. Wang, Park, et al., 2015; Wu et al., 2013) although there are studies exploring the use of bio-electrochemical systems for contaminant remediation (Adelaja et al., 2014; S.-H. Liu et al., 2018; Nguyen et al., 2016).

The use of bio-electrochemical systems for remediation is based on the idea that anaerobic microbial degradation of contaminants can be accelerated by providing an alternative electron acceptor and an external circuit between the contaminated anaerobic zone and an aerobic zone. The electrode would foster the oxidation of the reduced contaminant, and couple it to the reduction of a readily available oxidant, such as oxygen, present in the aerobic zone. The resulting electron flux can then be harvested for bioelectricity or monitored as a proxy for oxidation rates at depth.

This technique is particularly appealing because it can be applied as a passive in-situ treatment, especially in the case of reduced contaminants with typically slow anaerobic degradation rates, such as polycyclic aromatic hydrocarbons (PAHs). PAHs are one of the most common groundwater contaminants in urban areas and are particularly important because of their toxicity, continued emission, persistence and mobility in the environment (Cachada et al., 2016). For example, the naphthalene half-life under aerobic conditions is reported to be 0.5-20 days, while under anaerobic conditions it is 25-258 days (Howard, 2017). Under anaerobic conditions, naphthalene oxidation is coupled to the reduction of alternative electron acceptors, like nitrate, iron oxides, or sulfate (Dou et al., 2009; Kleemann & Meckenstock, 2011; Meckenstock et al.,

2000), therefore the availability of these compounds can be a limiting factor for the degradation rate.

Removal of hydrocarbons, such as benzene, toluene and naphthalene, accompanied by electricity production has been previously demonstrated in MFCs, and the in-situ implementation of this technology for remediation purposes is promising (Adelaja et al., 2014; Daghio et al., 2016; Hedbavna et al., 2016; Matturro et al., 2017; Morris & Jin, 2012). However, hydrocarbon-contaminated aquifers are often under reducing conditions, and other reduced species could be electrochemically oxidized. In some MFC experiments, oxidation of inorganic compounds such as sulfide has been observed in addition to hydrocarbon oxidation (Daghio et al., 2016; Rakoczy et al., 2013), while in others, the purpose is specifically sulfide removal via electrochemical oxidation (Daghio et al., 2018; Zhao et al., 2008). Ferrous iron, has the potential of being oxidized at the anode in a MFC achieving complete removal (Cheng et al., 2007).

In this study we developed batch bioreactor experiments to test the degradation of naphthalene and the possible influence of high concentrations of ferrous iron over naphthalene removal and energy production. We used naphthalene as a simple model for other hydrocarbons which are common refractory contaminants in aquifers. Our setup aims to mimic an aquifer with high ferrous iron concentration in a batch reactor where the anode and cathode are separated by a permeable sand layer, and the cathode is under aerobic conditions while the anode is under anoxic conditions.

3.2 Methods

3.2.1 Reactor construction

The bioreactors consisted of two vertically stacked 1-L glass chambers, connected by a threaded PVC connector (Figure 3.4). The top cylinder contained the cathode, and the bottom the anode. The cathode chamber contained 10 cm of pure quartz sand (40-100 mesh; ACROS Organics), separated from the lower anode chamber by a fine mesh (50-µm pore size). The anode chamber was permanently stirred by a Teflon-coated stir bar to eliminate mass-transfer limitations at the anode. The anodes were plain carbon cloth (CC6 Plain; Fuel Cell Earth), while the cathodes were

Pt-coated carbon cloth (0.5 mg/cm² 20% Pt on Carbon Cloth; Fuel Cell Earth). The 5x5 cm^2 square electrodes were attached to stainless steel wires with conductive carbon epoxy (AA-CARB 61; Atom Adhesives). The anode and cathode chambers were filled with naphthalene-spiked anaerobic media (aqueous solution), inside an anaerobic chamber to ensure anaerobic conditions.

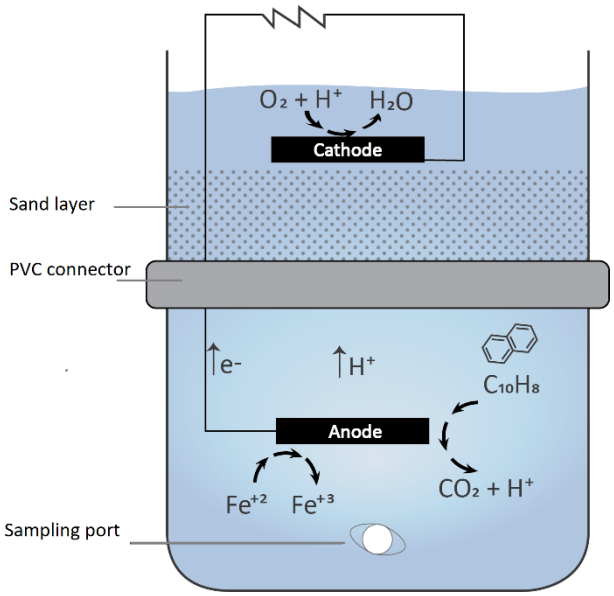

Figure 3.4. Schematic representation and conceptualization of the two-chamber reactor configuration. The anode and cathode chambers are separated by a 10-cm layer of quartz sand, and the electrodes are connected to an external load (1 kΩ) through a conductive wire.

The media was prepared after Widdel and Bak (1992), with modified sulfate and iron concentrations to resemble local iron-rich groundwater. The media was prepared with 1 g/L NaCl, 0.4 g/L $MgCl_2 \cdot 6H_2O$, 0.1 g/L $CaCI_2 \cdot 2H_2O$, 0.6 g/L Na_2SO_4, 0.25 NH_4Cl, 0.2 g/L KH_2PO_4, and 0.5 g/L KCl. After autoclaving, 30 mL of 1M bicarbonate solution, 1 mL of mixed vitamins solution, vitamin B12, trace elements, selenate-tungstate solutions were aseptically added under a CO_2/N_2 atmosphere (20/80). The resulting pH of the media was between 7.3 and 7.4. Naphthalene (15 mg/L) was dissolved into the prepared media and 5 ml of 360 mM $FeCl_2$ solution was added inside an anaerobic chamber. The media was inoculated with 10 mL/L of inoculum. The inoculum was prepared by shaking 200 cc of prepared media with 200 cc (~380

g) of PAH-contaminated fine sands taken from an anaerobic section of the Fraser River aquifer (River District site, well MW14-05, at 60' – 65' depth).

The reactors were assembled and loaded with the anaerobic media and sand inside an anaerobic chamber (0 ppm O_2, 2.1% H_2, 97.9% N_2 atmosphere). Reactors were brought outside the chamber to run the experiment, so that oxygen was available at the cathode. The final sampling of anode material and mineral precipitates in the anode chamber was done inside an anaerobic chamber (4-8 ppm O_2, 2.5% H_2, 97.5% N_2 atmosphere).

3.2.2 MFC operation

Five conditions were tested (Table 3.1): the base case was an inoculated closed-circuit reactor with naphthalene and iron in the media; for the no iron experiments no $FeCl_2$ was used in the media; the natural degradation control was an open-circuit reactor; the no naphthalene experiment did not contain naphthalene; and the abiotic control was not inoculated. All experiments were performed in duplicate.

Table 3.1. Summary of the conditions tested in MFC experiments.

Experiment	Reactor ID	Naphthalene	Ferrous iron	Electrical circuit	Inoculation
Base Case closed-circuit	BC_a BC_b	0.11 mM	1.8 mM	Closed	Yes
No iron	NF_a NF_b	0.11 mM	-	Closed	Yes
Natural degradation	ND_a ND_b	0.11 mM	1.8 mM	Open	Yes
Abiotic	A_a A_b	0.11 mM	1.8 mM	Closed	No
No naphthalene	NN_a NN_b	-	1.8 mM	Closed	Yes

Experiments ran for seven weeks. Ten mL aqueous samples were collected and analyzed to monitor the geochemical evolution of the reactors. The first samples of solution from the reactors were collected approximately three hours after reactor set up, after reactor vessels were brought outside of the anaerobic chamber. Solution samples were collected weekly from the reactors for five weeks, and the last sample was collected two weeks later. At the end of the experiment, reactors were disassembled in an anaerobic chamber where anode samples were collected for

Scanning Electron Microscopy (SEM) analysis and mineral precipitates from the anode chamber were collected for SEM and X-Ray Diffraction (XRD) analysis.

3.2.3 Chemical analyses

Each 10 mL sample was split for different chemical analyses. Cation and anion samples were filtered through a 0.22 μm PVDF membrane filter. Cation samples were preserved with 2% HNO_3. Major cation and anion concentrations were determined by inductively coupled plasma – optical emission spectrometry (ICP-OES) and ion chromatography, respectively. For ICP-OES analysis, a Varian 725-ES Optical Emission Spectrometer was used with external calibration standards, and scandium as the internal standard. Alkalinity was determined by acidimetric titration following standard procedures (Rounds, 2012). Anion samples were diluted 1/10 prior to analysis. Anions (Cl^-, NO_3^- and SO_4^{2-}) were analyzed using a Dionex ICS 2000 ion chromatograph; a 20 μL aliquot was injected onto an Ion Pac AS18 anion column (Dionex Corporation) and then separated by isocratic elution using 35.0 mM potassium hydroxide, a flow rate of 1.0 mL/min, and column temperature of 30°C.

Naphthalene was quantified by gas chromatography–mass spectrometry analysis. A volume of 0.5 mL unfiltered sample was mixed with hexane (1:1 by volume) and vortexed. The hexane supernatant was analyzed for naphthalene with an Agilent GC 7890A/7000A GC/MS Triple Quad equipped with an Agilent 19091S-433HP-5MS 5% Phenyl Methyl Silox column. The carrier gas was helium, and the temperature program was 40 °C (2 min isothermal), ramp of 20 °C/min to 280 °C for 1 min, 280 °C (isothermal for 15 min). The following MS conditions were used: selected ion monitoring mode (selected mass of 128), ionization energy of 70 eV, source temperature of 230 °C.

3.2.4 SEM imaging

Anode samples were fixed in a 2.5% glutaraldehyde 50 mM sodium cacodylate buffer solution, washed with distilled de-ionized water, and then dehydrated stepwise in a gradient series of water/ethanol solutions (30%, 50%, 70%, 90%, 95%, 100% ethanol). The dehydrated samples

were dried by critical point drying with CO_2 (Autosamdri 815B-B, Tousimis). Dried samples were coated with ~20 nm of Pt/Au.

Mineral precipitates present in the anode chamber were also collected at the end of the experiments for SEM imaging. Samples were collected, decanted and frozen under an anaerobic environment. They were subsequently freeze dried and coated with carbon prior to SEM imaging.

Anode and mineral samples were examined using a Philips XL30 electron microscope with a Bruker Quantax 200 energy-dispersion X-ray microanalysis system. Operating conditions were 15-20 keV accelerating voltage, spot size of 4-5, and working distance of ~10 mm. Secondary electron (SE) detection was used to obtain topographic images of the surface of the anode samples and to recognize the morphology microorganisms and mineral phases, and their textural relationships. Energy-dispersive X-ray spectrometry (EDS) was used to determine the major elements of individual mineral phases, and backscatter electron detection was used to image mineral phases in the precipitate samples.

3.2.5 X-Ray diffraction

Samples of mineral precipitates and media were collected from the anode compartment of the reactor at the end of the experimental run. Wet samples were collected, flash frozen inside the anaerobic chamber, and subsequently freeze dried in a freeze drier. Dried samples were ground into fine powder using a corundum mortar and smeared on to a zero-diffraction quartz plate with ethanol. Step-scan X-ray powder-diffraction data were collected over a range 3-80°2θ with CoKα radiation on a Bruker D8 Advance Bragg-Brentano diffractometer equipped with an Fe monochromator foil, 0.6 mm (0.3°) divergence slit, incident- and diffracted-beam Soller slits and a LynxEye-XE detector. The long fine-focus Co X-ray tube was operated at 35 kV and 40 mA, using a take-off angle of 6°.

Mineral phases were identified using the International Centre for Diffraction Database PDF-4 and Search-Match software by Bruker. Mineral abundances (%) were estimated.

3.2.6 Electrochemical analysis

The electrode potential was measured every 30 seconds with a Campbell Scientific CR1000 data logger. The measurements collected over a 30-minute interval were averaged and recorded. The current was calculated using Ohm's Law: $V = I \cdot R$, where V [V] is the voltage drop across the external load, I is the current (A), and R is the external load (1 kΩ). Current production was plotted over time to identify the time to the start of electricity generation, peak current and peak length. Peak length was calculated as the number of days in which the voltage was above a voltage threshold. The threshold was calculated as half of the maximum voltage. The current density (A/cm^2) was then calculated by normalizing the current to the cathode area (surface area 25 cm^2). The maximum current and duration of the polarization of the reactors was tested to determine their internal resistance. The polarization curve represents the voltage as a function of current density. For the test, the resistance was varied stepwise starting at a low resistance and increasing every 20 minutes. The open circuit voltage (OCV) was measured 1 hr after the open circuit was established. Then the polarization test was repeated in the same manner for decreasing resistances, and averages of the obtained values are reported. Polarization tests were performed during the peak of voltage generation in each reactor.

Power [W] was calculated at each step as $P = I \cdot V = V^2/R$. The power curve describes the power density as a function of the current density. The internal resistance (R_{int}) of the reactors was calculated as the slope of the polarization curve.

3.2.7 Sorption experiment

The degree to which naphthalene is sorbed onto the different materials used in the MFC experiment was measured in a separate experiment. The glass (used in the MFC reactor vessels), quartz sand, carbon cloth and the Fe precipitate that forms when adding $FeCl_2$ solution to naphthalene-spiked media were tested in independent experiments. The mass-to-volume ratio of tested material (sand and cloth) to naphthalene-spiked media matched that of the MFC experiments. The sorption experiment media and the MFC media were identical in composition,

except for the iron concentration (Table 3.2); iron was only added to the sorption experiment testing naphthalene sorption onto iron precipitates (S_Fe experiments).

Table 3.2. Summary of experimental conditions tested in the sorption experiments. Media composition was identical to that used in the MFC experiments, except iron was only added to the iron precipitates sorption experiment.

Experiment	Experiment ID	Media composition
Glass vial (blank)	S_B1 S_B2 S_B3	Naphthalene-spiked media, no iron
Quartz sand	S_S1 S_S2 S_S3	Naphthalene-spiked media, no iron
Carbon cloth	S_C1 S_C2 S_C3	Naphthalene-spiked media, no iron
Iron precipitates	S_Fe1 S_Fe2 S_Fe3	Naphthalene-spiked media, 1.8 mM Fe

Sorption experiments were done in triplicate, two of the three experiments were sampled 3 hrs after set-up, matching the first sampling event in the MFC experiment. The third experiment was sampled 7 days after set-up, matching the second sampling event in MFC experiment. Experiments were sampled in duplicate in each sampling event. Naphthalene was measured in these samples as described above.

The amount of naphthalene sorbed was calculated using $Q_e = \frac{(C_i - C_e)\,V}{m}$, where Q_e is the naphthalene sorbed per unit mass of sorbent (mg/g), C_i is the initial naphthalene concentration (mg/L), C_e is the equilibrium naphthalene concentration measured at each time point (mg/L), V is the volume of media (L), and m is the mass of sorbent (g). The distribution coefficient K_d (g/L) was calculated according to $Q_e = K_d\, C_e$.

3.2.8 Chemical data analysis

Using the experimentally determined distribution coefficients and dissolved naphthalene data, we determined naphthalene degradation and removal efficiency in the MFCs. We calculated the naphthalene mass sorbed to the carbon cloth anode at each sampling time point using the K_d of the carbon cloth. The amount of naphthalene removed from the anode chamber at each time

point corresponds to the difference between the total naphthalene added to the reactor initially and the dissolved naphthalene measured at each time point. Naphthalene loss in the anode chamber can be due to either sorption to the cloth anode, microbial degradation, or diffusion to the cathode chamber. To account for naphthalene loss (or gain) due to diffusion between cathode and anode chambers, we first calculated the amount of naphthalene sorbed to the cathode and sand in the cathode chamber using the initial naphthalene added and the experimental K_d. Then we calculated the initial dissolved naphthalene in the cathode chamber with a mass balance. Then, based on the dissolved naphthalene gradient between anode and cathode chamber, a mass flux was calculated using $J = -D\theta\frac{\Delta C}{\Delta x}$, with D the diffusion coefficient of naphthalene (7.5e-06 cm^2/s), θ the sand porosity (0.216), ΔC the difference between naphthalene measured concentration in the anode chamber and dissolved naphthalene concentration calculated in the cathode chamber after sorption to sand and cathode, Δx the sand layer length (0.1 m). Dissolved naphthalene in the cathode chamber was adjusted trough time by adding or subtracting the mass flux to the anode and recalculating the naphthalene sorbed to sand and cathode accordingly.

3.2.9 Microbial methods

Inoculum, media, and anode samples were used to characterize the microbial community composition. Aqueous samples (15 mL of inoculum suspension and 50 mL of reactor media, collected in triplicate at the end of the experiments) were centrifuged at 10,000 RCF for 20 minutes, then the supernatant was decanted, and the pellets were kept for analysis. Anode samples (1 cm x 1 cm) we also collected in triplicate, at the end of the experiments. All microbiological samples were stored frozen at -80 °C until DNA extraction.

DNA was extracted using the Qiagen DNeasy PowerSoil Kit according to the manufacturer's protocol. DNA quantity was assessed using the PicoGreen Assay for dsDNA, measured on a TECAN™ M200 (with excitation set at 480 nm and emission at 520 nm). The V4 region of the 16S rRNA gene was amplified using primers 515F/806R (Apprill et al., 2015; Parada et al., 2016). The PCR products were amplified using a 25 µL reaction mixture containing 1 µL of DNA template, 0.2 µM of each primer, 0.2 mM deoxynucleoside triphosphate, 0.4 U of *Taq* DNA polymerase, and 2.5 µL 10X PCR buffer to a final concentration of 1.5 mM $MgCl_2$. PCR

amplification was performed with an initial denaturing step at 94 °C (3 min), followed by 30 cycles of denaturation at 94 °C (30 s), annealing at 55 °C (1 min) and extension at 72 °C (1 min), followed by a final extension at 72 °C for 10 min. Controls without template DNA were included to ensure no contamination. PCR product quality was checked using gel electrophoresis of a 1 µL aliquot on a 1.5% agarose gel, using 1 µL /mL SYBER safe DNA gel stain. Amplicon samples were pooled at equimolar concentrations into a single library using an Invitrogen SequalPrep kit. Amplicon library was analyzed on an Agilent Bioanalyzer; High Sensitivity DS DNA assay was used to determine library fragment size and check for integrity. KAPA Library Quantification Kit was used to determine pooled library concentration. Library pools were diluted to 4 nM and denatured into single strands using fresh 0.2 N NaOH. The final library was loaded at a concentration of 8 pM, with an additional PhiX spike-in of 5–20%. Sequencing was conducted at the University of British Columbia sequencing center (https://sequencing.ubc.ca/).

Sequences were processed using Mothur (www.mothur.org) as described in Schloss et al. (2009). Sequences were removed if they contained ambiguous characters, had homopolymers longer than 8 bp and did not align to a reference alignment. Unique sequences and their frequency were identified for each sample, and a pre-clustering algorithm was used to remove noise sequences (Schloss et al., 2011). Unique sequences were aligned against a SILVA reference alignment (http://www.mothur.org/wiki/Silva_reference_alignment). Chimeric sequences were checked using UCHIME 3 (Edgar et al., 2011) and removed from the analysis. Reads were clustered into OTUs at 97% similarity using OptiClust (Westcott & Schloss, 2017). OTUs were classified using the SILVA reference taxonomy database (release 138, available at http://www.mothur.org/wiki/Silva_reference_files). For alpha and beta diversity measures, samples were subsampled to the lowest coverage depth and calculated in Mothur (Schloss et al., 2009).

Analysis of molecular variance (AMOVA) was used to determine whether the differences found in the microbial population between reactors and sample types was statistically significant. Linear discriminant analysis effect size (LEfSe; Segata et al., 2011) was used to determine whether there were any OTUs differentially represented in different groups. For the LEfSe the grouping used considered the whole community (anode and media) between reactor types. The

threshold for the logarithmic discriminant analysis (LDA) score was 3.0, and for p-values the threshold was 0.05.

All detected OTUs were paired to known metabolic functions by using the FAPROTAX database (http://www.loucalab.com/archive/FAPROTAX/) (Louca et al., 2016), which contains metabolic and other ecologically important functions for cultured strains. Then the relative abundance of organisms capable of these metabolic functions was mapped for each sample and reactor type.

3.3 Results

3.3.1 Naphthalene sorption

Table 3.3 summarizes the sorption experiment results. The most significant sorbent for naphthalene per unit mass was the carbon cloth; the K_d obtained for iron precipitates is two orders of magnitude smaller, and K_d of the quartz sand is one order or magnitude smaller than that. The glass vial (blank experiment) represents a minimal sink for sorbed naphthalene. The experiments sampled after 3 hours and the ones sampled after 7 days showed no systematic difference in the distribution coefficient, suggesting naphthalene sorption occurs relatively fast.

Table 3.3. Distribution coefficient of reactor materials used in MFC experiments, average and standard deviation from triplicate experiments.

Sorption experiment	K_d (ml/g)	K_d SD (ml/g)
Blank (glass)	0.11	0.09
Cloth	259	97
Fe precipitates	2.53	1.57
Sand	0.39	0.21

The mass of naphthalene initially removed due to sorption to reactor materials in the MFC experiments was estimated based on the mass of each sorbent material and the distribution coefficients K_d (ml/g) obtained experimentally. In the anode chamber, the main sorbent is the carbon cloth anode, which sorbed 2.7±0.02 mg (21±0.2 μmol). In the cathode chamber, even though the K_d of the quartz sand is small, it constitutes an important sink for naphthalene; sand sorbed 1.1±0.5 mg (8.7±4.3 μmol) of naphthalene.

In the MFC experiments, the naphthalene measured in the first sample, collected approximately three hours after reactor-set-up, was generally lower than the amount of naphthalene added to the media. According to our calculations, this difference is reasonably well explained by sorption of naphthalene to the anode materials.

3.3.2 Naphthalene removal in MFCs

Aqueous naphthalene concentration in the anode media decreased with time in all reactors (Figure 3.5A), first rapidly and then more slowly. In all reactors, the first naphthalene concentration, measured in samples collected three hours after reactor set-up, was lower than what was initially added to the media, indicating sorption to reactor materials is a relevant process. Naphthalene concentration in the anode chamber in the closed-circuit BC experiment decreased from 116 μM initially added to the reactors to 22 μM in BC_a, and to 8 μM in BC_b, measured after 48 days. In the natural degradation experiment ND, naphthalene decreased from 118 μM to 18 μM in ND_a, and to 7 μM in ND_b. In the experiment with no iron NF, the naphthalene concentration decreased from 115 μM to below detection limit in NF_a, and from 116 μM to 3 μM in NF_b.

The total mass of naphthalene degraded in the closed-circuit BC experiment was 92 and 109 μmoles for reactors BC_a and BC_b, respectively. The degradation achieved in the open-circuit natural degradation controls was 98 and 111 μmoles for reactors ND_a and ND_b, respectively. The reactors with no ferrous iron in the media, NF experiments, show the highest naphthalene degradation. The total naphthalene degraded was 119 and 115 μmoles for reactors NF_a and NF_b, respectively. The amount of naphthalene degraded in NF_a is higher that the naphthalene initially present in the anode chamber, due to diffusion from the cathode chamber. By the end of the experiment, the estimated net mass transfer of naphthalene was from the cathode chamber to the anode chamber for all experiments and varied between 4 and 9 μmoles (Figure 3.5B).

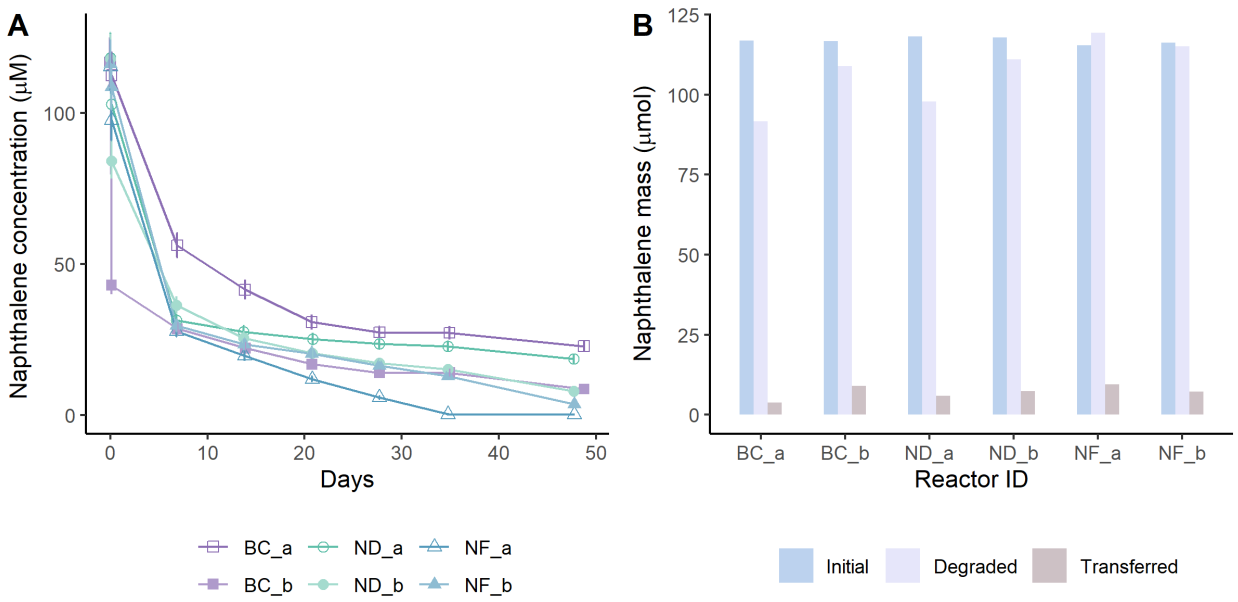

Figure 3.5. Naphthalene evolution in the MFC reactors. (A) Dissolved naphthalene concentration measured in the anode chamber through time. (B) Total naphthalene mass degraded by the end of the experiment, compared to the initial naphthalene and total mass transferred from the cathode to anode chamber by diffusion.

3.3.3 Geochemical evolution

Dissolved ferrous iron measured immediately after MFC reactor set-up was consistently lower than the iron added to the media in all experiments, and after the first week of operation dissolved iron remained at about 0.04 mM in all reactors. The difference initial iron concentration and the first measurement corresponds to about 1.5 mM. In the first sample phosphate concentration was about 1.1 mM lower than initially added and remained below 10 µM throughout the experimental run. This is consistent with the precipitation of vivianite ($Fe_3(PO_4)_2$ H_2O), an iron and phosphate mineral that is present in XRD analysis of samples from all reactors containing iron (Table 3.4). Vivianite is also oversaturated according to speciation calculations performed in Phreeqc. According to the change in Fe and P, we can estimate that between 0.5 and 0.55 millimoles (or between 0.22 and 0.24 mg) of vivianite precipitated at the beginning of the experiments.

Most of the geochemical parameters monitored during the experiments remain relatively stable. Alkalinity and pH trends slightly upwards in time in all experiments (Figure 3.7). In experiments ND and NF, some of the samples analyzed had trace amounts of nitrate (0.01 mM), but it generally remains below this detection limit. Sulfate concentration tends to increase in BC reactors. It stays relatively stable at 4.5 mM in ND experiments, with a slight decrease of 0.15mM during the last 28 days of the experiment in ND_b but not in ND_a. Sulfate remains stable in NF experiments. In NN experiments the trend of sulfate is to slightly decrease from 3.8 mM to reach 3.6 mM.

According to the XRD results, samples collected from the bottom of the anode chamber, which included aqueous media and solid precipitates, are comprised of phosphate, chloride, and sulfate minerals (Table 3.4). Halite, sylvite, nahcolite, aphthitalite and struvite were identified, however these are very soluble minerals likely to have precipitated from the aqueous phase of the sample during the freeze-drying step of preparation prior to XRD analysis. Vivianite and elemental sulfur likely correspond to solid phases present in equilibrium with the media. Elemental sulfur is present is both BC duplicates but only one of the ND and NN duplicate reactors. Vivianite is present in all the reactors where iron was available in the media (all except NF experiments).

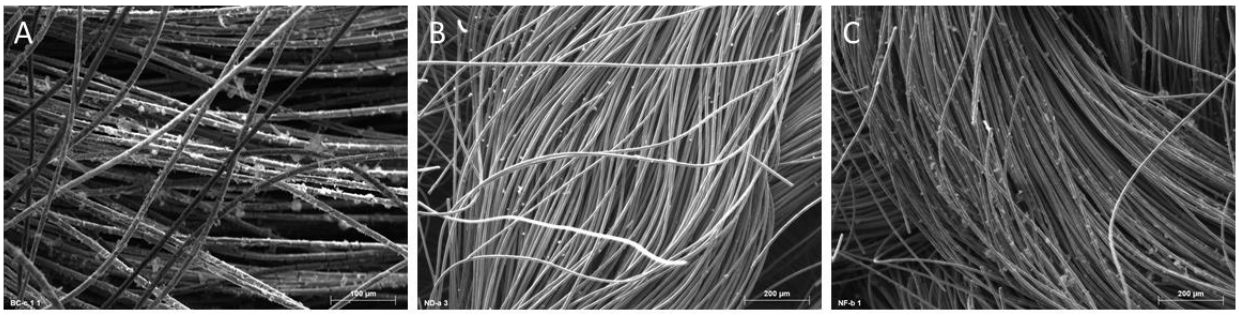

Figure 3.7. SEM images of anode samples collected at the end of the experiments. (A) BC anode, (B) ND anode, and (C) NF anode. Mineral precipitates are present in all anodes. EDX analysis indicates mineral precipitates are mainly composed of P, Fe and Ca.

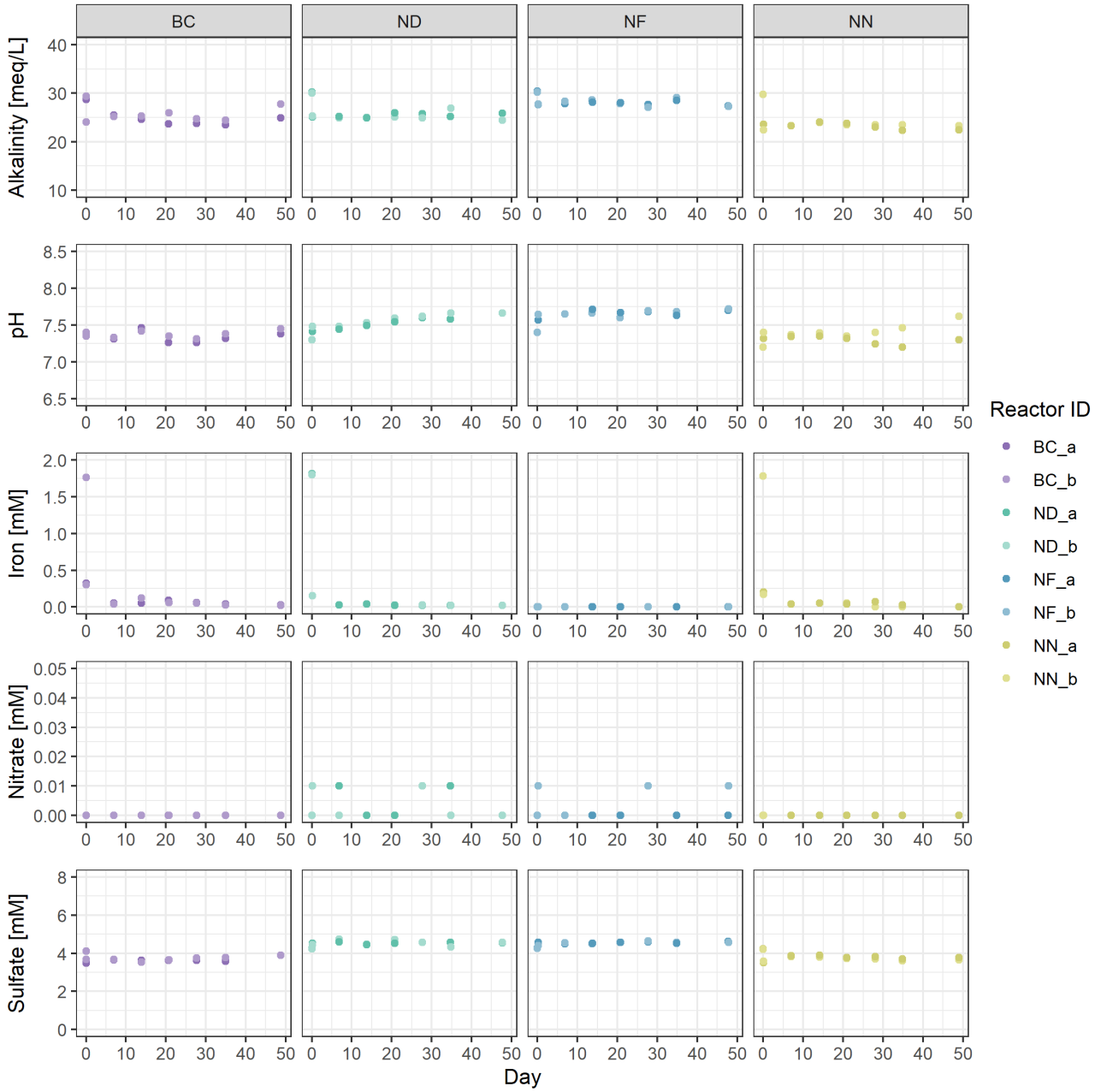

Figure 3.7. Geochemical evolution of MFC experiments

According to the SEM-EDX analysis of particles attached to the carbon fibers in the anodes, most of the particles in BC and NN experiments are mainly composed of P and Fe, in agreement with the XRD findings. Some particles in these samples also show small concentration of other elements such as Ca, Na and Mg. In NN anode samples, Fe and P are also the main components of the precipitates, with occasional minor Mg and Ca content. In NF anode samples, particles

were composed of P, Al, Si, Ca, K, Na and Mg, occasionally some particles were mainly composed of S.

Table 3.4. Approximate abundance and mineralogy in samples of solid precipitate, collected at the end of the experiments, according to XRD analysis.

Mineral	**BC_a**	**BC_b**	**ND_a**	**ND_b**	**NF_a**	**NF_b**	**NN_a**	**NN_b**
Vivianite, $Fe_3(PO_4)_2$ $8(H_2O)$	34%	46%	77%	62%			18%	66%
Halite, NaCl	30%	24%	18%	15%	45%	39%	42%	14%
Nahcolite, $NaHCO_3$	19%	14%		8%	20%	27%	21%	
Aphthitalite, $(K,Na)_3Na(SO_4)_2$	6%	4%	4%	2%	8%	8%	4%	
Struvite, $(NH_4)MgPO_4{\cdot}6H_2O$					22%	16%		
Sylvite, KCl	3%	4%	1%	3%	2%	4%	8%	
Quartz, SiO_2	1%	1%		8%	1%	5%	1%	12%
Sulfur, S_8	6%	6%		2%			5%	
Corundum, Al_2O_3								5%
Ankerite-Dolomite, $Ca(Fe^{2+},Mg,Mn)(CO_3)_2$ – $CaMg(CO_3)_2$							?	?
Amorphous	X			X	X	X		

"X" indicates the presence of amorphous phases. Unclear mineral identification is indicated with "?"

3.3.4 Microbiology

A total of 2,275,704 16S rRNA gene sequences were obtained from 74 out of 75 samples (the PCR product did not amplify for one of the samples). The number of reads in each sample ranged between 5,952 and 79,204. A total of 4,154 OTUs were obtained for all samples. High coverage was achieved in all samples (mean 0.993, range 0.977-0.998), indicating that the sequencing results are reliable to characterize the true microbial community composition.

The OTUs identified in all samples correspond mainly to Bacteria (83-100%), with few Archaea present in the samples. The microbial community in the reactor samples is mostly comprised of Proteobacteria (3.3-97%), Desulfobacterota (0-95%), Bacteroidota (0.1-16%), Firmicutes (0-16%), Verrucomicrobiota (0-9%), and several other lesser abundant phyla (<1% on average across reactor samples). The microbial community in the inoculum is similar, comprised mostly of Proteobacteria (59-65%), Desulfobacterota (6.6-27%), Bacteroidota (5-7.5%), Verrucomicrobiota (0.95-4.2%), unclassified Bacteria (1.7-3.8%), Acidobacteriota (1.4-2.9%),

Planctomycetota (0.91-2.7%), and other lesser abundant phyla (<1% on average across inoculum samples).

Across anode and media samples, the most abundant genera belong to Proteobacteria and Desulfobacterota phyla (Figure 3.9). Within the Proteobacteria phylum they mainly consist of unclassified genera of the Pseudomonadaceae family (22%), *Immundisolibacter* (5.5%), and *Hydrogenophaga* (4.2%). The most abundant genera within the Desulfobacterota phylum are *Candidatus Deferrimonas* (10.9%%), *Geothermobacter* (6.2%), and unclassified genera of the Desulfuromonadaceae order (5.8%). The most abundant genera in the inoculum samples also belong to the Proteobacteria and Desulfobacterota phyla; Pseudomonas (10.4%), Citrifermentans (7.4%), Sulfurifustis (3.1%) and Thiobacillus (3.1%) are among the most abundant. Although, several of the most abundant OTUs belong to unclassified genus of Gammaproteobacteria, (5.2%), Alphaproteobacteria (4.4%), Bacteria (2.8%), Pseudomonadaceae (2.5%), Burkholderiales (2.3%), and Desulfuromonadaceae (2.1%).

The microbial community developed in each of the experiments are significantly different (AMOVA p-value <0.05). Within experiments BC and NF, the anode microbial community composition is significantly different than that of the media (AMOVA p-values <0.001 and 0.02, respectively), while there is no significant difference between anode and media microbial community in ND and NN (AMOVA p-values 0.2 and 0.15, respectively).

LEfSe was used to identify taxonomic differences among the different experiments. BC reactors were enriched with the anaerobic iron- and electrode-reducer *Candidatus Deferrimonas* and the anaerobic elemental sulfur- and iron-reducer Desulfuromonadia (Garrity, Schleifer, et al., 2005; Waite et al., 2020); both are enriched in anode compared to media samples constituting 46-57% and 18% of the microbial community of the anodes, respectively. BC experiments were also enriched with unclassified genus in the Geobacteraceae family. The Geobacteraceae family includes iron- and electrode-reducing bacteria, as well as monoaromatic hydrocarbon degraders; *Geobacter* species is capable of inter species electron transfer and is one of the most studied in the context of MFCs (Röling, 2014).

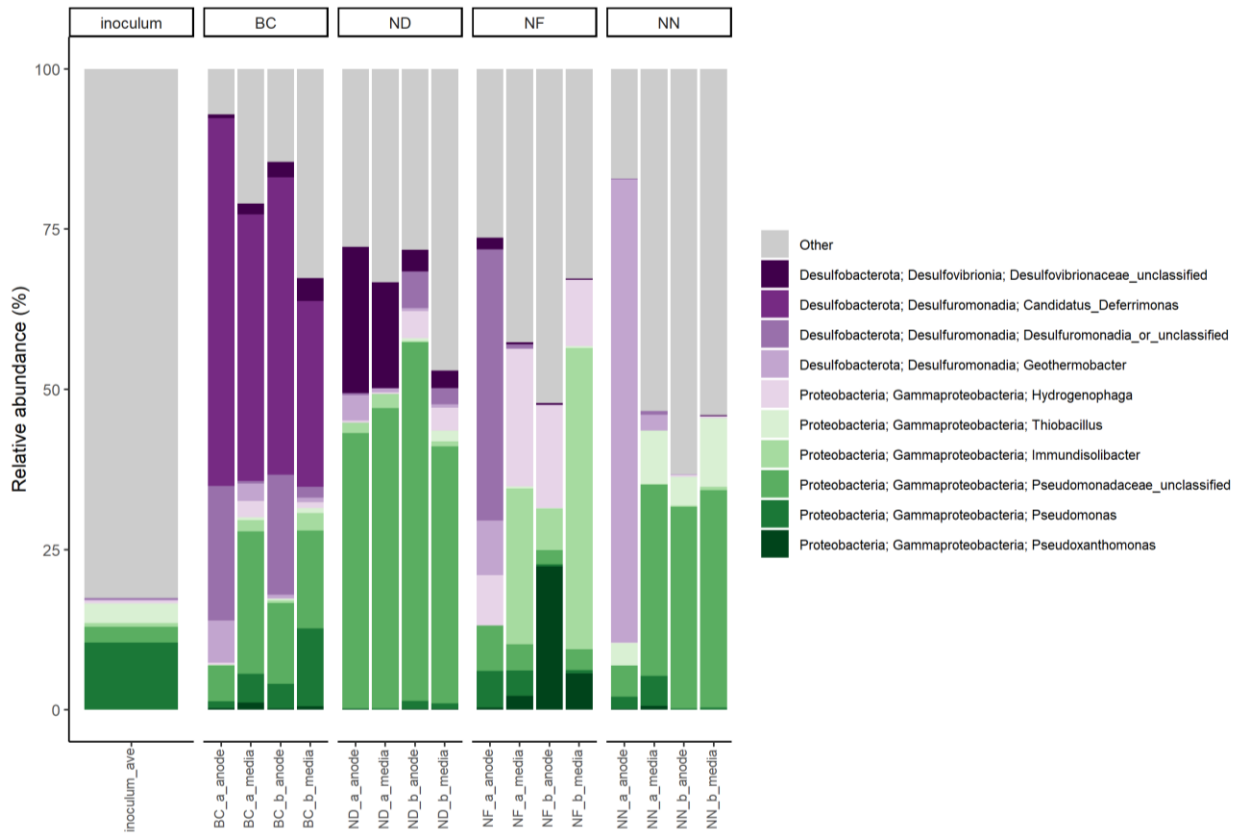

Figure 3.9. Relative abundance of the ten most abundant genera in the microbial community in anode and media samples from bioreactors, and in inoculum samples; lesser abundant taxa are aggregated in the "other" category. Data corresponds to averaged triplicate samples. Taxonomy shown corresponds to Phylum; Class; Genus.

For the natural degradation control, open-circuit ND experiment, several of the significant taxa are anaerobic sulfur-reducers, within Desulfosporosinus, Desulfatitalea, and Desulfovibrionaceae, Desulfocapsaceae (Garrity, Schleifer, et al., 2005; Higashioka et al., 2013; Kuever, 2014; Robertson et al., 2001; Stackebrandt et al., 2003); the type genus Desulfocapsa within Desulfocapsaceae is capable of disproportionation of elemental sulfur to sulfide and sulfate (Janssen et al., 1996). Significant taxa also include fermenters such as Rhodocyclaceae, Paludibacteraceae, Prolixibacteraceae and Christensenellaceae (Huang et al., 2014; Morotomi et al., 2012; Ueki et al., 2006; Ormerod et al., 2016). Uncultured members of Rhodocyclaceae, which includes aromatic compound degraders, sulfur oxidizing chemoautotrophs, methylotrophs and anaerobic fermenters are also enriched in ND reactors (Oren, 2014). No significant

difference in the abundance of these taxa in anode compared to media samples was observed in this group.

In the closed-circuit reactors with no iron, NF, the aerobic hydrogen oxidizer *Hydrogenophaga* is the most abundant of the significant taxa; some species in this genus can degrade aromatic hydrocarbons (Banerjee et al., 2019; Fahy et al., 2008), and one species can generate electricity via oxidation of hydrogen in a pure culture MFC (Kimura & Okabe, 2013). Most of the enriched species are aerobic, some facultatively anaerobic, and several are hydrocarbon degraders such as *Immundisolibacter*, *Pseudorhodoplanes*, *Parvibaculum*, Sphingomonadaceae, and the methane oxidizer Pedosphaeraceae (Corteselli et al., 2017; Garrity, Schleifer, et al., 2005; Martins et al., 2010; Rosario-Passapera et al., 2012; Schleheck et al., 2004; Tirandaz et al., 2015). *Immundisolibacter* and *Hydrogenopahga* are more abundant in the media compared to the anode samples, while Sphingomonadaceae, Desulfuromonadaceae and *Chryseobacterium* are more abundant in the anodes than in the media.

In the closed-circuit reactors with no naphthalene, NN, the iron-oxidizers *Gallionella* and *Ferrovibrio,* and the sulfide oxidizer *Thiobacillus* are among the significant taxa. The iron-reducer *Geothermobacter* is also particularly enriched in anode samples compared to media samples, as well as the sulfur-reducer *Desulfurivibrio,* to a lesser extent.

3.3.5 Electricity production in MFCs

All reactors produced current 11 to 16 days after set-up, except for the abiotic control (Figure 3.10). Electricity production in the closed-circuit BC experiment (see Table 3.1 for list of experiments) started 14 days after reactor set-up. The current increased steadily, reaching a maximum of 0.24 mA on day 17. In NF reactors, where no iron was available in the media, electricity production started after 14 and 11 days, in the respective duplicate reactors, increasing exponentially and reaching a maximum current of 0.08 and 0.12 mA on days 20 and 13, respectively. The duration of the peak was shorter for the BC experiment, with a length of 5 days, compared to the NF reactors, where electricity production lasted for 5 and 10 days in the duplicate reactors. The NN experiment, where no naphthalene was available, electricity

production started after 10 days for both duplicate reactors; the current increased slowly, reaching a first maximum of 0.06 mA and 0.05 mA on days 16 and 14, respectively for each reactor; the current then decreased until it spiked to an overall maximum of 0.17 mA and 0.43 mA on days 27 and 25, respectively. For NN experiments, the duration of the first peak was 8 and 6 days for the respective duplicates, and the second peak lengths were 4 and 16 days. The abiotic control, set-up with autoclaved media, did not produce significant voltage, the average current measurement was 4±6 μA and 7±3 μA for the respective duplicate reactors.

The total accumulated electron flux measured in BC experiment was 269 C and 114 C for reactors BC_a and BC_b, respectively. A total of 65 and 88 C were transferred in the NF_a and NF_b experiments, respectively; and a total charge of 144 and 634 C in NN_a and NN_b experiments, respectively. The total electron flux in the NF experiment was lower than that of the BC experiment. On average, the flux was the highest for the NN experiment, however one of the duplicates generated a higher flux than BC, and one generating a lower flux.

For the BC experiment, the maximum power output was 4.3 mW/m^2 of electrode surface area, and the internal resistance was 0.5 kΩ, according to the polarization test (Appendix A). For the NN experiment, the maximum power output was 2.6±2.0 mW/m^2 of electrode surface area and the internal resistance was 0.7±0.1 kΩ. For the NF experiment, the maximum power output was 3.0±1.2 mW/m^2 of electrode surface area and the internal resistance was 0.5±0.1 kΩ. The open circuit voltage was 340 mV in the BC experiment, 351±9 mV in the NN experiment, and 615 in the NF experiment.

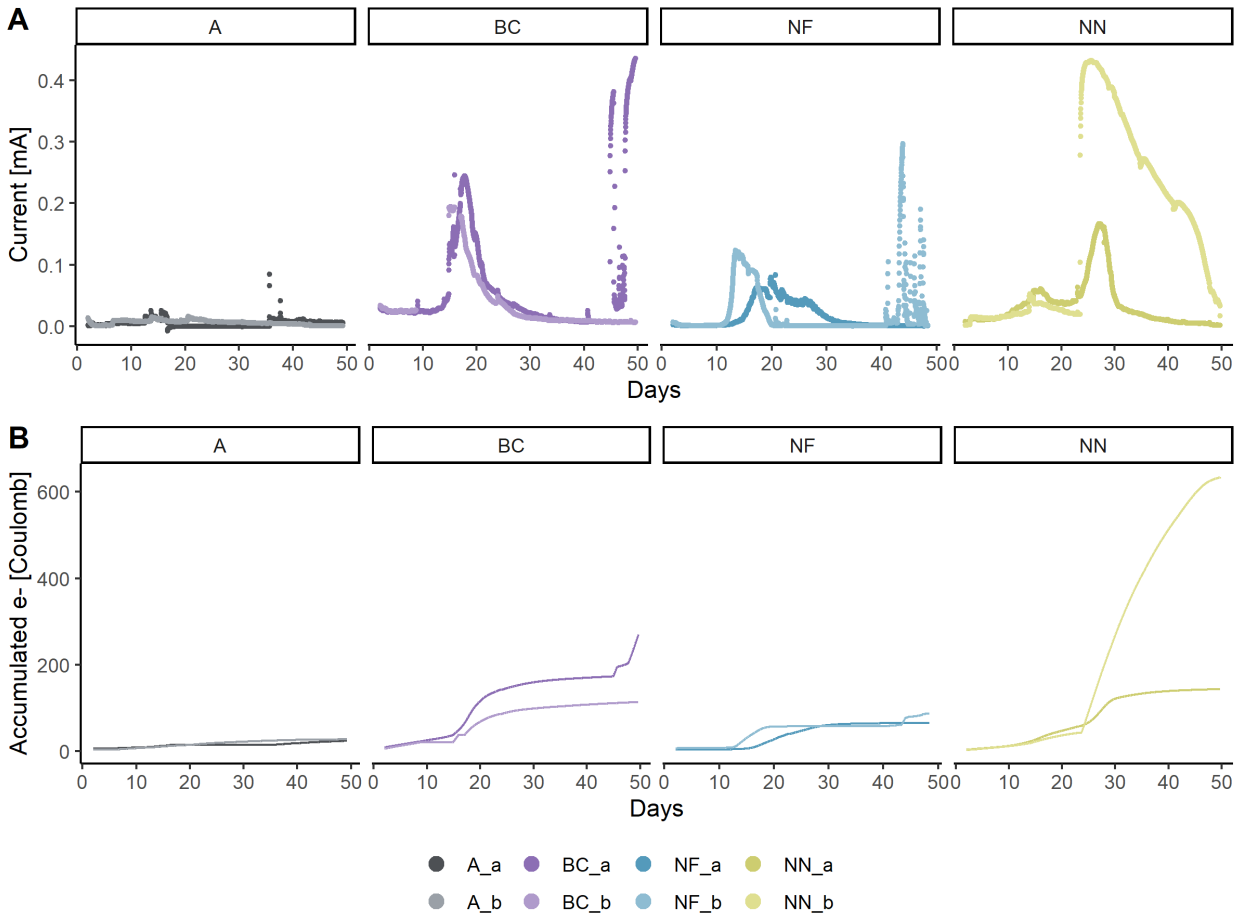

Figure 3.10. Electricity production in the MFCs. (A) Current production through time in all reactors. (B) Accumulated coulomb generation in the MFCs.

3.4 Discussion

There are several biological and chemical reactions expected to occur in the bioreactors, including: microbial degradation of naphthalene to carbon dioxide via organic metabolites, with iron oxides or sulfate as electron acceptor; microbial respiration with the anode as electron acceptor; diffusion of dissolved species between the anode and cathode chambers; sorption of naphthalene and organic metabolites to the surface of electrodes and mineral precipitation and dissolution.

First, we will analyze the processes affecting naphthalene, compare the degradation efficiency in the natural degradation control and the closed-circuit experiments, and analyze the effect of iron.

Then, we will evaluate the electricity generation in the MFC experiments. And finally, we present the conceptual model of the system, including all the processes occurring in the bioreactors.

3.4.1 Naphthalene removal efficiency

The change in naphthalene concentration measured in the media sampled from the anode chamber does not translate directly to total naphthalene removal via microbial degradation. Sorption to reactor materials and mass transfer due to diffusion need to be considered. Figure 3.11 depicts the mass of naphthalene stored in aqueous and sorbed form in the anode chamber, and the mass degraded through time in all experiments, taking into account mass transfer between anode and cathode chamber.

At the beginning of the experiment, sorption to sand and carbon cloth electrode in the cathode chamber removed about 25 μmol of naphthalene from the media, according to our calculations, which resulted in a concentration of 0.05 mM. This generated a naphthalene concentration gradient driving diffusion from the anode chamber (0.11 mM) to the cathode chamber. However, after one week, naphthalene in the anode chamber had decreased significantly reversing the gradient, so that naphthalene mass transfer was towards the anode chamber.

Two experiments, BC_b and ND_b, show some naphthalene being degraded in the first timepoint, which corresponds to the sample taken immediately after experiment set up according to our calculations., however this is unrealistic and probably due to underestimation of some processes. In the case of BC_b, the first dissolved naphthalene measurement is significantly lower than expected, suggesting a sampling, analysis, or experiment set-up error. For ND_b, the first dissolved naphthalene measurement is reasonable, so we hypothesize that sorption or diffusion are underestimated, because it is unlikely that the true process removing naphthalene in the short time between reactor set-up and the first sample is degradation.

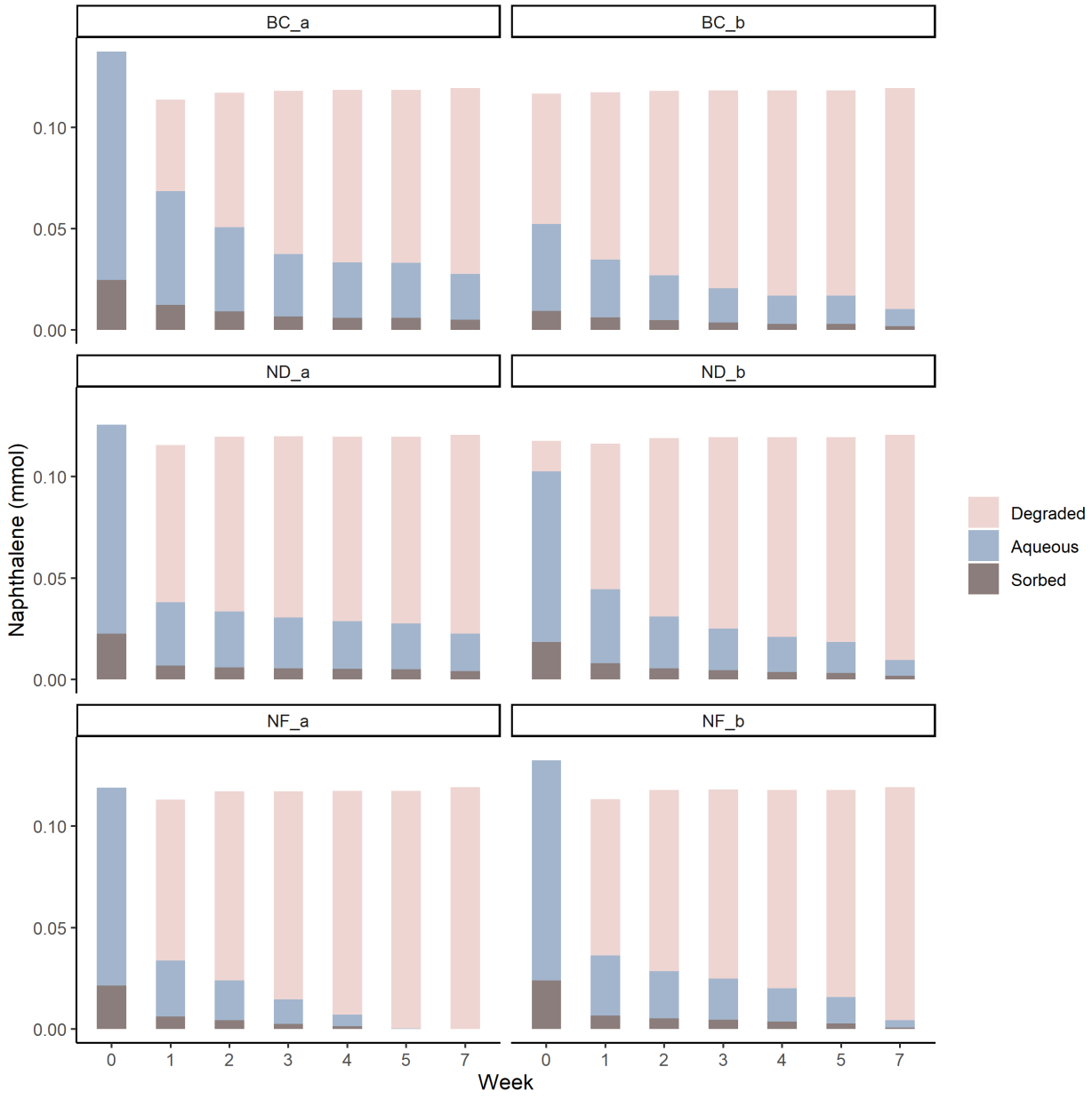

Figure 3.11. Distribution of naphthalene mass in the anode chamber in the different MFC reactors. Aqueous naphthalene corresponds to dissolved naphthalene weekly measurement. The mass sorbed to the carbon cloth anode was determined based on the aqueous concentration and the experimental K_d obtained from the sorption experiment. Degraded naphthalene was determined based on a mass balance and considering diffusion between anode and cathode chambers.

Dissolved naphthalene decreases with time according to our measurements, and therefore so does the amount sorbed to the carbon cloth anode, which was calculated based on the experimentally determined distribution coefficient. After 48 days, most of the naphthalene is

degraded in all experiments, and a small amount stays sorbed. Overall, the naphthalene degradation efficiency is highest in NF reactors, removing 103% and 99% of the initial naphthalene in the anode chamber in NF_a and NF_b respectively. Note that diffusion transfers naphthalene from the cathode to the anode chamber in all experiments (Figure 3.5B), increasing the available naphthalene in the anode chamber. In contrast, in the closed-circuit experiments, the degradation efficiency is lower, achieving 78% and 93% in BC_a and BC_b respectively. This reveals that the presence of ferrous iron in the media decreases the naphthalene removal efficiency of the MFC as constructed.

The removal achieved in the natural degradation control is similar to that of the closed-circuit experiments, with 82 and 94% of the initial naphthalene degraded by the end of the experiment in ND_a and ND_b respectively. This indicates that the MFC as constructed does not provide enhance naphthalene removal.

3.4.2 Electricity, redox reactions, and microbial community

The peak electrical current obtained from our MFC experiments varied between 0.12 and 0.43 mA, similar to that of other published works (Wu et al., 2013; Wei et al., 2013; Lee et al., 2014; Q. Liu et al., 2017; Kumar et al., 2017; Q. Liu et al., 2018; Mancílio et al., 2020). Both the peak current and the total charge transferred through time was lower in the NF reactors without iron compared to BC experiments and NN reactors, where iron was available.

The media in the BC, ND and NN reactors contain relatively small amounts of dissolved ferrous iron (1.8 mM). Because of vivianite precipitation at the beginning of the experiment, the dissolved iron concentration remained low throughout the experiment in all reactors (about 0.04 mM). The fact that the experiments where iron is available show better electrical performance compared to those with no iron suggests iron oxidation plays a role in electricity production in our reactors. Iron oxidation is further supported by the presence of iron reducers and oxidizers in all the experiments where iron was available, furthermore, the iron-reducers *Candidatus Deferrimonas* and *Geothermobacter* are one of the most abundant taxa in BC and NN experiments. Since no evidence of iron oxyhydroxides was found in our reactors and dissolved

iron remained stable throughout the experiment, partial oxidation of vivianite-bound iron is more likely to have occurred.

The observation of elemental sulfur suggests the possibility of abiotic sulfide oxidation with Fe(III) reduction, since elemental sulfur is not formed by sulfate reduction but as an intermediate of sulfide oxidation (Jørgensen et al., 2019). Elemental sulfur is absent in NF reactors, where no iron was available, which supports the idea that elemental sulfur formation occurs via abiotic Fe(III) reduction. It is also possible that vivianite-bound Fe(II) oxidation was slower than the Fe(III) reduction coupled to sulfide oxidation, which can be relatively fast (Jørgensen et al., 2019) . Vivianite oxidation has been shown to progress slowly at room temperature, and tends to stabilize at 50% Fe(III) after 300 days under oxidizing conditions (Rouzies & Millet, 1993).

Since it is possible that iron was oxidized by the anode during the experiment, it is important to analyze the possible effects of both ferrous and ferric iron in the MFC. The effect of ferrous iron on the electrical performance of MFCs is complex. Electrical performance may be enhanced by Fe^{+2} because it acts as a redox site in enzymes catalyzing electron transfer and redox reactions (Z. Lu et al., 2015). Small amounts of ferrous iron (100-200 μM) can facilitate biofilm formation and stimulate the electrochemical activity in MFCs during start-up, but not enhance power output in the long term (Q. Liu et al., 2017). In their experiment, availability of Fe^{+2} resulted in an enrichment of exoelectrogenic bacteria in the anode biofilms. However, Fe^{+2} concentrations higher than 0.9 mM can have a negative effect on the power density in the long-term operation of the MFC (Wei et al., 2013). Our experimental results are in agreement with the findings by Liu et al. (2017); the reactors with small amounts of dissolved iron available show increased electricity generation.

There is evidence that ferric iron enhances electricity generation in MFCs. For example, increased electricity generation by *Shewanella oneidensis* was observed in a lactate-fed MFC when ferric citrate was added to the media (Wu et al., 2013). The mechanism of electricity enhancement in that experiment was related to the ability of *S. oneidensis* to synthesise flavins from the reduction of Fe(III) oxide, and use them as electron shuttles for transferring electrons to the anode. *Shewanella* and *Geothrix* both have been proposed to secrete electron shuttles to

promote Fe(III) reduction (Nevin & Lovley, 2002; Newman & Kolter, 2000), so it is possible that secretion of electron shuttles by iron reducers, such as *Geothrix*, which was found in our experiments, contribute to high electricity generation in BC and NN experiments.

Iron reducers *Candidatus Deferrimonas*, *Geobacter* and *Ferribacterium*, and iron oxidizers, like *Gallionella*, were found in BC experiments, suggesting a cycle of iron oxidation and reduction may be at play in the anode chamber. We hypothesize that ferrous iron was oxidized at the anode possibly generating electricity, and then ferric iron could be used as electron shuttle, enhancing electricity production in a similar fashion to S. oneidensis in the study by Wu et al. (2013). This biotic process would be competing with abiotic iron reduction driven by sulfide oxidation.

BC reactors show an enrichment of *Geothrix* in the anodes compared to the inoculum. These genera were not observed to be enriched in the NF reactors. *Geothrix* are typical of Fe(III) reducing environments; some species, such as *Geothrix fermentans*, can use flavin-based electron shuttles for electrode and FeOOH respiration (Mehta-Kolte & Bond, 2012). High electricity production in BC experiments compared to the NF experiment may be related to secretion of electron shuttles by *Geothrix* species in a similar way that *Shewanella* species has been shown to enhance electricity production (Wu et al., 2013).

The NN experiment also presents both iron-reducers and iron-oxidizers. The iron-reducer *Geothermobacter* is particularly enriched in anode compared to media samples and is one of the taxa that were identified as the most significantly enriches in NN reactors. Other significant taxa include *Thiobacillus* and *Gallionella*. *Thiobacillus* are typically sulfide-oxidizers but there is one species that can also oxidize ferrous iron while depositing elemental sulfur outside the cell (Lens, 2009). And *Gallionella* are typically iron-oxidizers in microaerophilic environments (L. E.-L. Hallbeck & Pedersen, 2015).

The highest electrical performance was obtained in NN experiments, which contained iron but not naphthalene. This high electrical performance might be related to the cyclic oxidation and reduction of sulfur compounds. Although, this cycle may occur in all reactors, NN reactors have the highest abundance of sulfide oxidizers among all experiments. Sulfide oxidizers in NN

reactors include mainly *Thiothrix* and *Thiobacillus*, which are also significantly more abundant in NN experiments than in all other experiments. Sulfur reducers such as *Syntrophobacter*, *Desulfovibrio*, *Desulfobulbus* and *Sulfospirilum*, are also particularly abundant in anode samples from NN experiments, further supporting the idea that sulfur redox cycling may be linked to electricity production. It is possible that with no naphthalene in the media, the environmental conditions favored the reproduction of sulfur reducers and oxidizers in the NN experiment.

Research on the effect of sulfur in MFCs' performance has shown sulfate can be converted to sulfide, which can act as an electron shuttle, and be oxidized to elemental sulfur at the anode, which can be reduced again to sulfide, or oxidized via the anode back to sulfate (Daghio et al., 2016; Kumar et al., 2017; Matturro et al., 2017; Rakoczy et al., 2013). In particular, in a MFC designed for sulfate removal, a pure culture of *Desulfovibrio desulfuricans* was responsible for sulfate reduction to sulfide, which was then chemically oxidized at the anode accompanied by power generation and resulting in elemental sulfur formation in the anode chamber (Zhao et al., 2008). The presence of Desulfovibrio or other sulfur reducers such as *Syntrophobacter*, *Desulfomicrobium* and *Desulfobulbus* in our experiments, together with the presence of elemental sulfur as part of mineral precipitates in the anode chamber suggest a similar mechanism might contribute to electricity production in all our experiments.

The reason the duplicate NN_a produced significantly more electricity than NN_b may be due to the particular syntrophic interactions within the microbial community. For example, the higher abundance of sulfide oxidizer *Thiobacillus* in NN_b compared to NN_a, may contribute to a more rapid sulfur cycling and more electricity production.

3.4.3 Conceptual model of the reactor

The MFC reactors constructed in these experiments form a complex system where several inorganic and biological reactions coexist (Figure 3.12). The microbiological and mineralogical analyses help elucidate their extent and interactions; however, some processes remain unexplored. Here we present a summary of these processes and the extent of our understanding of them.

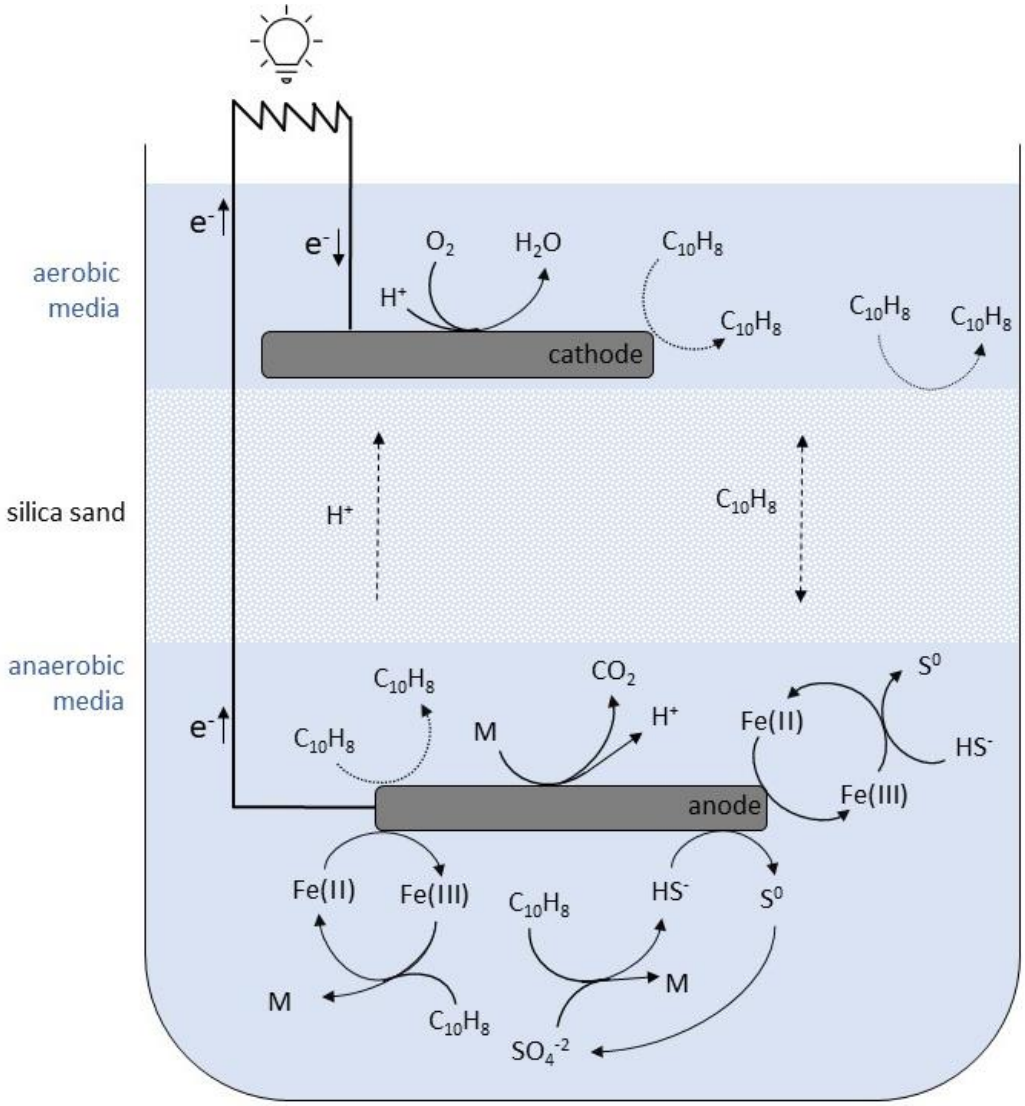

Figure 3.12. Schematic representation of the main processes occurring in the MFC reactors (when iron is available). The solid lines represent biotic and abiotic reactions, the dashed line represents diffusion of naphthalene through the silica sand layer, and the dotted lines represent sorption and desorption of naphthalene to reactor materials. M refers to naphthalene metabolites.

(1) Microbial degradation of naphthalene to carbon dioxide via organic metabolites, with iron oxides or sulfate as electron acceptor:

Naphthalene is likely degraded to intermediate metabolites with iron or sulfate as electron acceptor. The anode is unlikely to act as electron acceptor for the initial steps of naphthalene degradation, since no electricity is observed during the first 11-16 days of the experiments, but

naphthalene concentration decreased further than what can be explained due to sorption and diffusion during the first and second week of the experiment.

Sulfate is a more likely electron acceptor for naphthalene degradation than iron even in the reactors where iron was available because no macroscopic or microscopic evidence of iron oxidation was observed. Anode samples observed under the SEM did not show iron oxides, and the mineral precipitates observed under naked eye in the bottom of the reactors were green or black, and not red. However, iron co-precipitated with phosphate as vivianite could be at least partially oxidized since its color changed from white to green during the experiment. Also, the abundance of iron oxidizers such as *Gallionella* and *Ferrovibrionales,* and iron reducers such as *Geobacter*, *Deferrimonas*, *Geothermobacter* or *Ferribacterium* suggest iron redox reactions may take place at least at a micro-environmental level.

2) Microbial respiration with the anode as electron acceptor:

Electricity generation indicates this process occurs in the reactors, after a lag phase of 11-16 days. This lag phase is an indication of two possible processes: the degradation of naphthalene to intermediate metabolites and the build-up of electroactive bacteria on the electrode (Hedbavna et al., 2016; Logan et al., 2006).

Because no current was produced in the reactors while naphthalene concentration decreased, beyond what is expected due to sorption, during the first 10-14 days of the experiment, it is likely that naphthalene first degrades to intermediate metabolites. Only then these metabolites, rather than naphthalene, are oxidized with the anode as electron acceptor, generating electricity. The oxidation of metabolites rather than the contaminant at the anode has been previously reported in MFCs, for example, phenol was first fermented to acetate, and acetate was the carbon source for electricity generation in MFC experiments by Hedbavna et al. (2016).

Electricity production in the blank experiment where no naphthalene was available (NN reactors) suggests redox cycling of inorganic species likely contributes significantly to electricity production.

(4) Electron transfer from the anode to the cathode via the electrical circuit, generating electricity:

It is clear from the voltage measurements in the closed-circuit experiments that the anode acted as electron acceptor for oxidation reactions in the lower chamber, and the electron transfer occurred via the wire to the cathode in the upper chamber. Reduction of oxygen in the cathode chamber was paired to the oxidation in the anode chamber but was not actively monitored.

(5) Sorption of naphthalene and organic metabolites to the surface of electrodes:

Sorption experiment results indicate that the difference between the naphthalene initially added to the reactors and the first measurement can be reasonably well explained by sorption of naphthalene, mainly to the carbon cloth electrodes, but also to the quartz sand in the cathode chamber.

In the cathode chamber, an average of 25 μmoles are sorbed to the carbon cloth anode, which constitutes 18% of the initial naphthalene available in the anode chamber. The distribution between aqueous and sorbed naphthalene however was dynamic, responding to changes in the aqueous concentration due to naphthalene degradation and to diffusion between the anode and cathode chambers. By the end of the experiments, in average, only 0.1% of the initial naphthalene remained sorbed in the anode chamber, and 0.4% of the initial naphthalene in the cathode chamber.

(6) Diffusion of dissolved species between the anode and cathode chambers:

The difference in the sorption capacity between the materials in the anode and cathode chambers generated concentration gradients that drove naphthalene diffusion towards the cathode chamber initially. However, after a week, the sharp decrease in naphthalene concentration in the anode chamber reversed the gradient, which resulted in some reactors degrading more naphthalene than what was initially available in the anode chamber by the end of the experiment.

(7) Mineral precipitation and dissolution:

Vivianite precipitation occurred in all reactors containing iron. We observed colloidal precipitates after the addition of iron to the reactor media during experiment set-up. Geochemical simulations indicate vivianite supersaturation in the media used, and XRD analysis detected vivianite in the precipitates collected from the anode chamber at the end of the experiments. Vivianite precipitation removed dissolved iron from in the anode chamber; iron dropped from 1.8 mM initially added to 0.3 mM in the first sample, immediately after set-up and was maintained below 10 μM throughout the experimental run. Vivianite dissolution and precipitation kinetics further complicates the iron mass balance in the reactors, since we do not have data about the variation of the mass of vivianite in the reactor through time. It is possible that vivianite was partially oxidized during the course of the experiment, however, its composition is at most 50% Fe(III) (Rouzies & Millet, 1993). At higher values of Fe(III), vivianite shows a different XRD pattern, either amorphous or that of metavivianite (Chiba et al., 2020; Miot et al., 2009).

The presence of elemental sulfur in both BC experiments as well as in ND_b and NN_a but not in NF reactors, where no iron was available suggests abiotic sulfide oxidation with Fe(III) reduction .

3.5 Conclusions

This study presents insights on the effects of the availability of reduced species, such as ferrous iron, over the feasibility of using bio-electrochemical systems for the remediation of reduced contaminants like naphthalene. Increased electricity production was obtained in the reactors were iron was available, compared to the experiments where it was not, both in terms of the total electron flux and the maximum voltage measured. However, in terms degradation efficiency, the experiment with no iron achieved higher removal of naphthalene, compared to the experiment where iron was available. The mechanism by which ferrous iron hinders naphthalene removal in these experiments is not immediately obvious. We hypothesize that the overall oxidation capacity of the anode could be used to oxidize iron instead of the target contaminant.

Additionally, microbial community composition and competing metabolic processes may favor inorganic redox reactions over naphthalene degradation.

In our closed-circuit MFC experiments, iron, sulfate, and naphthalene metabolites were likely involved in electricity production. Therefore, only measuring electricity production is no substitute for direct measurement of contaminant biodegradation if this technology is deployed in the field when there are additional electron donors like ferrous iron present in the aquifer.

Chapter 4: Conclusions and recommendations

This project investigated the mechanisms and controls involved in the bio-electrochemical degradation of naphthalene in an MFC. The principal aim of this research was to test whether a bio-electrical system inoculated with a native microbial community could successfully remediate naphthalene contamination in a reducing environment where iron was potentially an electron donor. Batch bioreactor experiments were constructed and monitored for 49 days, including two experiments where iron and naphthalene were available, two no-iron experiments with naphthalene, two no-naphthalene controls, two natural degradation controls, and two abiotic controls. All experiments except the natural degradation control were closed-circuit experiments, where the electrodes in the reducing and oxidizing zones of the reactor were connected by a conductive wire and a 1 kΩ resistor. The monitoring of the experiments consisted in regular sampling and chemical analysis of water from the anodic compartment and continuous measurement of electrical current across the resistor. Mineralogical analysis of solid precipitates from the anode compartment, and microbiological characterization of the microbial community in anodes and media were performed at the end of the experiments.

A sorption experiment was also developed to properly address the possibility of naphthalene sorption to electrodes and other MFC reactor materials. Distribution coefficients were obtained for: (1) glass, used in the MFC reactor vessels; (2) silica sand, used as permeable separator between the reducing and the oxidizing compartments of the MFC; and (3) carbon cloth, used as electrode material.

4.1 Key findings

The carbon cloth electrodes exhibited the highest sorption per unit mass of all the materials tested. The silica sand used in our MFCs showed a small degree of affinity for naphthalene per unit mass. However, given the large sand mass present in the reactors, sorption of naphthalene by sand was even more significant than sorption by the carbon cloth electrodes in our experimental design. These results highlight the importance of addressing the influence of sorption to the materials used in BES, especially when carbon cloth is used for the electrodes.

This is relevant in the MFC research field, especially when these systems are tested as remediation devices for hydrocarbon contamination, however, hydrocarbon sorption is rarely addressed in scientific reports of such systems.

Sorption of naphthalene to the silica sand used as permeable separator between anode and cathode chamber in our MFC experimental design resulted in marked naphthalene concentration gradient. This gradient drove a diffusive flux in the direction of the anode chamber initially, however, naphthalene degradation in the anode chamber resulted in a shift in the gradient direction during the experimental run. The effects of sorption and the diffusion process had to be accounted for to properly evaluate naphthalene degradation and removal efficiency in the MFCs.

The MFC experiments presented here did not find any advantage in providing an electrical connection between reducing and oxidizing zones of the bioreactors in terms of naphthalene degradation achieved in the system. Both the closed-circuit experiment and the open-circuit natural degradation control achieved similar naphthalene removal efficiency; however, the former did demonstrate the additional benefit of generating a small current.

Electricity was produced in all the closed-circuit experiments but not in the abiotic control. Therefore, the additional electron acceptor provided by the anode in the reducing zone of the bioreactor was indeed utilized by electro-active bacteria to oxidize compounds present in the media. The fact that electricity production started several days after inoculation suggests that there is an adaptation period necessary before bacterial electron transfer begins and/or naphthalene was not utilized directly by exoelectrogenic bacteria, instead it was first degraded to simpler metabolites.

A higher total electricity produced in the experiments where both naphthalene and iron were available compared to the no-iron control suggests that both iron and naphthalene were oxidized at the anode. Interestingly, the highest electricity was generated in one of the reactors where iron but no naphthalene was available. This, added to the occurrence of elemental sulfur and sulfur reducing and oxidizing bacteria, suggests that given an appropriate microbial community composition, sulfur redox reactions are also an important process in the bio-reactors. Moreover,

microbial reduction of inorganic compounds, combined with oxidation of the product of these reactions may fuel electricity production in the MFCs.

The electrical current produced in BES used for remediating hydrocarbon-contaminated soils has been proposed as proxy for monitoring the extent of the remediation (L. Lu, Huggins, et al., 2014; Mao et al., 2016). However, in our MFC experiments naphthalene metabolites, as well as inorganic components such as iron and sulfur were likely involved in electricity production. Our results imply that when additional electron donors like ferrous iron are present in a contaminated aquifer, measuring electricity production in the BES is no substitute for direct measurement of contaminant biodegradation

In terms of naphthalene removal, the highest was achieved in the closed-circuit experiment where no iron was available. Ferrous iron in the media decreases the naphthalene removal efficiency of the MFC as constructed. This indicates that likely part of the oxidation potential of the electrode was used to oxidize inorganic compounds, which is not the target of the BES aiming for hydrocarbon remediation. Possibly, iron is oxidized and reduced in the anode chamber in a cycle powered by iron reducers like *Candidatus Deferrimonas* and *Geothermobacter*, one of the most abundant taxa, and iron oxidizers like *Gallionella and Ferrovibrio*.

As is expected in any laboratory experiment, the microbial community composition in the reactor's final samples was significantly different than the inoculum. The final closed-circuit experiments were enriched in anaerobic iron- and electrode-reducer *Candidatus Deferrimonas* and anaerobic elemental sulfur- and iron-reducer bacteria in the Desulfuromonadia class. Both taxa were enriched in the anodes compared to the media. The base case MFC experiments were also enriched with unclassified genera in the Geobacteraceae family, which includes iron- and electrode-reducing bacteria. In contrast, the inoculum was dominated by uncultured or unclassified genera in alpha- and gammaproteobacteria, as well as the ferric iron reducers *Citrifermantans* and the sulfur oxidizer *Sulfurifustis* (Kojima et al., 2015; Straub & Buchholz-Cleven, 2001; Waite et al., 2020). A shift in the microbial community composition towards genera that were better adapted to the environment provided in the reactors was observed.

The microbial community was also affected by the availability of iron in the bioreactors, the abundance of iron oxidizers in all reactors where iron was available was similar to that of the inoculum. Few iron bacteria were identified in the no-iron control.

Because we used a well buffered media, the effects of both naphthalene degradation and the electrical connection between anode and cathode chambers on the were relatively small. No important changes in pH or alkalinity in the media were observed. However, elemental sulfur precipitation was observed. Elemental sulfur precipitation is a potentially important process, since mineral precipitation could result in the isolation of the electrically conductive anode from the media, hindering the electron transfer between bacteria and the electrode and threatening the long-term performance of the BES.

4.2 Limitations and recommendations

Naphthalene was selected as the model contaminant for this study because it is a relatively simple hydrocarbon, and its biodegradation has been well documented in the scientific literature. Naphthalene is also one of the main contaminants in former industrial sites currently being developed for urban use, like in the Braid Street Site, the field site motivating this study. However, the hydrophobic nature and poor solubility of naphthalene, and its ability to sorb onto some materials added practical challenges to the experiment design and operation.

Iron removal from the aqueous phase due to vivianite precipitation prevented accurately tracking the effects of ferrous iron concentration on naphthalene degradation and electricity production. Vivianite formation was triggered by relatively high phosphate and iron concentrations. Phosphate was used as a pH buffer in the media, following standard procedures, however, using other buffers that do not interact with iron would simplify ferrous iron dynamics in the system.

The iron redox cycle hypothesis presented in this thesis involves the partial oxidation of vivianite-bound ferrous iron, since no evidence of iron oxyhydroxides was found. To confirm this idea, it would be appropriate to accurate measure the oxidation states of iron via X-ray absorption spectroscopy.

We used 16S rRNA gene sequences analysis to determine the taxonomic composition of the microbial community and make broad inferences about potential metabolic functions. Many of the OTUs identified in the inoculum and reactor samples have not yet been cultivated, and limited metabolic information was available. Additionally, we identified taxa only at the genus level; a taxonomic classification at the species and strain levels would provide more detailed information about potential metabolism of the microbial community.

Moreover, a functional gene approach would be more effective than the taxonomic characterization to study more definitively the metabolic functions and interactions within the microbial communities in our reactors. The quantification of key genes such as the ones encoding naphthalene degradation, extracellular electron transfer, and sulfur and iron reduction and oxidation would be particularly important. A metatranscriptomic approach with RNA sequencing would be even better suited to address questions around microbial activity (Shakya et al., 2019).

In this study, sampling was done at the end of the experiments, and so the microbial community composition obtained for anode and media samples is more representative of late stage in the experiment, when electric current production was in decline or completely inexistent. Sampling at different operational stages would allow for a better understanding of microbial community dynamics. Changes liked to electricity production and naphthalene and iron concentration changes are of particular interest. However, because sampling collection is destructive, sampling at different stages would require multiple replicates of the same experiment, and given the variability observed in this study between duplicates of the same experiment, variability among replicates would need to be carefully considered.

A natural next step in this research would be to use the insights from these batch experiments to draw conclusions about practical implications for the remediation of hydrocarbons in high-iron groundwater through geochemical modelling. Some research questions that could be addressed could include: (1) what would be the effect of the *in-situ* application of an up-scaled MFC system over aquifer geochemistry and contaminant transport? And (2) would this be an effective alternative remediation strategy?

References

Abraham, W.-R., Strömpl, C., Meyer, H., Lindholst, S., Moore, E. R. B., Christ, R., Vancanneyt, M., Tindall, B. J., Bennasar, A., Smit, J., & Tesar, M. (1999). Phylogeny and polyphasic taxonomy of Caulobacter species. Proposal of Maricaulis gen. Nov. With Maricaulis maris (Poindexter) comb. Nov. As the type species, and emended description of the genera Brevundimonas and Caulobacter. *International Journal of Systematic and Evolutionary Microbiology*, *49*(3), 1053–1073. https://doi.org/10.1099/00207713-49-3-1053

Adelaja, O., Keshavarz, T., & Kyazze, G. (2014). Enhanced biodegradation of phenanthrene using different inoculum types in a microbial fuel cell. *Engineering in Life Sciences*, *14*(2), 218–228. https://doi.org/10.1002/elsc.201300089

Aggarwal, P. K., Means, J. L., & Hinchee, R. E. (1991). Formulation of nutrient solutions for in situ bioremediation. *In Situ Bioreclamation: Applications and Investigations for Hydrocarbon and Contaminated Site Remediation*, 51–66.

al-Bashir, B., Cseh, T., Leduc, R., & Samson, R. (1990). Effect of soil/contaminant interactions on the biodegradation of naphthalene in flooded soil under denitrifying conditions. *Applied Microbiology and Biotechnology*, *34*(3), 414–419.

Anderson, R. T., & Lovley, D. R. (1999). Naphthalene and Benzene Degradation under Fe(III)-Reducing Conditions in Petroleum-Contaminated Aquifers. *Bioremediation Journal*, *3*(2), 121–135. https://doi.org/10.1080/10889869991219271

Anthony, T. (1998). *An investigation of the natural attenuation of a dissolved creosote and a pentachlorophenol plume*. University of Waterloo, Earth Sciences.

Appelo, C. A. J., & Postma, D. (2004). *Geochemistry, Groundwater and Pollution, Second Edition*. CRC Press.

Apprill, A., McNally, S., Parsons, R., & Weber, L. (2015). Minor revision to V4 region SSU rRNA 806R gene primer greatly increases detection of SAR11 bacterioplankton. *Aquatic Microbial Ecology*, *75*(2), 129–137. https://doi.org/10.3354/ame01753

Aulenta, F., Reale, P., Canosa, A., Rossetti, S., Panero, S., & Majone, M. (2010). Characterization of an electro-active biocathode capable of dechlorinating trichloroethene and cis-dichloroethene to ethene. *Biosensors and Bioelectronics*, *25*(7), 1796–1802. https://doi.org/10.1016/j.bios.2009.12.033

Badalamenti, J. P., Krajmalnik-Brown, R., & Torres, C. I. (2013). Generation of High Current Densities by Pure Cultures of Anode-Respiring Geoalkalibacter spp. Under Alkaline and Saline Conditions in Microbial Electrochemical Cells. *MBio*, *4*(3), e00144-13. https://doi.org/10.1128/mBio.00144-13

Badalamenti, J. P., Summers, Z. M., Chan, C. H., Gralnick, J. A., & Bond, D. R. (2016). Isolation and Genomic Characterization of 'Desulfuromonas soudanensis WTL', a Metal- and Electrode-Respiring Bacterium from Anoxic Deep Subsurface Brine. *Frontiers in Microbiology*, *7*. https://doi.org/10.3389/fmicb.2016.00913

Banerjee, S., Táncsics, A., Tóth, E., Révész, F., Bóka, K., & Kriszt, B. (2019). Hydrogenophaga aromaticivorans sp. Nov., isolated from a para-xylene-degrading enrichment culture, capable of degrading benzene, meta- and para-xylene. *International Journal of Systematic and Evolutionary Microbiology*, *71*(3). https://doi.org/10.1099/ijsem.0.004743

Bernardet, J.-F., Nakagawa, Y., & Holmes, B. (2002). Proposed minimal standards for describing new taxa of the family Flavobacteriaceae and emended description of the family. *International Journal of Systematic and Evolutionary Microbiology*, *52*(3), 1049–1070. https://doi.org/10.1099/00207713-52-3-1049

Bianchin, M., Smith, L., Barker, J. F., & Beckie, R. (2006). Anaerobic degradation of naphthalene in a fluvial aquifer: A radiotracer study. *Journal of Contaminant Hydrology*, *84*(3–4), 178–196. https://doi.org/10.1016/j.jconhyd.2005.12.006

Bieber, C. (2003). *Field sampling and modeling of creosote-derived contamination in a tidally forced aquifer*. University of British Columbia, Earth and Ocean Sciences.

Bond, D. R., Holmes, D. E., Tender, L. M., & Lovley, D. R. (2002). Electrode-Reducing Microorganisms That Harvest Energy from Marine Sediments. *Science*, *295*(5554), 483–485. https://doi.org/10.1126/science.1066771

Bond, D. R., & Lovley, D. R. (2003). Electricity Production by Geobacter sulfurreducens Attached to Electrodes. *Applied and Environmental Microbiology*, *69*(3), 1548–1555. https://doi.org/10.1128/AEM.69.3.1548-1555.2003

Boopathy, R. (2004). Anaerobic biodegradation of no. 2 diesel fuel in soil: A soil column study. *Bioresource Technology*, *94*, 143–151.

Bouchez-Naïtali, M., Rakatozafy, H., Marchal, R., Leveau, J. Y., & Vandecasteele, J. P. (1999). Diversity of bacterial strains degrading hexadecane in relation to the mode of substrate uptake. *Journal of Applied Microbiology*, *86*(3), 421–428. https://doi.org/10.1046/j.1365-2672.1999.00678.x

Cachada, A., Ferreira da Silva, E., Duarte, A. C., & Pereira, R. (2016). Risk assessment of urban soils contamination: The particular case of polycyclic aromatic hydrocarbons. *Science of The Total Environment*, *551–552*, 271–284. https://doi.org/10.1016/j.scitotenv.2016.02.012

Cao, M., Huang, J., Li, J., Qiao, Z., & Wang, G. (2017). Edaphobaculum flavum gen. Nov., sp. Nov., a member of family Chitinophagaceae, isolated from grassland soil. *International Journal of Systematic and Evolutionary Microbiology*, *67*(11), 4475–4481. https://doi.org/10.1099/ijsem.0.002316

Cao, W., Yin, L., Zhang, D., Wang, Y., Yuan, J., Zhu, Y., & Dou, J. (2019). Contamination, Sources, and Health Risks Associated with Soil PAHs in Rebuilt Land from a Coking Plant, Beijing, China. *International Journal of Environmental Research and Public Health*, *16*(4), 670. https://doi.org/10.3390/ijerph16040670

Cerniglia, C. E. (1992). Biodegradation of polycyclic aromatic hydrocarbons. *Biodegradation*, *3*(2–3), 351–368. https://doi.org/10.1007/BF00129093

Chaudhuri, S. K., & Lovley, D. R. (2003). Electricity generation by direct oxidation of glucose in mediatorless microbial fuel cells. *Nature Biotechnology*, *21*(10), 1229–1232. https://doi.org/10.1038/nbt867

Chen, W., Duan, L., & Zhu, D. (2007). Adsorption of Polar and Nonpolar Organic Chemicals to Carbon Nanotubes. *Environmental Science & Technology*, *41*(24), 8295–8300. https://doi.org/10.1021/es071230h

Cheng, S., Dempsey, B. A., & Logan, B. E. (2007). Electricity Generation from Synthetic Acid-Mine Drainage (AMD) Water using Fuel Cell Technologies. *Environmental Science & Technology*, *41*(23), 8149–8153. https://doi.org/10.1021/es0712221

Cheng, S., Liu, H., & Logan, B. E. (2006). Power Densities Using Different Cathode Catalysts (Pt and CoTMPP) and Polymer Binders (Nafion and PTFE) in Single Chamber Microbial Fuel Cells. *Environmental Science & Technology*, *40*(1), 364–369. https://doi.org/10.1021/es0512071

Chiba, K., Takahashi, M., Ohshima, E., Kawamata, T., & Sugiyama, K. (2020). The synthesis of metavivianite and the oxidation sequence of vivianite. *Journal of Mineralogical and Petrological Sciences*, *advpub*. https://doi.org/10.2465/jmps.200417

Chin, K. J., Liesack, W., & Janssen, P. H. (2001). Opitutus terrae gen. Nov., sp. Nov., to accommodate novel strains of the division “Verrucomicrobia” isolated from rice paddy soil. *International Journal of Systematic and Evolutionary Microbiology*, *51*(6), 1965–1968. https://doi.org/10.1099/00207713-51-6-1965

Christensen, N., Batstone, D. J., He, Z., Angelidaki, I., & Schmidt, J. E. (2004). Removal of polycyclic aromatic hydrocarbons (PAHs) from sewage sludge by anaerobic degradation. *Water Science and Technology*, *50*(9), 237–244.

Clauwaert, P., Rabaey, K., Aelterman, P., De Schamphelaire, L., Pham, T. H., Boeckx, P., Boon, N., & Verstraete, W. (2007). Biological Denitrification in Microbial Fuel Cells. *Environmental Science & Technology*, *41*(9), 3354–3360. https://doi.org/10.1021/es062580r

Corteselli, E. M., Aitken, M. D., & Singleton, D. R. (2017). Description of Immundisolibacter cernigliae gen. Nov., sp. Nov., a high-molecular-weight polycyclic aromatic hydrocarbon-degrading bacterium within the class Gammaproteobacteria, and proposal of Immundisolibacterales ord. Nov. And Immundisolibacteraceae fam. Nov. *International Journal of Systematic and Evolutionary Microbiology*, *67*(4), 925–931. https://doi.org/10.1099/ijsem.0.001714

Daghio, M., Vaiopoulou, E., Aulenta, F., Sherry, A., Head, I., Franzetti, A., & Rabaey, K. (2018). Anode potential selection for sulfide removal in contaminated marine sediments. *Journal of Hazardous Materials*, *360*, 498–503. https://doi.org/10.1016/j.jhazmat.2018.08.016

Daghio, M., Vaiopoulou, E., Patil, S. A., Suárez-Suárez, A., Head, I. M., Franzetti, A., & Rabaey, K. (2016). Anodes Stimulate Anaerobic Toluene Degradation via Sulfur Cycling in Marine Sediments. *Applied and Environmental Microbiology*, *82*(1), 297–307. https://doi.org/10.1128/AEM.02250-15

Dahal, R. H., & Kim, J. (2018). Ferrovibrio soli sp. Nov., a novel cellulolytic bacterium isolated from stream bank soil. *International Journal of Systematic and Evolutionary Microbiology*, *68*(1), 427–431. https://doi.org/10.1099/ijsem.0.002527

Daniel, G., Kosmala, T., Brombin, F., Mazzucato, M., Facchin, A., Dalconi, M. C., Badocco, D., Pastore, P., Granozzi, G., & Durante, C. (2021). Highly Graphitized Fe-N-C Electrocatalysts Prepared from Chitosan Hydrogel Frameworks. *Catalysts*, *11*(3), 390. https://doi.org/10.3390/catal11030390

Das, S. (2014). *Microbial Biodegradation and Bioremediation*. Elsevier. http://ebookcentral.proquest.com/lib/ubc/detail.action?docID=1741074

Delle Site, A. (2001). Factors Affecting Sorption of Organic Compounds in Natural Sorbent/Water systems and Sorption Coefficients for Selected Pollutants. A Review. *Journal Of Physical And Chemical Reference Data*, *30*(1).

Doronina, N. V., Trotsenko, Y. A., Krausova, V. I., Boulygina, E. S., & Tourova, T. P. (1998). Methylopila capsulata gen. Nov., sp. Nov., a novel non-pigmented aerobic facultatively methylotrophic bacterium. *International Journal of Systematic Bacteriology*, *48 Pt 4*, 1313–1321. https://doi.org/10.1099/00207713-48-4-1313

Dou, J., Liu, X., & Ding, A. (2009). Anaerobic degradation of naphthalene by the mixed bacteria under nitrate reducing conditions. *Journal of Hazardous Materials*, *165*(1–3), 325–331. https://doi.org/10.1016/j.jhazmat.2008.10.002

Edgar, R. C., Haas, B. J., Clemente, J. C., Quince, C., & Knight, R. (2011). UCHIME improves sensitivity and speed of chimera detection. *Bioinformatics (Oxford, England)*, *27*(16), 2194–2200. https://doi.org/10.1093/bioinformatics/btr381

Ewing, T., Ha, P. T., Babauta, J. T., Tang, N. T., Heo, D., & Beyenal, H. (2014). Scale-up of sediment microbial fuel cells. *Journal of Power Sources*, *272*, 311–319. https://doi.org/10.1016/j.jpowsour.2014.08.070

Fahy, A., Ball, A. S., Lethbridge, G., Timmis, K. N., & McGenity, T. J. (2008). Isolation of alkali-tolerant benzene-degrading bacteria from a contaminated aquifer. *Letters in Applied Microbiology*, *47*(1), 60–66. https://doi.org/10.1111/j.1472-765X.2008.02386.x

Famiglietti, J. S. (2014). The global groundwater crisis. *Nature Climate Change*, *4*(11), 945–948. https://doi.org/10.1038/nclimate2425

Fukunaga, Y., Kurahashi, M., Sakiyama, Y., Ohuchi, M., Yokota, A., & Harayama, S. (2009). Phycisphaera mikurensis gen. Nov., sp. Nov., isolated from a marine alga, and proposal

of Phycisphaeraceae fam. Nov., Phycisphaerales ord. Nov. And Phycisphaerae classis nov. In the phylum Planctomycetes. *The Journal of General and Applied Microbiology*, *55*(4), 267–275. https://doi.org/10.2323/jgam.55.267

Garrity, G., Brenner, D. J., Krieg, N. R., & Staley, J. R. (2005). *Bergey's Manual® of Systematic Bacteriology: Volume 2: the Proteobacteria, Part B: the Gammaproteobacteria*. Springer. http://ebookcentral.proquest.com/lib/ubc/detail.action?docID=603682

Garrity, G., Schleifer, K.-H., Staley, J. T., Brenner, D. J., Krieg, N. R., Boone, D. R., De Vos, P., Goodfellow, M., Rainey, F. A., & Garrity, G. M. (2005). *Bergey's Manual® of Systematic Bacteriology: Volume Two: the Proteobacteria (Part C)*. Springer. http://ebookcentral.proquest.com/lib/ubc/detail.action?docID=302700

Ghasemi, M., Shahgaldi, S., Ismail, M., Kim, B. H., Yaakob, Z., & Wan Daud, W. R. (2011). Activated carbon nanofibers as an alternative cathode catalyst to platinum in a two-chamber microbial fuel cell. *International Journal of Hydrogen Energy*, *36*(21), 13746–13752. https://doi.org/10.1016/j.ijhydene.2011.07.118

Golder Associates Limited. (1997). *Environmental site assessment report, 25 Braid Street Wood Preserving Facility, Coquitlam, British Columbia*. *962–1877*.

Greene, A. C. (2014). The Family Desulfuromonadaceae. In E. Rosenberg, E. F. DeLong, S. Lory, E. Stackebrandt, & F. Thompson (Eds.), *The Prokaryotes: Deltaproteobacteria and Epsilonproteobacteria* (pp. 143–155). Springer. https://doi.org/10.1007/978-3-642-39044-9_380

Grishchenkov, V. G., Townsend, R. T., McDonald, T. J., Autenrieth, R. L., Bonner, J. S., & Boronin, A. M. (2000). Degradation of petroleum hydrocarbons by facultative anaerobic bacteria under aerobic and anaerobic conditions. *Process Biochemistry*, *35*(9), 889–896. https://doi.org/10.1016/S0032-9592(99)00145-4

Hallbeck, L. E.-L., & Pedersen, K. (2015). Gallionella. *Bergey's Manual of Systematics of Archaea and Bacteria*, 1–10.

Hallbeck, L., Sthl, F., & Pedersen, K. (1993). Phytogeny and phenotypic characterization of the stalk-forming and iron-oxidizing bacterium Gallionella ferruginea. *Microbiology*, *139*(7), 1531–1535. https://doi.org/10.1099/00221287-139-7-1531

Haritash, A. K., & Kaushik, C. P. (2009). Biodegradation aspects of Polycyclic Aromatic Hydrocarbons (PAHs): A review. *Journal of Hazardous Materials*, *169*(1–3), 1–15. https://doi.org/10.1016/j.jhazmat.2009.03.137

Hasan, K., Reddy, K. V. R., Eßmann, V., Górecki, K., Conghaile, P. Ó., Schuhmann, W., Leech, D., Hägerhäll, C., & Gorton, L. (2015). Electrochemical Communication Between Electrodes and Rhodobacter capsulatus Grown in Different Metabolic Modes. *Electroanalysis*, *27*(1), 118–127. https://doi.org/10.1002/elan.201400456

Hedbavna, P., Rolfe, S. A., Huang, W. E., & Thornton, S. F. (2016). Biodegradation of phenolic compounds and their metabolites in contaminated groundwater using microbial fuel cells. *Bioresource Technology*, *200*, 426–434. https://doi.org/10.1016/j.biortech.2015.09.092

Hess, S., Suthaus, A., & Melkonian, M. (2016). "Candidatus Finniella" (Rickettsiales, Alphaproteobacteria), Novel Endosymbionts of Viridiraptorid Amoeboflagellates (Cercozoa, Rhizaria). *Applied and Environmental Microbiology*, *82*(2), 659–670. https://doi.org/10.1128/AEM.02680-15

Higashioka, Y., Kojima, H., Watanabe, M., & Fukui, M. (2013). Desulfatitalea tepidiphila gen. Nov., sp. Nov., a sulfate-reducing bacterium isolated from tidal flat sediment. *International Journal of Systematic and Evolutionary Microbiology*, *63*(Pt_2), 761–765. https://doi.org/10.1099/ijs.0.043356-0

Hirsch, P., & Müller, M. (1985). Planctomyces limnophilus sp. Nov., a Stalked and Budding Bacterium from Freshwater. *Systematic and Applied Microbiology*, *6*(3), 276–280. https://doi.org/10.1016/S0723-2020(85)80031-X

Hördt, A., López, M. G., Meier-Kolthoff, J. P., Schleuning, M., Weinhold, L.-M., Tindall, B. J., Gronow, S., Kyrpides, N. C., Woyke, T., & Göker, M. (2020). Analysis of 1,000+ Type-

Strain Genomes Substantially Improves Taxonomic Classification of Alphaproteobacteria. *Frontiers in Microbiology*, *11*. https://doi.org/10.3389/fmicb.2020.00468

Howard, P. H. (2017). *Handbook of Environmental Degradation Rates*. CRC Press. https://doi.org/10.1201/9780203719329

Hua, T., Li, S., Li, F., Ondon, B. S., Liu, Y., & Wang, H. (2019). Degradation performance and microbial community analysis of microbial electrolysis cells for erythromycin wastewater treatment. *Biochemical Engineering Journal*, *146*, 1–9. https://doi.org/10.1016/j.bej.2019.02.008

Huang, X.-F., Liu, Y. J., Dong, J.-D., Qu, L.-Y., Zhang, Y.-Y., Wang, F.-Z., Tian, X.-P., & Zhang, S. (2014). Mangrovibacterium diazotrophicum gen. Nov., sp. Nov., a nitrogen-fixing bacterium isolated from a mangrove sediment, and proposal of Prolixibacteraceae fam. Nov. *International Journal of Systematic and Evolutionary Microbiology*, *64*(Pt 3), 875–881. https://doi.org/10.1099/ijs.0.052779-0

Iino, T., Mori, K., Uchino, Y., Nakagawa, T., Harayama, S., & Suzuki, K. (2010). Ignavibacterium album gen. Nov., sp. Nov., a moderately thermophilic anaerobic bacterium isolated from microbial mats at a terrestrial hot spring and proposal of Ignavibacteria classis nov., for a novel lineage at the periphery of green sulfur bacteria. *International Journal of Systematic and Evolutionary Microbiology*, *60*(6), 1376–1382. https://doi.org/10.1099/ijs.0.012484-0

Iino, T., Sakamoto, M., & Ohkuma, M. (2015). Prolixibacter denitrificans sp. Nov., an iron-corroding, facultatively aerobic, nitrate-reducing bacterium isolated from crude oil, and emended descriptions of the genus Prolixibacter and Prolixibacter bellariivorans. *International Journal of Systematic and Evolutionary Microbiology*, *65*(Pt_9), 2865–2869. https://doi.org/10.1099/ijs.0.000343

Ite, A. E., & Semple, K. T. (2012). Biodegradation of petroleum hydrocarbons in contaminated soil. In A. Rajesh (Ed.), *Microbial biotechnology: Energy and environment* (pp. 250–278). CABI. http://www.cabi.org/cabebooks/ebook/20123375154

Janssen, P. H., Schuhmann, A., Bak, F., & Liesack, W. (1996). Disproportionation of inorganic sulfur compounds by the sulfate-reducing bacterium Desulfocapsa thiozymogenes gen. Nov., sp. Nov. *Archives of Microbiology*, *166*(3), 184–192. https://doi.org/10.1007/s002030050374

Jia, K. (2015). *Iron and manganese reduction driven by organic matter and mixing of fresh and saline groundwater in the Fraser River delta aquifer, Vancouver, Canada* [Master's Thesis]. University of British Columbia.

Jørgensen, B. B., Findlay, A. J., & Pellerin, A. (2019). The Biogeochemical Sulfur Cycle of Marine Sediments. *Frontiers in Microbiology*, *10*. https://doi.org/10.3389/fmicb.2019.00849

Kashefi, K., Holmes, D. E., Baross, J. A., & Lovley, D. R. (2003). Thermophily in the Geobacteraceae: Geothermobacter ehrlichii gen. nov., sp. nov., a Novel Thermophilic Member of the Geobacteraceae from the "Bag City" Hydrothermal Vent. *Applied and Environmental Microbiology*, *69*(5), 2985–2993. https://doi.org/10.1128/AEM.69.5.2985-2993.2003

Kimura, Z., & Okabe, S. (2013). Hydrogenophaga electricum sp. Nov., isolated from anodic biofilms of an acetate-fed microbial fuel cell. *The Journal of General and Applied Microbiology*, *59*(4), 261–266. https://doi.org/10.2323/jgam.59.261

Kleemann, R., & Meckenstock, R. U. (2011). Anaerobic naphthalene degradation by Gram-positive, iron-reducing bacteria. *FEMS Microbiology Ecology*, *78*(3), 488–496. https://doi.org/10.1111/j.1574-6941.2011.01193.x

Kojima, H., Shinohara, A., & Fukui, M. (2015). Sulfurifustis variabilis gen. Nov., sp. Nov., a sulfur oxidizer isolated from a lake, and proposal of Acidiferrobacteraceae fam. Nov.

And Acidiferrobacterales ord. Nov. *International Journal of Systematic and Evolutionary Microbiology*, *65*(10), 3709–3713. https://doi.org/10.1099/ijsem.0.000479

Konikow, L. F., & Kendy, E. (2005). Groundwater depletion: A global problem. *Hydrogeology Journal*, *13*(1), 317–320. https://doi.org/10.1007/s10040-004-0411-8

Kuever, J. (2014). The Family Desulfovibrionaceae. In E. Rosenberg, E. F. DeLong, S. Lory, E. Stackebrandt, & F. Thompson (Eds.), *The Prokaryotes: Deltaproteobacteria and Epsilonproteobacteria* (pp. 107–133). Springer. https://doi.org/10.1007/978-3-642-39044-9_272

Kumar, S. S., Malyan, S. K., Basu, S., & Bishnoi, N. R. (2017). Syntrophic association and performance of Clostridium, Desulfovibrio, Aeromonas and Tetrathiobacter as anodic biocatalysts for bioelectricity generation in dual chamber microbial fuel cell. *Environmental Science and Pollution Research*, *24*(19), 16019–16030. https://doi.org/10.1007/s11356-017-9112-4

Langwaldt, J. H., & Puhakka, J. A. (2000). On-site biological remediation of contaminated groundwater: A review. *Environmental Pollution*, *107*(2), 187–197. https://doi.org/10.1016/S0269-7491(99)00137-2

Lee, D.-J., Liu, X., & Weng, H.-L. (2014). Sulfate and organic carbon removal by microbial fuel cell with sulfate-reducing bacteria and sulfide-oxidising bacteria anodic biofilm. *Bioresource Technology*, *156*, 14–19. https://doi.org/10.1016/j.biortech.2013.12.129

Lens, P. (2009). Sulfur Cycle. In M. Schaechter (Ed.), *Encyclopedia of Microbiology (Third Edition)* (pp. 361–369). Academic Press. https://doi.org/10.1016/B978-012373944-5.00057-2

Lesser, L. E. (2000). *Laboratory and field evidence of anaerobic biodegradation of naphthalene*. University of Waterloo, Earth Sciences.

Li, W.-W., & Yu, H.-Q. (2015). Electro-assisted groundwater bioremediation: Fundamentals, challenges and future perspectives. *Bioresource Technology*, 677–684.

Liu, Q., Liu, B., Li, W., Zhao, X., Zuo, W., & Xing, D. (2017). Impact of Ferrous Iron on Microbial Community of the Biofilm in Microbial Fuel Cells. *Frontiers in Microbiology*, *8*. https://doi.org/10.3389/fmicb.2017.00920

Liu, Q., Yang, Y., Mei, X., Liu, B., Chen, C., & Xing, D. (2018). Response of the microbial community structure of biofilms to ferric iron in microbial fuel cells. *Science of The Total Environment*, *631–632*, 695–701. https://doi.org/10.1016/j.scitotenv.2018.03.008

Liu, S.-H., Lai, C.-Y., Ye, J.-W., & Lin, C.-W. (2018). Increasing removal of benzene from groundwater using stacked tubular air-cathode microbial fuel cells. *Journal of Cleaner Production*, *194*, 78–84. https://doi.org/10.1016/j.jclepro.2018.05.138

Logan, B. E., Hamelers, B., Rozendal, R., Schröder, U., Keller, J., Freguia, S., Aelterman, P., Verstraete, W., & Rabaey, K. (2006). Microbial Fuel Cells: Methodology and Technology†. *Environmental Science & Technology*, *40*(17), 5181–5192. https://doi.org/10.1021/es0605016

Louca, S., Parfrey, L. W., & Doebeli, M. (2016). Decoupling function and taxonomy in the global ocean microbiome. *Science*, *353*(6305), 1272–1277. https://doi.org/10.1126/science.aaf4507

Lowy, D. A., Tender, L. M., Zeikus, J. G., Park, D. H., & Lovley, D. R. (2006). Harvesting energy from the marine sediment–water interface II: Kinetic activity of anode materials. *Biosensors and Bioelectronics*, *21*(11), 2058–2063. https://doi.org/10.1016/j.bios.2006.01.033

Lu, L., Huggins, T., Jin, S., Zuo, Y., & Ren, Z. J. (2014). Microbial Metabolism and Community Structure in Response to Bioelectrochemically Enhanced Remediation of Petroleum Hydrocarbon-Contaminated Soil. *Environmental Science & Technology*. https://doi.org/10.1021/es4057906

Lu, L., Yazdi, H., Jin, S., Zuo, Y., Fallgren, P. H., & Ren, Z. J. (2014). Enhanced bioremediation of hydrocarbon-contaminated soil using pilot-scale bioelectrochemical systems. *Journal of Hazardous Materials*, *274*, 8–15. https://doi.org/10.1016/j.jhazmat.2014.03.060

Lu, X., Zhang, T., Han-Ping Fang, H., Leung, K. M. Y., & Zhang, G. (2011). Biodegradation of naphthalene by enriched marine denitrifying bacteria. *International Biodeterioration & Biodegradation*, *65*(1), 204–211. https://doi.org/10.1016/j.ibiod.2010.11.004

Lu, Z., Chang, D., Ma, J., Huang, G., Cai, L., & Zhang, L. (2015). Behavior of metal ions in bioelectrochemical systems: A review. *Journal of Power Sources*, *275*, 243–260. https://doi.org/10.1016/j.jpowsour.2014.10.168

Majone, M., Verdini, R., Aulenta, F., Rossetti, S., Tandoi, V., Kalogerakis, N., Agathos, S., Puig, S., Zanaroli, G., & Fava, F. (2015). In situ groundwater and sediment bioremediation: Barriers and perspectives at European contaminated sites. *New Biotechnology*, *32*(1), 133–146. https://doi.org/10.1016/j.nbt.2014.02.011

Mancílio, L. B. K., Ribeiro, G. A., Lopes, E. M., Kishi, L. T., Martins-Santana, L., de Siqueira, G. M. V., Andrade, A. R., Guazzaroni, M.-E., & Reginatto, V. (2020). Unusual microbial community and impact of iron and sulfate on microbial fuel cell ecology and performance. *Current Research in Biotechnology*, *2*, 64–73. https://doi.org/10.1016/j.crbiot.2020.04.001

Mao, D., Lu, L., Revil, A., Zuo, Y., Hinton, J., & Ren, Z. J. (2016). Geophysical Monitoring of Hydrocarbon-Contaminated Soils Remediated with a Bioelectrochemical System. *Environmental Science & Technology*. https://doi.org/10.1021/acs.est.6b00535

Marsili, E., Baron, D. B., Shikhare, I. D., Coursolle, D., Gralnick, J. A., & Bond, D. R. (2008). Shewanella secretes flavins that mediate extracellular electron transfer. *Proceedings of the National Academy of Sciences*, *105*(10), 3968–3973. https://doi.org/10.1073/pnas.0710525105

Martins, G., Peixoto, L., Ribeiro, D. C., Parpot, P., Brito, A. G., & Nogueira, R. (2010). Towards implementation of a benthic microbial fuel cell in lake Furnas (Azores): Phylogenetic affiliation and electrochemical activity of sediment bacteria. *Bioelectrochemistry*, *78*(1), 67–71. https://doi.org/10.1016/j.bioelechem.2009.07.003

Matturro, B., Cruz Viggi, C., Aulenta, F., & Rossetti, S. (2017). Cable Bacteria and the Bioelectrochemical Snorkel: The Natural and Engineered Facets Playing a Role in Hydrocarbons Degradation in Marine Sediments. *Frontiers in Microbiology*, *8*. https://doi.org/10.3389/fmicb.2017.00952

McNally, D. L., Mihelcic, J. R., & Lueking, D. R. (1998). Biodegradation of Three- and Four-Ring Polycyclic Aromatic Hydrocarbons under Aerobic and Denitrifying Conditions. *Environ. Sci. Technol.*, *32*, 2633–2639.

Meckenstock, R. U., Annweiler, E., Michaelis, W., Richnow, H. H., & Schink, B. (2000). Anaerobic Naphthalene Degradation by a Sulfate-Reducing Enrichment Culture. *Applied and Environmental Microbiology*, *66*(7), 2743–2747. https://doi.org/10.1128/AEM.66.7.2743-2747.2000

Mehta-Kolte, M. G., & Bond, D. R. (2012). Geothrix fermentans Secretes Two Different Redox-Active Compounds To Utilize Electron Acceptors across a Wide Range of Redox Potentials. *Applied and Environmental Microbiology*, *78*(19), 6987–6995. https://doi.org/10.1128/AEM.01460-12

Mihelcic, J. R., & Luthy, R. G. (1988). Microbial-Degradation Of Acenaphthene And Naphthalene Under Denitrification Conditions In Soil-Water Systems. *Applied And Environmental Microbiology*, *54*(5), 1188–1198.

Min, B., Cheng, S., & Logan, B. E. (2005). Electricity generation using membrane and salt bridge microbial fuel cells. *Water Research*, *39*(9), 1675–1686. https://doi.org/10.1016/j.watres.2005.02.002

Miot, J., Benzerara, K., Morin, G., Bernard, S., Beyssac, O., Larquet, E., Kappler, A., & Guyot, F. (2009). Transformation of vivianite by anaerobic nitrate-reducing iron-oxidizing bacteria. *Geobiology*, *7*(3), 373–384. https://doi.org/10.1111/j.1472-4669.2009.00203.x

Mittal, M., & Rockne, K. J. (2008). Indole production by Pseudomonas stutzeri strain NAP-3 during anaerobic naphthalene biodegradation in the presence of dimethyl formamide. *Journal of Environmental Science and Health. Part A, Toxic/Hazardous Substances & Environmental Engineering*, *43*(9), 1027–1034. https://doi.org/10.1080/10934520802059896

Mohan, S. V., & Chandrasekhar, K. (2011). Self-induced bio-potential and graphite electron accepting conditions enhances petroleum sludge degradation in bio-electrochemical system with simultaneous power generation. *Bioresource Technology*, *102*(20), 9532–9541. https://doi.org/10.1016/j.biortech.2011.07.038

Morotomi, M., Nagai, F., & Watanabe, Y. (2012). Description of Christensenella minuta gen. Nov., sp. Nov., isolated from human faeces, which forms a distinct branch in the order Clostridiales, and proposal of Christensenellaceae fam. Nov. *International Journal of Systematic and Evolutionary Microbiology*, *62*(1), 144–149. https://doi.org/10.1099/ijs.0.026989-0

Morris, J. M., & Jin, S. (2007). Feasibility of using microbial fuel cell technology for bioremediation of hydrocarbons in groundwater. *Journal of Environmental Science and Health, Part A*, *43*(1), 18–23. https://doi.org/10.1080/10934520701750389

Morris, J. M., & Jin, S. (2012). Enhanced biodegradation of hydrocarbon-contaminated sediments using microbial fuel cells. *Journal of Hazardous Materials*, *213–214*, 474–477. https://doi.org/10.1016/j.jhazmat.2012.02.029

Morris, J. M., Jin, S., Crimi, B., & Pruden, A. (2009). Microbial fuel cell in enhancing anaerobic biodegradation of diesel. *Chemical Engineering Journal*, *146*(2), 161–167. https://doi.org/10.1016/j.cej.2008.05.028

Mu, Y., Rabaey, K., Rozendal, R. A., Yuan, Z., & Keller, J. (2009). Decolorization of Azo Dyes in Bioelectrochemical Systems. *Environmental Science & Technology*, *43*(13), 5137–5143. https://doi.org/10.1021/es900057f

Mueller, J. G., Chapman, P. J., & Pritchard, P. H. (1989). Creosote-contaminated sites. Their potential for bioremediation. *Environmental Science & Technology*, *23*(10), 1197–1201. https://doi.org/10.1021/es00068a003

Nevin, K. P., & Lovley, D. R. (2002). Mechanisms for Accessing Insoluble Fe(III) Oxide during Dissimilatory Fe(III) Reduction by Geothrix fermentans. *Applied and Environmental Microbiology*, *68*(5), 2294–2299. https://doi.org/10.1128/AEM.68.5.2294-2299.2002

Newman, D. K., & Kolter, R. (2000). A role for excreted quinones in extracellular electron transfer. *Nature*, *405*(6782). https://doi.org/10.1038/35011098

Nguyen, V. K., Park, Y., Yu, J., & Lee, T. (2016). Simultaneous arsenite oxidation and nitrate reduction at the electrodes of bioelectrochemical systems. *Environmental Science and Pollution Research*, 1–11. https://doi.org/10.1007/s11356-016-7225-9

Nicholson, A. C., Gulvik, C. A., Whitney, A. M., Humrighouse, B. W., Bell, M. E., Holmes, B., Steigerwalt, A. G., Villarma, A., Sheth, M., Batra, D., Rowe, L. A., Burroughs, M., Pryor, J. C., Bernardet, J.-F., Hugo, C., Kämpfer, P., Newman, J. D., & McQuiston, J. R. (2020). Division of the genus Chryseobacterium: Observation of discontinuities in amino acid identity values, a possible consequence of major extinction events, guides transfer of nine species to the genus Epilithonimonas, eleven species to the genus Kaistella, and three species to the genus Halpernia gen. nov., with description of Kaistella daneshvariae sp. nov. and Epilithonimonas vandammei sp. nov. derived from clinical specimens. *International Journal of Systematic and Evolutionary Microbiology*, *70*(8), 4432–4450. https://doi.org/10.1099/ijsem.0.003935

Oren, A. (2014). The Family Rhodocyclaceae. In E. Rosenberg, E. F. DeLong, S. Lory, E. Stackebrandt, & F. Thompson (Eds.), *The Prokaryotes: Alphaproteobacteria and*

Betaproteobacteria (pp. 975–998). Springer. https://doi.org/10.1007/978-3-642-30197-1_292

Ormerod, K. L., Wood, D. L. A., Lachner, N., Gellatly, S. L., Daly, J. N., Parsons, J. D., Dal'Molin, C. G. O., Palfreyman, R. W., Nielsen, L. K., Cooper, M. A., Morrison, M., Hansbro, P. M., & Hugenholtz, P. (2016). Genomic characterization of the uncultured Bacteroidales family S24-7 inhabiting the guts of homeothermic animals. *Microbiome*, *4*(1), 36. https://doi.org/10.1186/s40168-016-0181-2

Pagnier, I., Raoult, D., & La Scola, B. (2011). Isolation and characterization of Reyranella massiliensis gen. Nov., sp. Nov. From freshwater samples by using an amoeba co-culture procedure. *International Journal of Systematic and Evolutionary Microbiology*, *61*(9), 2151–2154. https://doi.org/10.1099/ijs.0.025775-0

Pant, D., Singh, A., Bogaert, G. V., Olsen, S. I., Nigam, P. S., Diels, L., & Vanbroekhoven, K. (2012). Bioelectrochemical systems (BES) for sustainable energy production and product recovery from organic wastes and industrial wastewaters. *RSC Advances*, *2*(4), 1248–1263. https://doi.org/10.1039/C1RA00839K

Parada, A. E., Needham, D. M., & Fuhrman, J. A. (2016). Every base matters: Assessing small subunit rRNA primers for marine microbiomes with mock communities, time series and global field samples. *Environmental Microbiology*, *18*(5), 1403–1414. https://doi.org/10.1111/1462-2920.13023

Peng, X., Yu, H., Wang, X., Zhou, Q., Zhang, S., Geng, L., Sun, J., & Cai, Z. (2012). Enhanced performance and capacitance behavior of anode by rolling Fe3O4 into activated carbon in microbial fuel cells. *Bioresource Technology*, *121*, 450–453. https://doi.org/10.1016/j.biortech.2012.06.021

Pérez-Rodríguez, I., Choi, J. K., Abuyen, K., Tyler, M., Ronkowski, C., Romero, E., Trujillo, A., Tremblay, J., Viney, I., Savalia, P., & Amend, J. P. (2021). Geothermobacter hydrogeniphilus sp. Nov., a mesophilic, iron(III)-reducing bacterium from

seafloor/subseafloor environments in the Pacific Ocean, and emended description of the genus Geothermobacter. *International Journal of Systematic and Evolutionary Microbiology*, *71*(4). https://doi.org/10.1099/ijsem.0.004739

Podosokorskaya, O. A., Kadnikov, V. V., Gavrilov, S. N., Mardanov, A. V., Merkel, A. Y., Karnachuk, O. V., Ravin, N. V., Bonch-Osmolovskaya, E. A., & Kublanov, I. V. (2013). Characterization of Melioribacter roseus gen. Nov., sp. Nov., a novel facultatively anaerobic thermophilic cellulolytic bacterium from the class Ignavibacteria, and a proposal of a novel bacterial phylum Ignavibacteriae. *Environmental Microbiology*, *15*(6), 1759–1771. https://doi.org/10.1111/1462-2920.12067

Qian, Y., Posch, T., & Schmidt, T. C. (2011). Sorption of polycyclic aromatic hydrocarbons (PAHs) on glass surfaces. *Chemosphere*, *82*(6), 859–865. https://doi.org/10.1016/j.chemosphere.2010.11.002

Rabaey, K., Boon, N., Siciliano, S. D., Verhaege, M., & Verstraete, W. (2004). Biofuel Cells Select for Microbial Consortia That Self-Mediate Electron Transfer. *Applied and Environmental Microbiology*, *70*(9), 5373–5382. https://doi.org/10.1128/AEM.70.9.5373-5382.2004

Rakoczy, J., Feisthauer, S., Wasmund, K., Bombach, P., Neu, T. R., Vogt, C., & Richnow, H. H. (2013). Benzene and sulfide removal from groundwater treated in a microbial fuel cell. *Biotechnology and Bioengineering*, *110*(12), 3104–3113. https://doi.org/10.1002/bit.24979

Reguera, G., & Kashefi, K. (2019). Chapter One—The electrifying physiology of Geobacter bacteria, 30 years on. In R. K. Poole (Ed.), *Advances in Microbial Physiology* (Vol. 74, pp. 1–96). Academic Press. https://doi.org/10.1016/bs.ampbs.2019.02.007

Robertson, W. J., Bowman, J. P., Franzmann, P. D., & Mee, B. J. (2001). Desulfosporosinus meridiei sp. Nov., a spore-forming sulfate-reducing bacterium isolated from gasolene-

contaminated groundwater. *International Journal of Systematic and Evolutionary Microbiology*, *51*(1), 133–140. https://doi.org/10.1099/00207713-51-1-133

Robinson, S. L., Novak, J. T., Widdowson, M. A., & Elliot, M. (2001). Microbial degradation of PAHs under various redox conditions at a creosote-contaminated site. *6th International In Situ and On-Site Bioremediation Symposium*, 1–8.

Rodrigo, J., Boltes, K., & Esteve-Nuñez, A. (2014). Microbial-electrochemical bioremediation and detoxification of dibenzothiophene-polluted soil. *Chemosphere*, *101*, 61–65. https://doi.org/10.1016/j.chemosphere.2013.11.060

Röling, W. F. M. (2014). The Family Geobacteraceae. In E. Rosenberg, E. F. DeLong, S. Lory, E. Stackebrandt, & F. Thompson (Eds.), *The Prokaryotes: Deltaproteobacteria and Epsilonproteobacteria* (pp. 157–172). Springer. https://doi.org/10.1007/978-3-642-39044-9_381

Rosario-Passapera, R., Keddis, R., Wong, R., Lutz, R. A., Starovoytov, V., & Vetriani, C. (2012). Parvibaculum hydrocarboniclasticum sp. Nov., a mesophilic, alkane-oxidizing alphaproteobacterium isolated from a deep-sea hydrothermal vent on the East Pacific Rise. *International Journal of Systematic and Evolutionary Microbiology*, *62*(Pt_12), 2921–2926. https://doi.org/10.1099/ijs.0.039594-0

Rossi, R., & Logan, B. E. (2021). Using an anion exchange membrane for effective hydroxide ion transport enables high power densities in microbial fuel cells. *Chemical Engineering Journal*, *422*, 130150. https://doi.org/10.1016/j.cej.2021.130150

Rossi, R., Wang, X., & Logan, B. E. (2020). High performance flow through microbial fuel cells with anion exchange membrane. *Journal of Power Sources*, *475*, 228633. https://doi.org/10.1016/j.jpowsour.2020.228633

Rothermich, M. M., Hayes, L. A., & Lovley, D. R. (2002). Anaerobic, sulfate-dependent degradation of polycyclic aromatic hydrocarbons in petroleum-contaminated harbor

sediment. *Environmental Science & Technology*, *36*(22), 4811–4817. https://doi.org/10.1021/es0200241

Rounds, S. A. (2012). *Alkalinity and Acid Neutralizing Capacity (version 6): USGS Water-Quality Information.* https://water.usgs.gov/owq/FieldManual/Chapter6/section6.6/

Rouzies, D., & Millet, J. M. M. (1993). Mössbauer study of synthetic oxidized vivianite at room temperature. *Hyperfine Interactions*, *77*(1), 19–28. https://doi.org/10.1007/BF02320295

Ryckelynck, N., Stecher, H. A., & Reimers, C. E. (2005). Understanding the Anodic Mechanism of a Seafloor Fuel Cell: Interactions between Geochemistry and Microbial Activity. *Biogeochemistry*, *76*(1), 113–139.

Sajana, T. K., Ghangrekar, M. M., & Mitra, A. (2016). In Situ Bioremediation Using Sediment Microbial Fuel Cell. *Journal of Hazardous, Toxic, and Radioactive Waste*. https://doi.org/10.1061/(ASCE)HZ.2153-5515.0000339

Santoro, C., Arbizzani, C., Erable, B., & Ieropoulos, I. (2017). Microbial fuel cells: From fundamentals to applications. A review. *Journal of Power Sources*, *356*, 225–244. https://doi.org/10.1016/j.jpowsour.2017.03.109

Schleheck, D., Tindall, B. J., Rosselló-Mora, R., & Cook, A. M. (2004). Parvibaculum lavamentivorans gen. Nov., sp. Nov., a novel heterotroph that initiates catabolism of linear alkylbenzenesulfonate. *International Journal of Systematic and Evolutionary Microbiology*, *54*(5), 1489–1497. https://doi.org/10.1099/ijs.0.03020-0

Schloss, P. D., Gevers, D., & Westcott, S. L. (2011). Reducing the Effects of PCR Amplification and Sequencing Artifacts on 16S rRNA-Based Studies. *PLOS ONE*, *6*(12), e27310. https://doi.org/10.1371/journal.pone.0027310

Schloss, P. D., Westcott, S. L., Ryabin, T., Hall, J. R., Hartmann, M., Hollister, E. B., Lesniewski, R. A., Oakley, B. B., Parks, D. H., Robinson, C. J., Sahl, J. W., Stres, B., Thallinger, G. G., Horn, D. J. V., & Weber, C. F. (2009). Introducing mothur: Open-

Source, Platform-Independent, Community-Supported Software for Describing and Comparing Microbial Communities. *Applied and Environmental Microbiology*, *75*(23), 7537–7541. https://doi.org/10.1128/AEM.01541-09

Scow, K. M., & Hicks, K. A. (2005). Natural attenuation and enhanced bioremediation of organic contaminants in groundwater. *Current Opinion in Biotechnology*, *16*(3), 246–253. https://doi.org/10.1016/j.copbio.2005.03.009

Segata, N., Izard, J., Waldron, L., Gevers, D., Miropolsky, L., Garrett, W. S., & Huttenhower, C. (2011). Metagenomic biomarker discovery and explanation. *Genome Biology*, *12*(6), R60. https://doi.org/10.1186/gb-2011-12-6-r60

Segers, P., Vacanneyt, M., Pot, B., Torck, U., Hoste, B., Dewetinck, D., Falsen, E., Kersters, K., & De Vos, P. (1994). Classification of Pseudomonas diminuta Leifson and Hugh 1954 and Pseudomonas vesicularis Büsing, Döll, and Freytag 1953 in Brevundimonas gen. Nov. As Brevundimonas diminuta comb. Nov. And Brevundimonas vesicularis comb. Nov., Respectively. *International Journal of Systematic and Evolutionary Microbiology*, *44*(3), 499–510. https://doi.org/10.1099/00207713-44-3-499

Seo, J.-S., Keum, Y.-S., & Li, Q. X. (2009). Bacterial Degradation of Aromatic Compounds. *International Journal of Environmental Research and Public Health*, *6*(1), 278–309. https://doi.org/10.3390/ijerph6010278

Shakya, M., Lo, C.-C., & Chain, P. S. G. (2019). Advances and Challenges in Metatranscriptomic Analysis. *Frontiers in Genetics*, *0*. https://doi.org/10.3389/fgene.2019.00904

Shi, B., Ngueleu, S. K., Rezanezhad, F., Slowinski, S., Pronk, G. J., Smeaton, C. M., Stevenson, K., Al-Raoush, R. I., & Van Cappellen, P. (2020). Sorption and Desorption of the Model Aromatic Hydrocarbons Naphthalene and Benzene: Effects of Temperature and Soil Composition. *Frontiers in Environmental Chemistry*, *0*. https://doi.org/10.3389/fenvc.2020.581103

Siddiqi, M. Z., Sok, W., Choi, G., Kim, S. Y., Wee, J.-H., & Im, W. T. (2020). Simplicispira hankyongi sp. Nov., a novel denitrifying bacterium isolated from sludge. *Antonie van Leeuwenhoek*, *113*(3), 331–338. https://doi.org/10.1007/s10482-019-01341-0

Song, T.-S., Yan, Z.-S., Zhao, Z.-W., & Jiang, H.-L. (2011). Construction and operation of freshwater sediment microbial fuel cell for electricity generation. *Bioprocess and Biosystems Engineering*, *34*(5), 621–627. https://doi.org/10.1007/s00449-010-0511-x

Sorokin, D. Yu., Tourova, T. P., Mußmann, M., & Muyzer, G. (2008). Dethiobacter alkaliphilus gen. nov. sp. nov., and Desulfurivibrio alkaliphilus gen. nov. sp. nov.: Two novel representatives of reductive sulfur cycle from soda lakes. *Extremophiles*, *12*(3), 431–439. https://doi.org/10.1007/s00792-008-0148-8

Sorokina, A. Y., Chernousova, E. Y., & Dubinina, G. A. (2012). Ferrovibrio denitrificans gen. Nov., sp. Nov., a novel neutrophilic facultative anaerobic Fe(II)-oxidizing bacterium. *FEMS Microbiology Letters*, *335*(1), 19–25. https://doi.org/10.1111/j.1574-6968.2012.02631.x

Stackebrandt, E., Schumann, P., Schüler, E., & Hippe, H. (2003). Reclassification of Desulfotomaculum auripigmentum as Desulfosporosinus auripigmenti corrig., comb. Nov. *International Journal of Systematic and Evolutionary Microbiology*, *53*(5), 1439–1443. https://doi.org/10.1099/ijs.0.02526-0

Straub, K. L., & Buchholz-Cleven, B. E. (2001). Geobacter bremensis sp. Nov. And Geobacter pelophilus sp. Nov., two dissimilatory ferric-iron-reducing bacteria. *International Journal of Systematic and Evolutionary Microbiology*, *51*(5), 1805–1808. https://doi.org/10.1099/00207713-51-5-1805

Stroo, H. F., Leeson, A., & Ward, C. H. (Eds.). (2013). *Bioaugmentation for Groundwater Remediation*. Springer New York. http://link.springer.com/10.1007/978-1-4614-4115-1

Strycharz, S. M., Woodard, T. L., Johnson, J. P., Nevin, K. P., Sanford, R. A., Löffler, F. E., & Lovley, D. R. (2008). Graphite Electrode as a Sole Electron Donor for Reductive

Dechlorination of Tetrachlorethene by Geobacter lovleyi. *Applied and Environmental Microbiology*, *74*(19), 5943–5947. https://doi.org/10.1128/AEM.00961-08

Sturman, P. J., Stewart, P. S., Cunningham, A. B., Bouwer, E. J., & Wolfram, J. H. (1995). Engineering scale-up of in situ bioremediation processes: A review. *Journal of Contaminant Hydrology*, *19*(3), 171–203. https://doi.org/10.1016/0169-7722(95)00017-P

Tegtmeier, D., Belitz, A., Radek, R., Heimerl, T., & Brune, A. (2018). Ereboglobus luteus gen. nov. sp. nov. from cockroach guts, and new insights into the oxygen relationship of the genera Opitutus and Didymococcus (Verrucomicrobia: Opitutaceae). *Systematic and Applied Microbiology*, *41*(2), 101–112. https://doi.org/10.1016/j.syapm.2017.10.005

Tender, L. M., Reimers, C. E., Stecher, H. A., Holmes, D. E., Bond, D. R., Lowy, D. A., Pilobello, K., Fertig, S. J., & Lovley, D. R. (2002). Harnessing microbially generated power on the seafloor. *Nature Biotechnology*, *20*(8), 821–825. https://doi.org/10.1038/nbt716

Thierrin, J., Davis, G. B., & Barber, C. (1995). A Ground-Water Tracer Test with Deuterated Compounds for Monitoring In Situ Biodegradation and Retardation of Aromatic Hydrocarbons. *Ground Water*, *33*(3), 469–475. https://doi.org/10.1111/j.1745-6584.1995.tb00303.x

Tian, T., & Yu, H.-Q. (2020). Iron-assisted biological wastewater treatment: Synergistic effect between iron and microbes. *Biotechnology Advances*, *44*, 107610. https://doi.org/10.1016/j.biotechadv.2020.107610

Tirandaz, H., Dastgheib, S. M. M., Amoozegar, M. A., Shavandi, M., de la Haba, R. R., & Ventosa, A. (2015). Pseudorhodoplanes sinuspersici gen. Nov., sp. Nov., isolated from oil-contaminated soil. *International Journal of Systematic and Evolutionary Microbiology*, *65*(Pt_12), 4743–4748. https://doi.org/10.1099/ijsem.0.000643

Ueki, A., Akasaka, H., Suzuki, D., & Ueki, K. (2006). Paludibacter propionicigenes gen. Nov., sp. Nov., a novel strictly anaerobic, Gram-negative, propionate-producing bacterium

isolated from plant residue in irrigated rice-field soil in Japan. *International Journal of Systematic and Evolutionary Microbiology*, *56*(1), 39–44. https://doi.org/10.1099/ijs.0.63896-0

US EPA. (2020). *Superfund Remedy Report, 16-th edition* (EPA-542-R-20-001). United States Environmental Protection Agency. https://www.epa.gov/sites/default/files/2020-07/documents/100002509.pdf

Vandamme, P., Bernardet, J.-F., Segers, P., Kersters, K., & Holmes, B. (1994). NOTES: New Perspectives in the Classification of the Flavobacteria: Description of Chryseobacterium gen. nov., Bergeyella gen. nov., and Empedobacter nom. rev. *International Journal of Systematic and Evolutionary Microbiology*, *44*(4), 827–831. https://doi.org/10.1099/00207713-44-4-827

Venkataraman, A., Rosenbaum, M., Arends, J. B. A., Halitschke, R., & Angenent, L. T. (2010). Quorum sensing regulates electric current generation of Pseudomonas aeruginosa PA14 in bioelectrochemical systems. *Electrochemistry Communications*, *12*(3), 459–462. https://doi.org/10.1016/j.elecom.2010.01.019

Waite, D. W., Chuvochina, M., Pelikan, C., Parks, D. H., Yilmaz, P., Wagner, M., Loy, A., Naganuma, T., Nakai, R., Whitman, W. B., Hahn, M. W., Kuever, J., & Hugenholtz, P. (2020). Proposal to reclassify the proteobacterial classes Deltaproteobacteria and Oligoflexia, and the phylum Thermodesulfobacteria into four phyla reflecting major functional capabilities. *International Journal of Systematic and Evolutionary Microbiology*, *70*(11), 5972–6016. https://doi.org/10.1099/ijsem.0.004213

Wang, H., Luo, H., Fallgren, P. H., Jin, S., & Ren, Z. J. (2015). Bioelectrochemical system platform for sustainable environmental remediation and energy generation. *Biotechnology Advances*, *33*(3–4), 317–334. https://doi.org/10.1016/j.biotechadv.2015.04.003

Wang, H., Park, J.-D., & Ren, Z. J. (2015). Practical Energy Harvesting for Microbial Fuel Cells: A Review. *Environmental Science & Technology*, *49*(6), 3267–3277. https://doi.org/10.1021/es5047765

Wang, Q., & Riley, T. V. (2015). Chapter 47—Erysipelothrix rhusiopathiae. In Y.-W. Tang, M. Sussman, D. Liu, I. Poxton, & J. Schwartzman (Eds.), *Molecular Medical Microbiology (Second Edition)* (pp. 859–872). Academic Press. https://doi.org/10.1016/B978-0-12-397169-2.00047-0

Wang, X., Cai, Z., Zhou, Q., Zhang, Z., & Chen, C. (2012). Bioelectrochemical stimulation of petroleum hydrocarbon degradation in saline soil using U-tube microbial fuel cells. *Biotechnology and Bioengineering*, *109*(2), 426–433. https://doi.org/10.1002/bit.23351

Wei, L., Han, H., & Shen, J. (2013). Effects of temperature and ferrous sulfate concentrations on the performance of microbial fuel cell. *International Journal of Hydrogen Energy*, *38*(25), 11110–11116. https://doi.org/10.1016/j.ijhydene.2013.01.019

Westcott, S. L., & Schloss, P. D. (2017). OptiClust, an Improved Method for Assigning Amplicon-Based Sequence Data to Operational Taxonomic Units. *MSphere*, *2*(2). https://doi.org/10.1128/mSphereDirect.00073-17

WHO. (2021). *Urban redevelopment of contaminated sites: A review of scientific evidence and practical knowledge on environmental and health issues (2021)* (WHO/EURO:2021-2187-41942-57585). WHO Regional Office for Europe. https://www.euro.who.int/en/health-topics/environment-and-health/urban-health/publications/2021/urban-redevelopment-of-contaminated-sites-a-review-of-scientific-evidence-and-practical-knowledge-on-environmental-and-health-issues-2021

Widdel, F., & Bak, F. (1992). Gram-Negative Mesophilic Sulfate-Reducing Bacteria. In A. Balows, H. G. Trüper, M. Dworkin, W. Harder, & K.-H. Schleifer (Eds.), *The Prokaryotes: A Handbook on the Biology of Bacteria: Ecophysiology, Isolation,*

Identification, Applications (pp. 3352–3378). Springer New York. https://doi.org/10.1007/978-1-4757-2191-1_21

Willems, A., De Ley, J., Gillis, M., & Kersters, K. (1991). NOTES: Comamonadaceae, a New Family Encompassing the Acidovorans rRNA Complex, Including Variovorax paradoxus gen. nov., comb. nov., for Alcaligenes paradoxus (Davis 1969). *International Journal of Systematic and Evolutionary Microbiology*, *41*(3), 445–450. https://doi.org/10.1099/00207713-41-3-445

Wolfson, S. J., Porter, A. W., Kerkhof, L. J., McGuinness, L. M., Prince, R. C., & Young, L. Y. (2018). Sulfate-Reducing Naphthalene Degraders Are Picky Eaters. *Microorganisms*, *6*(3), 59. https://doi.org/10.3390/microorganisms6030059

Wu, D., Xing, D., Lu, L., Wei, M., Liu, B., & Ren, N. (2013). Ferric iron enhances electricity generation by Shewanella oneidensis MR-1 in MFCs. *Bioresource Technology*, *135*, 630–634. https://doi.org/10.1016/j.biortech.2012.09.106

WWAP. (2016). *The United Nations World Water Development Report 2016: Water and Jobs*. United Nations World Water Assessment Programme. http://unesdoc.unesco.org/images/0024/002439/243938e.pdf

Yan Li, Y. W. (2015). Self-sustained reduction of multiple metals in a microbial fuel cell–microbial electrolysis cell hybrid system. *Bioresource Technology*, *192*. https://doi.org/10.1016/j.biortech.2015.05.030

Yan, Z., Song, N., Cai, H., Tay, J.-H., & Jiang, H. (2012). Enhanced degradation of phenanthrene and pyrene in freshwater sediments by combined employment of sediment microbial fuel cell and amorphous ferric hydroxide. *Journal of Hazardous Materials*, *199–200*, 217–225. https://doi.org/10.1016/j.jhazmat.2011.10.087

Yang, W., Wang, X., Son, M., & Logan, B. E. (2020). Simultaneously enhancing power density and coulombic efficiency with a hydrophobic Fe–N4/activated carbon air cathode for

microbial fuel cells. *Journal of Power Sources*, *465*, 228264. https://doi.org/10.1016/j.jpowsour.2020.228264

Yang, Y., Kong, G., Chen, X., Lian, Y., Liu, W., & Xu, M. (2017). Electricity Generation by Shewanella decolorationis S12 without Cytochrome c. *Frontiers in Microbiology*, *8*. https://doi.org/10.3389/fmicb.2017.01115

Zawierucha, I., & Malina, G. (2006). Bioaugmentation as a method of biodegradation enhancement in oil hydrocarbons contaminated soil. *Ecohydrology & Hydrobiology*, *6*(1–4), 163–169. https://doi.org/10.1016/S1642-3593(06)70138-0

Zhang, H., Zhu, D., Song, T., Ouyang, P., & Xie, J. (2015). Effects of the presence of sheet iron in freshwater sediment on the performance of a sediment microbial fuel cell. *International Journal of Hydrogen Energy*, *40*(46), 16566–16571. https://doi.org/10.1016/j.ijhydene.2015.09.045

Zhang, T., Gannon, S. M., Nevin, K. P., Franks, A. E., & Lovley, D. R. (2010). Stimulating the anaerobic degradation of aromatic hydrocarbons in contaminated sediments by providing an electrode as the electron acceptor. *Environmental Microbiology*, *12*(4), 1011–1020. https://doi.org/10.1111/j.1462-2920.2009.02145.x

Zhang, X., & Young, L. Y. (1997). Carboxylation as an initial reaction in the anaerobic metabolism of naphthalene and phenanthrene by sulfidogenic consortia. *Applied and Environmental Microbiology*, *63*(12), 4759–4764.

Zhao, F., Rahunen, N., Varcoe, J. R., Chandra, A., Avignone-Rossa, C., Thumser, A. E., & Slade, R. C. T. (2008). Activated Carbon Cloth as Anode for Sulfate Removal in a Microbial Fuel Cell. *Environmental Science & Technology*, *42*(13), 4971–4976. https://doi.org/10.1021/es8003766

Zhou, Y.-L., Yang, Y., Chen, M., Zhao, Z.-W., & Jiang, H.-L. (2014). To improve the performance of sediment microbial fuel cell through amending colloidal iron

oxyhydroxide into freshwater sediments. *Bioresource Technology*, *159*, 232–239. https://doi.org/10.1016/j.biortech.2014.02.082

Appendices

Appendix A – **MFC Supplementary Information**

Appendix A includes all supplementary information from Chapter 3.

A.1 SEM data

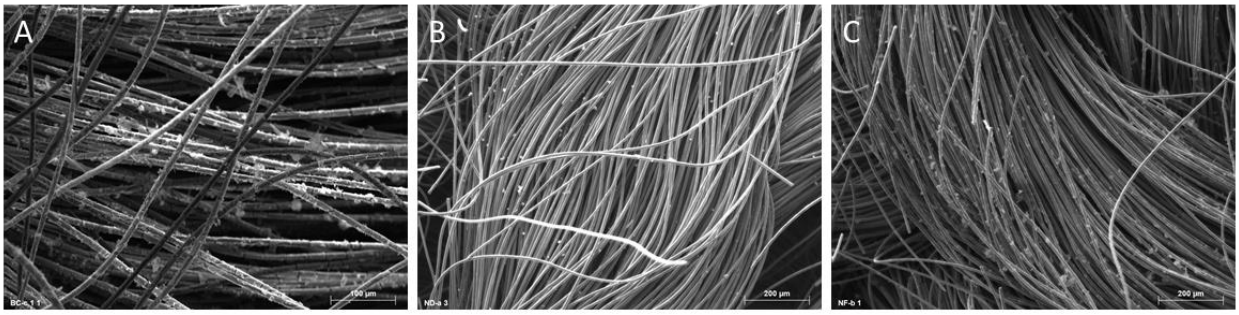

Figure A.1.1. SEM images of anode samples collected at the end of the experiments. (A) BC anode, (B) ND anode, and (C) NF anode. Mineral precipitates are present in all anodes. EDX analysis indicates mineral precipitates are mainly composed of P, Fe and Ca

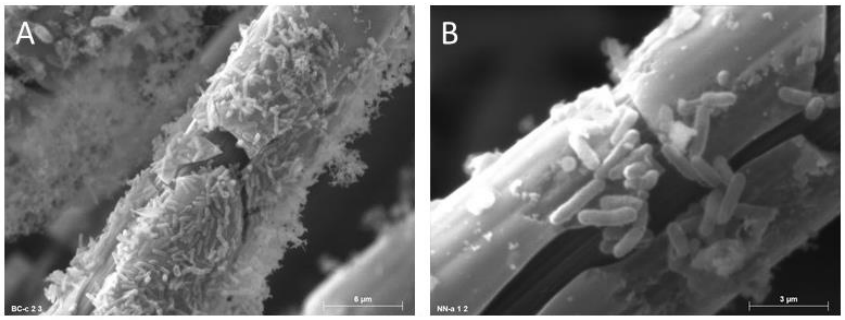

Figure A.1.2. SEM images showing bacteria attached to carbon cloth anode filaments. (A) BC_b anode, (B) NN_a anode

Table A.1.1. Normalized elemental mass (%) from SEM-EDX analysis of anode samples collected at the end of experiments. Spectrum denotes reactor IDs.

Spectrum	C	O	Na	Mg	Al	Si	P	S	Cl	K	Ca	Ti	Fe	Pd
BC-a 1 17	19.31	41.02	0.75	0.84	0.00	0.00	6.47	0.00	0.00	0.00	2.31	0.00	29.29	0.00
BC-a 1 18	15.08	43.69	3.05	1.35	0.00	0.00	6.07	0.00	0.00	0.00	3.42	0.00	27.34	0.00
BC-a 1 19	0.00	51.14	0.00	1.01	0.00	0.00	9.39	0.00	0.00	0.92	4.59	0.00	32.95	0.00
BC-a 1 16	12.54	38.67	1.35	0.95	0.00	0.00	7.07	0.00	0.00	0.00	2.85	0.00	36.57	0.00
BC-a 1 15	67.70	32.30	0.00	0.00	0.00	0.00	0.00	0.00	0.00	0.00	0.00	0.00	0.00	0.00
BC-a 1 13	67.47	21.51	0.00	0.00	0.00	0.00	2.13	0.00	0.00	0.00	0.00	0.00	8.89	0.00
BC-a 1 14.	37.16	28.97	0.00	0.00	0.82	4.67	5.08	0.00	0.00	0.00	2.61	0.00	20.68	0.00
BC-a 1 12.	16.72	43.62	1.23	0.00	0.00	0.00	6.93	0.00	0.00	0.51	2.90	0.00	28.08	0.00
BC-a 2 31	11.01	31.66	0.00	1.69	0.00	0.00	10.02	0.00	0.00	0.00	1.13	0.00	44.49	0.00
BC-a 2 30	19.53	41.57	0.40	0.47	0.00	0.00	7.17	0.00	0.00	0.83	2.63	0.00	27.40	0.00
BC-a 2 29	21.74	43.29	1.04	0.86	0.00	0.00	6.55	0.00	0.00	0.00	2.10	0.00	24.43	0.00
BC-a 2 28	23.70	41.34	0.49	0.00	0.00	0.00	6.94	0.00	0.00	0.81	2.58	0.00	24.15	0.00
BC-b 1 22	39.30	39.03	0.50	0.00	0.00	0.00	3.71	0.00	0.00	0.00	1.81	0.00	15.66	0.00
BC-b 1 23	24.50	28.75	0.85	1.13	0.00	0.00	8.19	0.00	0.00	0.00	3.60	0.00	32.97	0.00
BC-b 1 21	24.40	43.50	1.31	0.54	0.00	0.00	6.35	0.00	0.00	0.00	2.80	0.00	21.09	0.00
BC-b 1 20	25.69	39.61	1.18	0.83	0.53	0.00	6.50	0.00	0.00	0.67	2.36	0.00	22.62	0.00
BC-b 2 27	35.41	37.68	0.00	0.00	0.00	0.00	3.77	0.00	0.00	0.59	1.34	0.00	21.21	0.00
BC-b 2 26	15.76	45.25	1.47	1.02	0.00	0.00	7.36	0.00	0.00	0.00	1.36	0.00	27.77	0.00
BC-b 2 25	22.54	26.92	1.54	1.17	0.00	0.00	7.66	0.00	0.00	0.00	3.11	0.00	37.06	0.00
BC-b 2 24	20.82	40.18	1.29	0.64	0.00	0.00	5.94	0.00	0.00	0.00	3.10	0.00	28.03	0.00
NN-a 1 6	16.32	8.48	0.00	0.00	0.00	0.00	2.00	0.00	0.00	0.00	43.72	0.00	29.48	0.00
NN-a 1 5	90.40	9.60	0.00	0.00	0.00	0.00	0.00	0.00	0.00	0.00	0.00	0.00	0.00	0.00
NN-a 1 4	51.72	32.80	0.00	0.00	0.00	0.00	2.34	0.00	0.00	0.00	0.82	0.00	12.32	0.00
NN-a 1 3	13.26	41.96	1.21	1.33	0.00	0.00	8.66	0.00	0.00	0.93	3.31	0.00	29.36	0.00
NN-a 1 2	15.30	32.53	1.12	0.97	0.00	0.00	9.84	0.00	0.00	1.40	3.97	0.00	34.86	0.00
NN-a 1 1	10.87	39.17	1.44	0.97	0.00	0.00	8.57	0.00	0.00	1.41	4.07	0.00	33.52	0.00
NN-b 1 9	14.30	45.69	1.67	0.94	0.00	0.00	7.14	0.00	0.00	1.04	3.68	0.00	25.54	0.00

Spectrum	C	O	Na	Mg	Al	Si	P	S	Cl	K	Ca	Ti	Fe	Pd
NN-b 1 11	100.00	0.00	0.00	0.00	0.00	0.00	0.00	0.00	0.00	0.00	0.00	0.00	0.00	0.00
NN-b 1 10	26.80	41.83	0.89	0.52	0.00	0.00	4.91	0.00	0.00	0.92	3.52	0.00	20.60	0.00
NN-b 2 34	20.66	45.31	1.05	0.74	0.00	0.00	6.03	0.00	0.00	0.84	2.46	0.00	22.92	0.00
NN-b 2 33	13.77	47.70	2.18	0.56	0.00	0.00	8.26	0.00	0.00	0.47	0.73	0.00	26.33	0.00
NN-b 2 32	8.86	43.43	2.47	0.70	0.00	0.00	10.61	0.00	0.00	0.33	1.31	0.00	32.29	0.00
ND-b 1	38.41	35.72	0.00	0.62	0.00	0.00	5.53	0.00	0.00	0.00	0.21	0.00	19.51	0.00
ND-b 2	31.01	40.35	0.00	0.78	0.00	0.00	6.73	0.00	0.00	0.00	0.22	0.00	20.91	0.00
ND-b 3	26.11	9.15	0.00	1.09	0.00	0.00	14.01	0.00	0.00	0.00	0.00	0.00	49.65	0.00
ND-b 4	36.94	41.16	0.00	0.57	0.00	0.00	5.18	0.00	0.00	0.00	0.25	0.00	15.89	0.00
ND-b 5	30.16	44.50	0.00	0.62	0.00	0.00	6.37	0.00	0.00	0.00	0.25	0.00	18.10	0.00
ND-b 6	39.26	38.90	0.00	0.52	0.00	0.00	5.41	0.00	0.00	0.00	0.00	0.00	15.91	0.00
ND-b 7	47.78	32.66	0.00	0.62	0.00	0.00	4.37	0.00	0.00	0.00	0.19	0.00	14.38	0.00
NF-b 10	54.62	29.26	0.86	0.68	1.04	2.47	2.72	0.00	0.00	0.57	1.97	0.00	5.81	0.00
NF-b 11	18.11	44.58	1.24	0.90	4.36	7.26	4.30	0.00	0.21	2.88	4.18	0.00	10.33	1.65
NF-b 12	31.63	30.65	0.77	1.00	3.45	5.86	4.35	0.00	0.00	2.06	4.75	0.89	14.59	0.00
NF-b 13	75.75	5.06	0.00	0.00	0.36	0.59	0.00	1.89	0.00	0.00	0.00	0.00	0.99	0.00
NF-b 14	55.32	29.54	0.98	0.47	1.41	2.84	1.86	0.00	0.00	0.57	1.79	0.00	5.21	0.00
NF-b 15	34.84	37.63	1.30	1.19	2.39	4.46	2.71	0.00	0.00	1.16	3.25	0.00	10.19	0.88
NF-b 16	17.66	26.24	0.89	1.25	5.07	15.90	6.17	0.21	0.00	2.25	5.87	0.00	17.41	1.07
NF-b 17	34.85	38.28	0.91	0.54	2.12	3.10	2.59	0.00	0.00	1.50	3.99	0.00	9.10	2.02
NF-b 18	30.50	37.60	1.04	1.03	2.28	4.70	3.14	0.00	0.00	1.50	3.65	0.00	12.57	1.09
NF-b 19	31.01	33.65	1.18	0.80	7.56	3.76	4.29	0.00	0.00	1.25	3.84	0.00	10.99	0.44
NF-b 20	0.00	40.43	2.20	1.09	11.16	12.44	3.97	0.00	0.00	2.72	5.22	0.00	17.19	2.42
NF-b 8	51.70	23.49	0.51	0.72	1.36	2.62	3.36	0.00	0.00	1.50	3.28	0.00	11.47	0
NF-b 9	52.70	11.64	0.00	0.00	0.32	2.17	0.00	3.52	0.51	0.00	0.00	0.00	0.00	0

A.2 XRD data – diffractograms

Figure A.2.1. X-ray diffractogram of sample BC_a

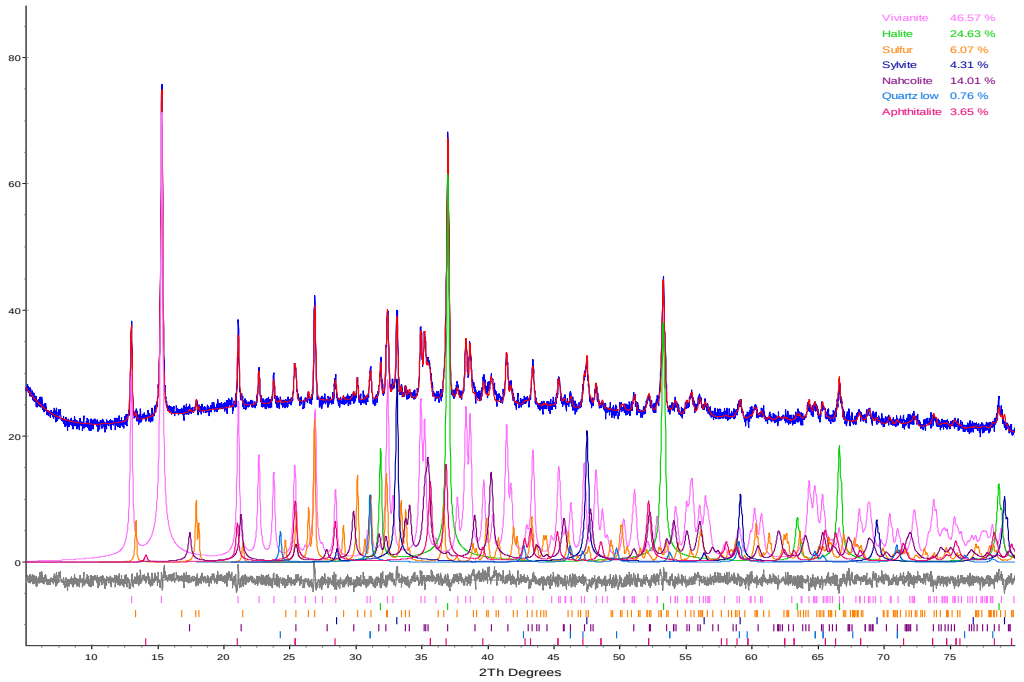

Figure A.2.2. X-ray diffractogram of sample BC_b

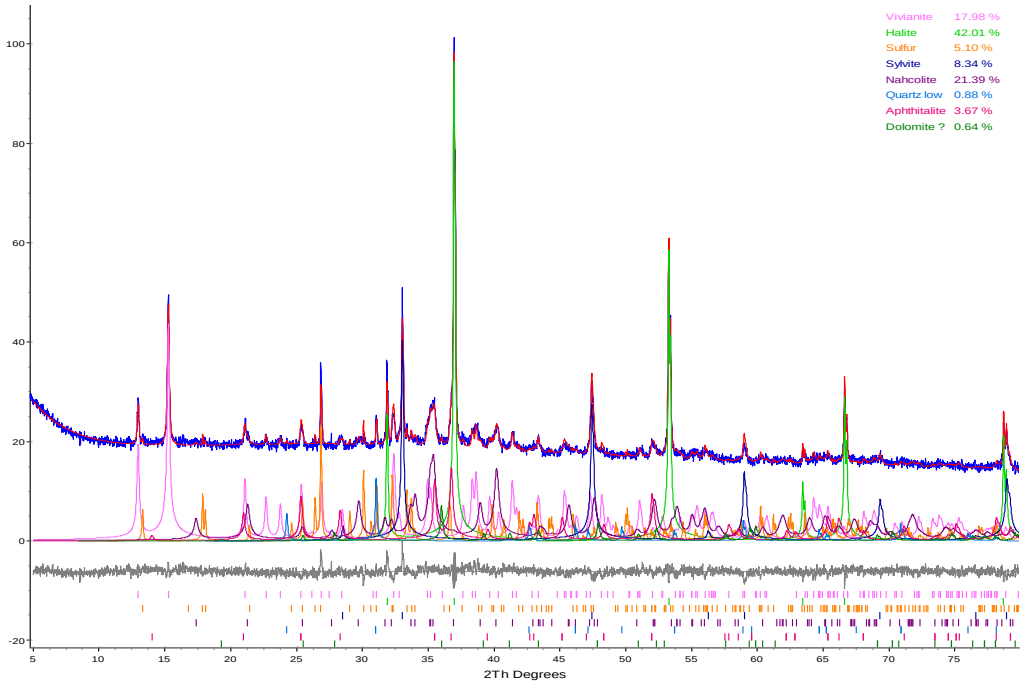

Figure A.2.3. X-ray diffractogram of sample NN_a

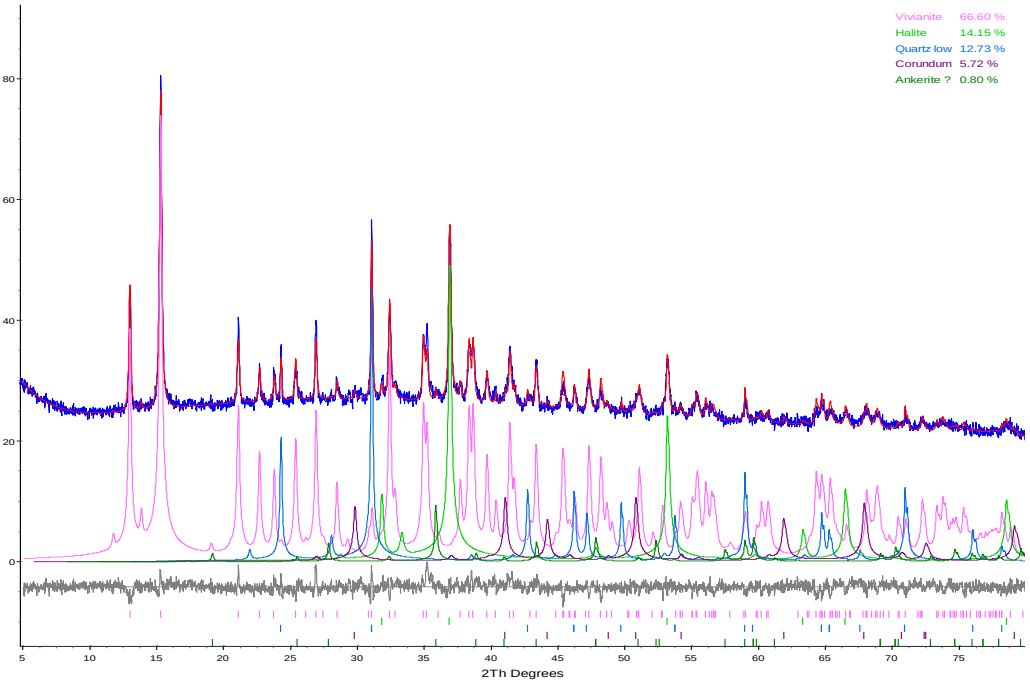

Figure A.2.4. X-ray diffractogram of sample NN_b

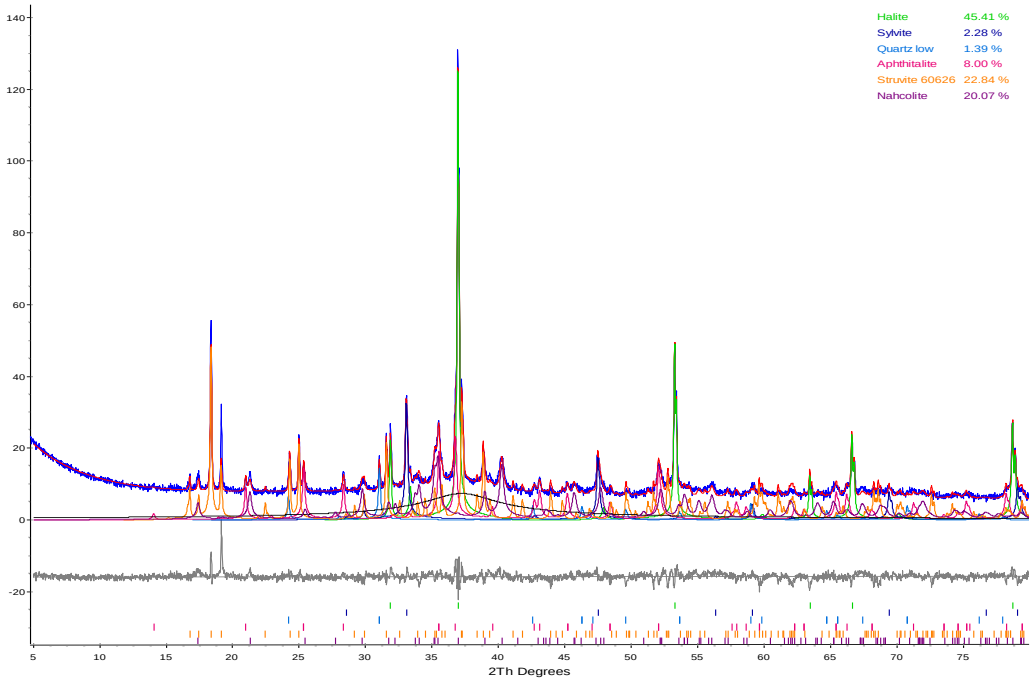

Figure A.2.5. X-ray diffractogram of sample NF_a

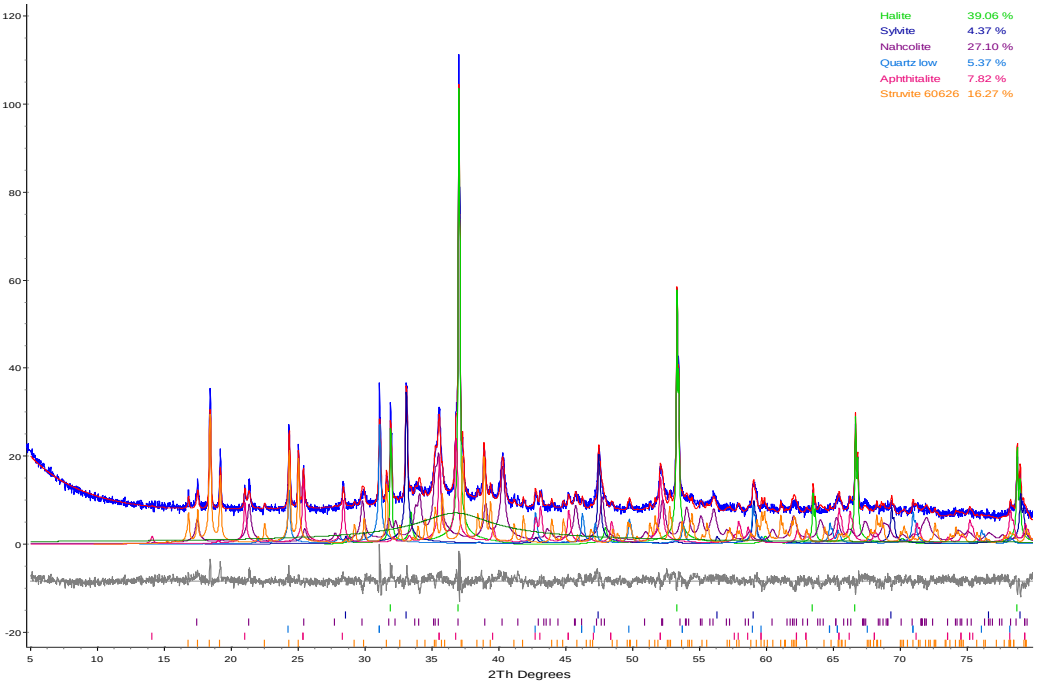

Figure A.2.6. X-ray diffractogram of sample NF_b

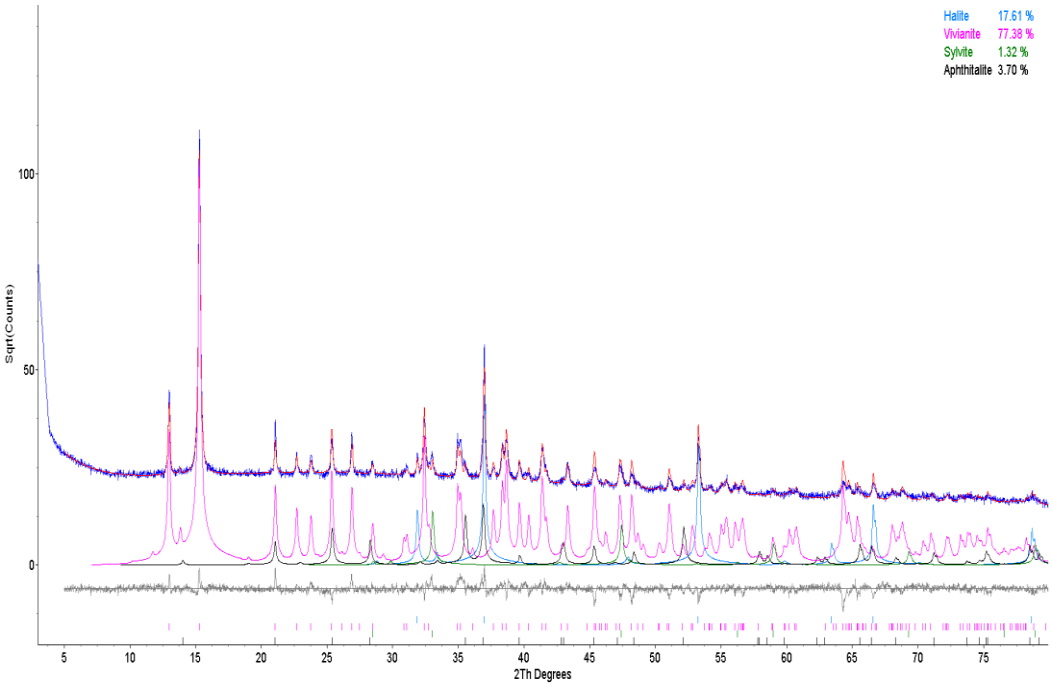

Figure A.2.7. X-ray diffractogram of sample ND_a

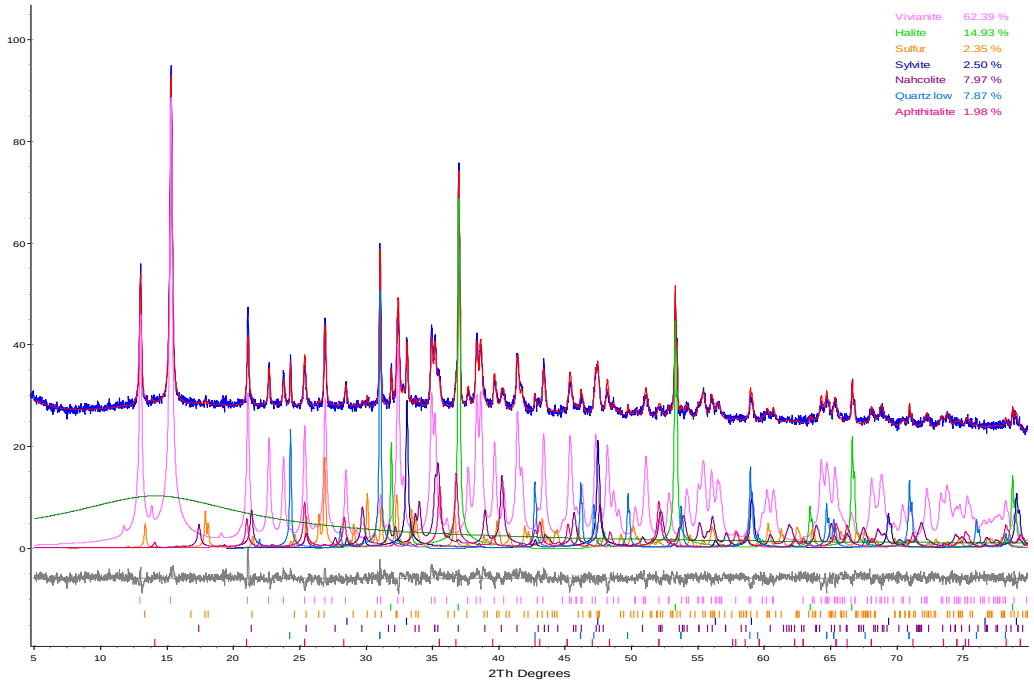

Figure A.2.8. X-ray diffractogram of sample ND_b

A.3 Polarization tests

Polarization tests were performed on the reactors to determine internal resistance. The test was performed when current production was highest. External load changes were done in 15-min steps, the last measurement was considered for calculations. Loads used were: 200 Ω, 470 Ω, 1 kΩ, 2.2 kΩ, 4.7 kΩ, 10 kΩ, 47 kΩ, 100 kΩ. The open circuit voltage (OCV) was measured after 1 hr of disconnecting the electrodes. The test was done for increasing and decreasing loads.

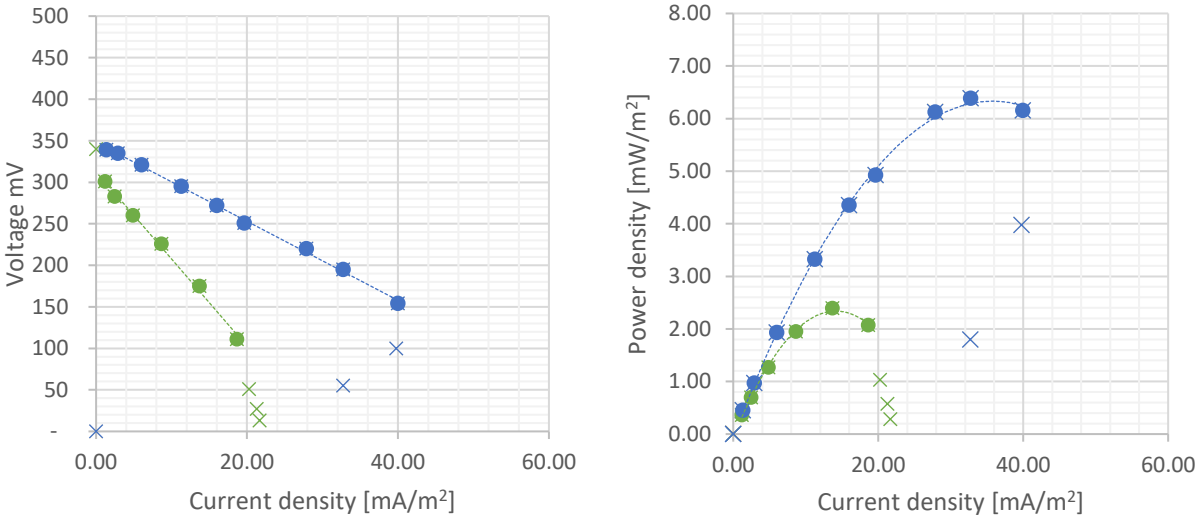

Figure A.3.1. Polarization and power curves for increasing (green) and decreasing (blue) resistance loads. Reactor BC_a

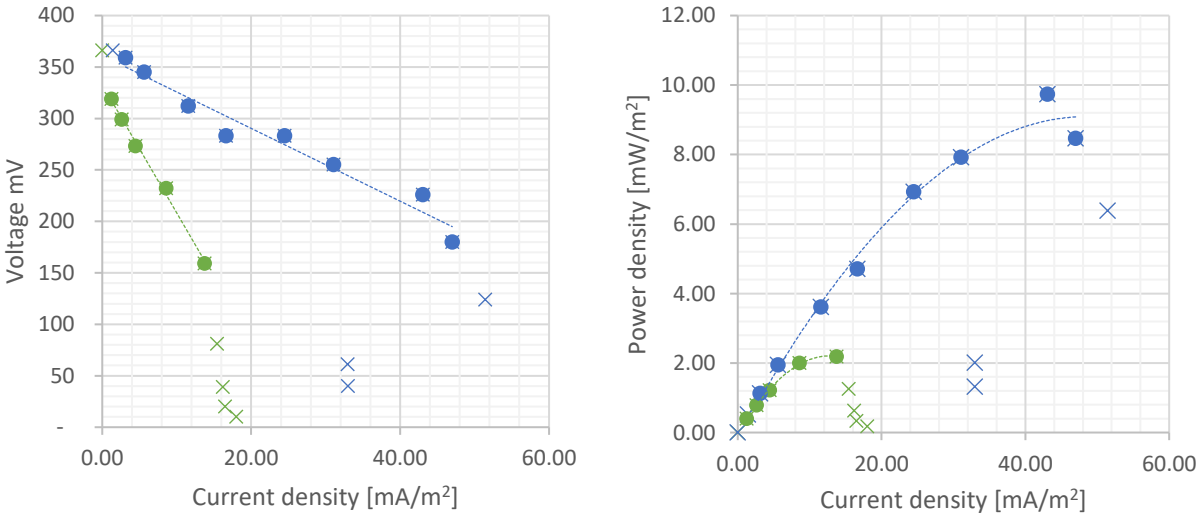

Figure A.3.2. Polarization and power curves for increasing (green) and decreasing (blue) resistance loads. Reactor BC_b

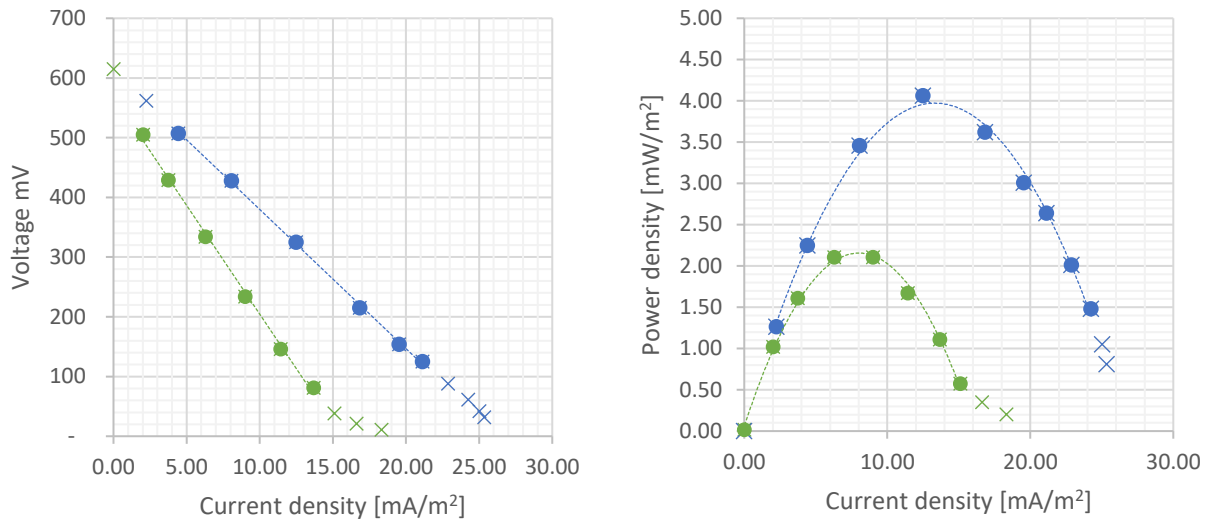

Figure A.3.3. Polarization and power curves for increasing (green) and decreasing (blue) resistance loads. Reactor NF_a

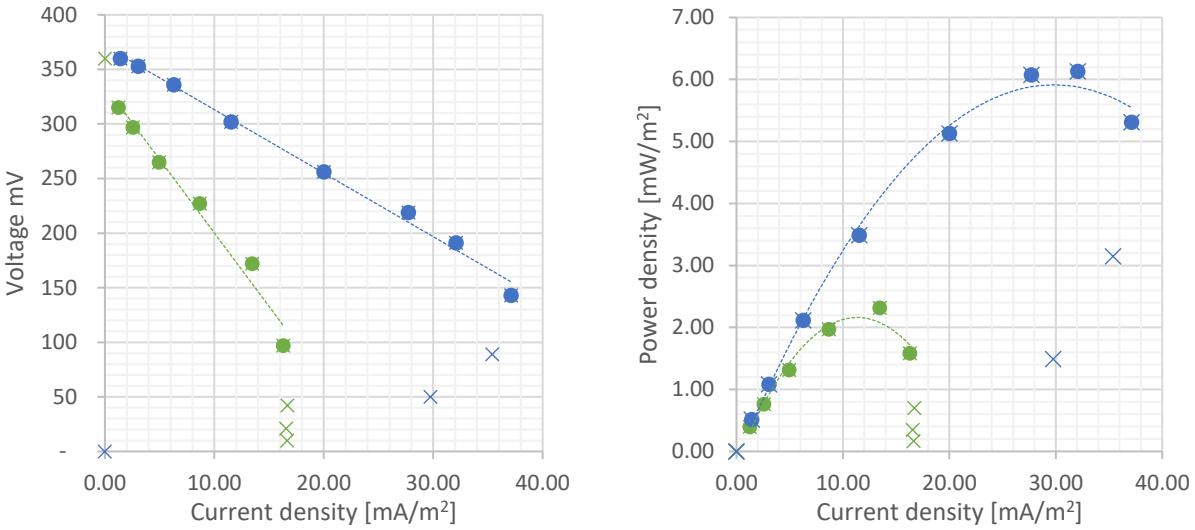

Figure A.3.4. Polarization and power curves for increasing (green) and decreasing (blue) resistance loads. Reactor NN_a

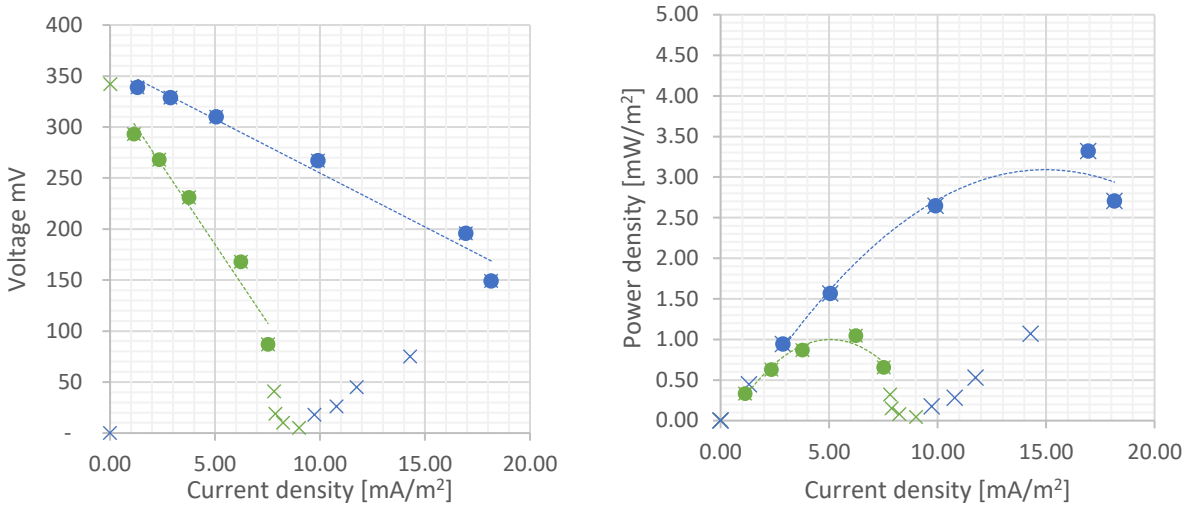

Figure A.3.5. Polarization and power curves for increasing (green) and decreasing (blue) resistance loads. Reactor NN_b

A.4 Sorption experiment plots

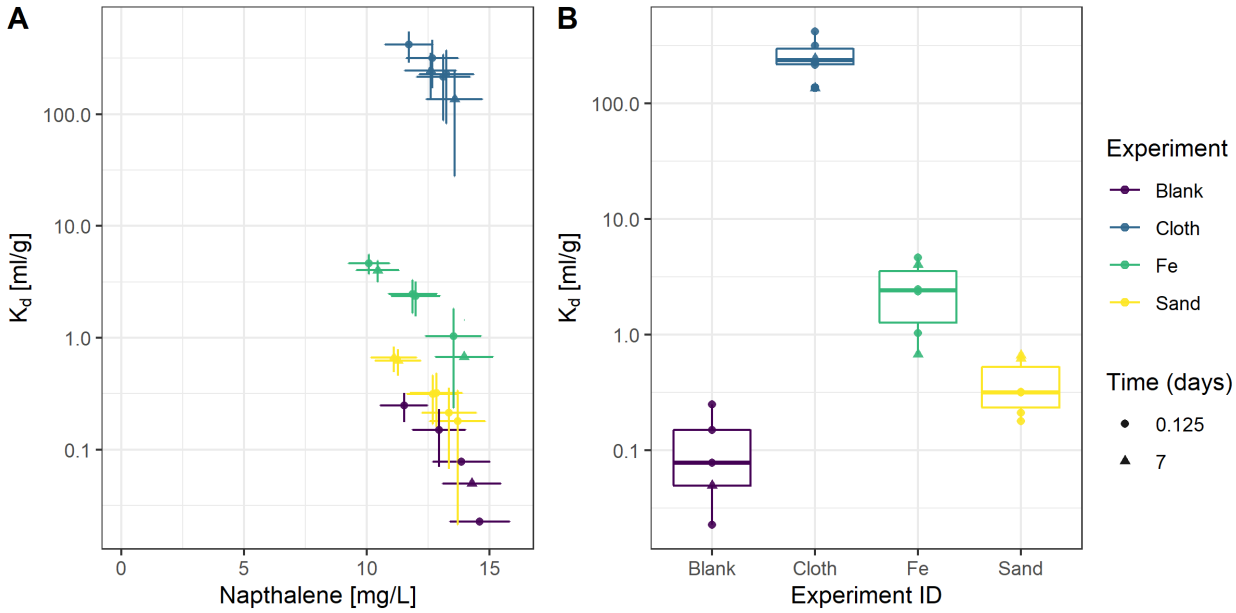

Figure A.4.1. Experimental sorption distribution coefficients for reactor materials according to sorption experiments. (A) Distribution coefficient versus measured naphthalene; error bars for the x-axis correspond to RSD calculated from triplicate IPC-MS measurements; error bars in the y-axis correspond to the calculated standard deviation of K_d. (B) Boxplot comparing of the distribution coefficient, Kd, determined for each experiment.

A.5 Microbial data and plots

Table A.5.1. Coverage data for microbiological samples

Reactor_type	Reactor_ID	Sample_type	Sample_ID	SEQ_ID	Coverage
inoculum	NN_in	inoculum	NN_in	CONI_2_3	0.988257
inoculum	BC_in	inoculum	BC_in	CONI_2_4	0.990891
inoculum	ND_NF_in	inoculum	ND_NF_in	CONI_2_2	0.991369
BC	BC_b	anode	BC_b_a2	CONI_21	0.99406
BC	BC_b	anode	BC_b_a3	CONI_22	0.994317
BC	BC_b	anode	BC_b_a1	CONI_19	0.994864
BC	BC_a	anode	BC_a_a3	CONI_20	0.995251
BC	BC_a	anode	BC_a_a1	CONI_17	0.996203
BC	BC_a	anode	BC_a_a2	CONI_18	0.996739
BC	BC_b	media	BC_b_m1	CONI_13	0.990206
BC	BC_a	media	BC_a_m1	CONI_11	0.991087
BC	BC_a	media	BC_a_m2	CONI_12	0.99125
BC	BC_a	media	BC_a_m3	CONI_14	0.992325
BC	BC_b	media	BC_b_m3	CONI_15	0.994017
BC	BC_b	media	BC_b_m2	CONI_16	0.995871
ND	ND_b	anode	ND_b_a2	CONI_3_5	0.99061
ND	ND_b	anode	ND_b_a3	CONI_3_6	0.991624
ND	ND_b	anode	ND_b_a1	CONI_3_4	0.991633
ND	ND_a	anode	ND_a_a2	CONI_3_2	0.994188
ND	ND_a	anode	ND_a_a1	CONI_3_1	0.994377
ND	ND_a	anode	ND_a_a3	CONI_3_3	0.996252
ND	ND_b	media	ND_b_m2	CONI_4	0.994885
ND	ND_b	media	ND_b_m3	CONI_5	0.99536
ND	ND_b	media	ND_b_m1	CONI_3	0.995431
ND	ND_a	media	ND_a_m1	CONI_1	0.996775
ND	ND_a	media	ND_a_m2	CONI_2	0.998177
NF	NF_b	anode	NF_b_a2	CONI_3_11	0.993358
NF	NF_b	anode	NF_b_a1	CONI_3_10	0.994135
NF	NF_a	anode	NF_a_a3	CONI_3_9	0.994676
NF	NF_b	anode	NF_b_a3	CONI_3_12	0.995854
NF	NF_a	anode	NF_a_a1	CONI_3_7	0.997022
NF	NF_a	anode	NF_a_a2	CONI_3_8	0.997109
NF	NF_a	media	NF_a_m2	CONI_7	0.980734
NF	NF_b	media	NF_b_m2	CONI_10	0.993703
NF	NF_b	media	NF_b_m1	CONI_9	0.993989
NF	NF_b	media	NF_b_m3	CONI_3_13	0.994488
NF	NF_a	media	NF_a_m1	CONI_6	0.995846
NF	NF_a	media	NF_a_m3	CONI_8	0.996564

Reactor_type	Reactor_ID	Sample_type	Sample_ID	SEQ_ID	Coverage
NN	NN_b	anode	NN_b_a2	CONI_27	0.977319
NN	NN_b	anode	NN_b_a3	CONI_28	0.985851
NN	NN_b	anode	NN_b_a1	CONI_26	0.994169
NN	NN_a	anode	NN_a_a2	CONI_24	0.994628
NN	NN_a	anode	NN_a_a1	CONI_23	0.995564
NN	NN_a	anode	NN_a_a3	CONI_25	0.995602
NN	NN_b	media	NN_b_m3	CONI_3_19	0.993041
NN	NN_b	media	NN_b_m1	CONI_3_17	0.993948
NN	NN_a	media	NN_a_m3	CONI_3_16	0.994164
NN	NN_b	media	NN_b_m2	CONI_3_18	0.994184
NN	NN_a	media	NN_a_m2	CONI_3_15	0.994957

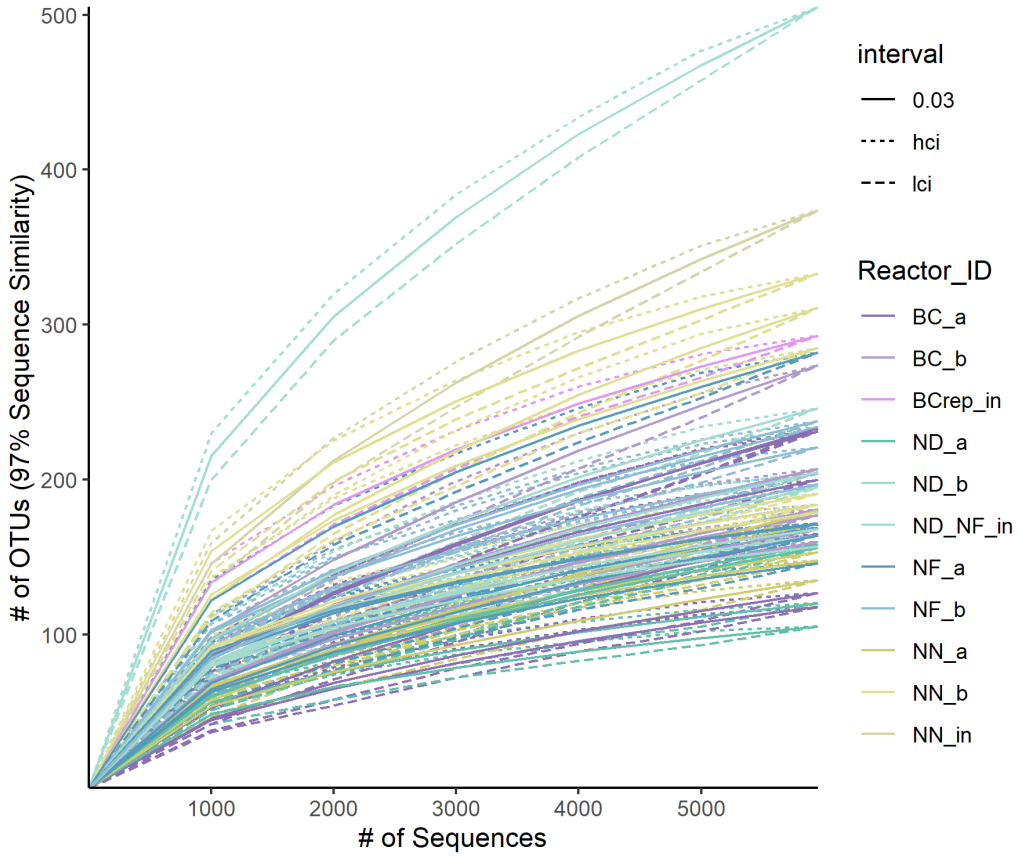

Figure A.5.1. Rarefaction curves rarefied 97%-OTU 16S rRNA gene amplicon data for each sample.

Table A.5.2. AMOVA results comparing total population (anode and media) between experiments BC-ND, BC-NF and BC-NN.

Comparator groups	**BC-ND**			**BC-NF**			**BC-NN**		
	Among	Within	Total	Among	Within	Total	Among	Within	Total
SS	3.52199	0.637275	4.15927	3.70171	3.77226	7.47396	3.05294	2.61484	5.66779
df	1	21	22	1	22	23	1	21	22
MS	3.52199	0.0303464		3.70171	0.171466		3.05294	0.124516	
Fs	116.06			21.59			24.52		
p-value	<0.001*			<0.001*			<0.001*		

Table A.5.3. AMOVA results comparing total population (anode and media) between experiments ND-NF, ND-NN and NF-NN.

Comparator groups	**ND-NF**			**ND-NN**			**NF-NN**		
	Among	Within	Total	Among	Within	Total	Among	Within	Total
SS	3.32179	3.43228	6.75407	0.74142	2.27487	3.01629	2.44967	5.40985	7.85952
df	1	21	22	1	20	21	1	21	22
MS	3.32179	0.163442		0.74142	0.113743		2.44967	0.257612	
Fs	20.32			6.52			9.51		
p-value	<0.001*			<0.001*			<0.001*		

Table A.5.4. AMOVA results: comparison between anode and media within reactor types. BC and ND reactors.

Comparator groups	**anode_BC-media_BC**			**anode_ND-media_ND**		
	Among	Within	Total	Among	Within	Total
SS	0.339549	0.149077	0.488626	0.0268885	0.12176	0.148649
df	1	10	11	1	9	10
MS	0.339549	0.0149077		0.0268885	0.0135289	
Fs	22.78			1.99		
p-value	<0.001*			0.202		

Table A.5.5. AMOVA results: comparison between anode and media within reactor types. NF and NN reactors.

Comparator groups	**anode_NF-media_NF**			**anode_NN-media_NN**		
	Among	Within	Total	Among	Within	Total
SS	0.90515	2.37848	3.28363	0.606723	1.5195	2.12622
df	1	10	11	1	9	10
MS	0.90515	0.237848		0.606723	0.168833	
Fs	3.81			3.59		
p-value	0.020			0.150		

Table A.5.6. AMOVA results: comparison anode to anode between reactor types

Comparator groups	**anode_BC-anode_ND**			**anode_BC-anode_NF**			**anode_BC-anode_NN**		
	Among	Within	Total	Among	Within	Total	Among	Within	Total
SS	2.34296	0.183494	2.52645	2.18534	1.44402	3.62936	1.9233	1.5247	3.448
df	1	10	11	1	10	11	1	10	11
MS	2.34296	0.0183494		2.18534	0.144402		1.9233	0.15247	
Fs	127.69			15.13			12.61		
p-value	0.002			<0.001*			0.001		

Table A.5.7. AMOVA results: comparison anode to anode between reactor types

Comparator groups	**media_BC-media_ND**			**media_BC-media_NF**			**media_BC-media_NN**		
	Among	Within	Total	Among	Within	Total	Among	Within	Total
SS	1.33693	0.0873435	1.42427	2.11086	1.08354	3.1944	1.41463	0.143874	1.5585
df	1	9	10	1	10	11	1	9	10
MS	1.33693	0.00970483		2.11086	0.108354		1.41463	0.015986	
Fs	137.76			19.48			88.49		
p-value	0.002			<0.001*			0.002		

Table A.5.8. Putative metabolism and description of taxa that are differentially represented in each reactor type according to LEfSe analysis (LDA > 3.0)**.**

Reactor	OTU	Taxa	Description	References
BC	Otu0002	Candidatus Deferrimonas	Iron reducing bacteria. Type species Deferrimonas soudanensis is a metal- and electrode-respiring bacterium from anoxic deep subsurface brine. Can form syntrophic associations with other bacteria (such as methanogens; Rotaru et al., 2015)	(Badalamenti et al., 2016; Waite et al., 2020)
BC	Otu0010	Desulfuromonadia class (unclassified order)	Strictly anaerobic; can reduce ferric iron and elemental sulfur to ferrous iron and sulfide	(Garrity, Schleifer, et al., 2005; Waite et al., 2020)
BC	Otu0056	Edaphobaculum	strictly aerobic bacterium from soil	(M. Cao et al., 2017)
BC	Otu0100	Simplicispira	denitrification; facultative anaerobe	(Siddiqi et al., 2020)
ND	Otu0001	Pseudomonadaceae family (unclassified genus)	Aerobic chemoorganotroph having respiratory metabolism with oxygen as terminal electron acceptor, some species fix nitrogen, some degrade aromatic hydrocarbons	(Garrity, Brenner, et al., 2005)
ND	Otu0012	Desulfovibrionaceae family (unclassified genus)	anaerobe; incomplete oxidation of organic susbtrates to acetate; reduces sulfate to sulfide	(Garrity, Schleifer, et al., 2005; Kuever, 2014)
ND	Otu0021	Rhodocyclaceae family (uncultured)	includes aromatic compound degraders, sulfur oxidizing chemoauthotrops, methylotrops, anaerobic fermenters	(Oren, 2014)
ND	Otu0018	Erysipelothrix	human pathogen	(Q. Wang & Riley, 2015)
ND	Otu0013	Prolixibacteraceae family (uncultured)	Genus Prolixibacter bellariivorans is facultative anaerobe, can ferment sugars, isolated from a fuel cell; genus Prolixibacter denitrificans is iron-corroding, facultative aerobic, nitrate-reducing isolated from crude oil.	(Huang et al., 2014; Iino et al., 2015)
ND	Otu0046	Desulfocapsaceae family (unclassified genus)	type genus Desulfocapsa are strictly anaerobic, capable of disproportionation of elemental sulfur to sulfide and sulfate	(Janssen et al., 1996)
ND	Otu0049	Desulfosporosinus	Genus: Sulfate and thiosulfate are reduced to sulfide in the presence of lactate, pyruvate and other carbon sources and electron donors. Incomplete oxidation of organic compounds to acetate occurs. Fumarate is sometimes used as a carbon and energy source for sulfate reduction. Nitrate is sometimes reduced to nitrite; Desulfosporosinus meridiei sp. nov., a sulfate-reducing bacterium isolated from BTEX-contaminated groundwater.	(Robertson et al., 2001; Stackebrandt et al., 2003)
ND	Otu0096	Desulfatitalea	Mesophilic, sulfate-reducing bacteria; can use sulfate and thiosulfate as electron acceptors.	(Higashioka et al., 2013)
ND	Otu0138	Paludibacteraceae family (unclassified)	Paludibacter genus: Strictly anaerobic. Fermentation of sugars to produce acetate, propionate and succinate	(Ormerod et al., 2016; Ueki et al., 2006)

Reactor	OTU	Taxa	Description	References
NF	Otu0006	Immundisolibacter	Aerobic bacteria; can grow on limited number of organic acids. Immundisolibacter cernigliae gen. nov., sp. nov., can grow on high-molecular-weight polycyclic aromatic hydrocarbon	(Corteselli et al., 2017)
NF	Otu0008	Hydrogenophaga	Aerobic; oxidize H_2 and use CO_2 as carbon source	(Garrity, Schleifer, et al., 2005)
NF	Otu0017	Chryseobacterium	Aerobic chemoorganotroph. Most species do not reduce nitrate or nitrite, and most do not produce H_2S	(Nicholson et al., 2020; Vandamme et al., 1994)
NF	Otu0014	Parvibaculum	Type species Parvibaculum lavamentivorans gen. nov., sp. nov. is an aerobic heterotrophic bacterium that can degrade the commercial surfactant linear alkylbenzenesulfonate, can also grow with acetate and octane; Parvibaculum hydrocarboniclasticum grows aerobically in artificial seawater with n-alkanes as sole carbon and energy sources	(Rosario-Passapera et al., 2012; Schleheck et al., 2004)
NF	Otu0035	Physicphaeraceae family (genus SM1A02)	Facultatively anaerobic bacteria; Physicphaera mikurensis sp. can reduce nitrate to nitrite	(Fukunaga et al., 2009)
NF	Otu0039	Rhodocyclaceae family (unclassified)	Family is metabolically and ecologically diverse, it includes aerobes, anaerobes and facultative anaerobes utilizing a number of electron acceptors (chlorate, perchlorate, Fe(III), nitrate, nitrite), fermentative bacteria, and nitrogen-fixing bacteria.	(Garrity, Schleifer, et al., 2005)
NF	Otu0051	Planctopirus	Type species Planctomyces limnophilus is aerobic, reported to perform dissimilatory nitrate reduction.	(Hirsch & Müller, 1985)
NF	Otu0084	Flavobacteriaceae family (unclassified)	The family includes aerobic, and microaerobic to anaerobic bacteria, chemoorganotrophs, some degrade cellullose, some are pathogens	(Bernardet et al., 2002)
NF	Otu0086	Opitutus	Facultatively anaerobic. Metabolism is both fermentative and respiratory. Nitrate can be reduced to nitrite	(Chin et al., 2001; Tegtmeier et al., 2018)
NF	Otu0108	Desulfuromonadaceae family (unclassified)	Desulfuromonadia class are strictly anaerobic, play important roles in organic matter degradation and are involved in syntrophic associations with methanogens and phototrophic green sulfur bacteria; some can reduce ferric iron and elemental sulfur to ferrous iron and sulfide	(Garrity, Brenner, et al., 2005; Greene, 2014; Waite et al., 2020)
NF	Otu0068	Ferrovibrionales order (unclassified family)	Ferrovibrio genus are facultative anaerobes, can grow coupling oxidation of Fe(II) with reduction of nitrate, with accumulation of Fe(III) oxides on the cell surface	(Sorokina et al., 2012)

Reactor	OTU	Taxa	Description	References
NF	Otu0085	Pseudorhodoplanes	Facultatively anaerobic, the type species Pseudorhodoplanes sinuspersici was isolated from an oil-contaminated site and can use pyruvate, yeast extract and tryptone as carbon sources	(Tirandaz et al., 2015)
NF	Otu0097	Acetobacteraceae family (uncultured)	aerobic, acetic acid bacteria (can oxidize ethanol to acetic acid aerobically), some can further oxidize the produced acetic acid to CO_2.	(Garrity, Schleifer, et al., 2005)
NF	Otu0082	Sphingomonadaceae family (unclassified genus)	Genus Sphingomonas is strict aerobe, some species can degrade dibenzo-p-dioxin (DD), dibenzofuran (DF), buphenyl, or aromatic hydrocarbons (including naphthalene sulfonic acids)	(Garrity, Schleifer, et al., 2005)
NF	Otu0121	Paracaedibacteraceae family (uncultured)	Obligate intracellular bacteria that colonize a wide range of eukaryotic hosts	(Hess et al., 2016)
NF	Otu0112	Reyranellaceae family (uncultured)	Reyranellaceae family, the type genus Reyranella massiliensis gen. nov., sp. nov. is a microaerophillic bacteria capable of nitrate reduction	(Hördt et al., 2020; Pagnier et al., 2011)
NF	Otu0144	Pedosphaeraceae family (unclassified genus)	Metane oxidizing microorganism potentially coupled to oxygen reduction, found in bioreactors under microaerophilic conditions. Methane oxidation coupled to iron reduction has also been proposed	(Martins et al., 2010)
NN	Otu0003	Geothermobacter	Mesophilic and thermophilic, strictly anaerobic bacteria growth by coupling the oxidation of acetate, pyruvate, dl-malate, glutamate, propionate, butyrate, ethanol, and methanol to the reduction of Fe(III) and nitrate. Geothermobacter hydrogeniphilus sp. can grow with H_2 as primary electron donor, CO_2 as carbon source and Fe(III) as terminal electron acceptor, and can also use S^0 and sulfate as electron acceptors (among other compounds).	(Kashefi et al., 2003; Pérez-Rodríguez et al., 2021)
NN	Otu0020	Desulfosporosinus	Genus: Sulfate and thiosulfate are reduced to sulfide in the presence of lactate, pyruvate and other carbon sources and electron donors. Incomplete oxidation of organic compounds to acetate occurs. Fumarate is sometimes used as a carbon and energy source for sulfate reduction. Nitrate is sometimes reduced to nitrite; Desulfosporosinus meridiei sp. nov., a sulfate-reducing bacterium isolated from BTEX-contaminated groundwater.	(Robertson et al., 2001; Stackebrandt et al., 2003)
NN	Otu0026	Thiobacillus	Sulfide oxidizer; one Fe(II) oxidizer,deposit S^0; all species grow aerobically, some species also grow anaerobically	(Lens, 2009)
NN	Otu0015	Desulfurivibrio	Obligately anaerobic with respiratory metabolism. Utilizes sulfur compounds, but not sulfate, as electron acceptor, and short-chain fatty acids and hydrogen as electron donors	(Sorokin et al., 2008)
NN	Otu0024	Thiobacillus	Sulfide oxidizer; one Fe(II) oxidizer,deposit S^0; All species grow aerobically, some species also grow anaerobically	(Lens, 2009)

Reactor	OTU	Taxa	Description	References
NN	Otu0025	Gallionella	Microaerophillic, and facultatively anaerobic, Fe(III) oxidizing bacteria, capable of chemolototrophic growth with CO_2 as sole carbon source and mixotrophic metabolism	(L. Hallbeck et al., 1993)
NN	Otu0044	Prolixibacteraceae family (uncultured)	Genus Prolixibacter bellariivorans is facultative anaerobe, can ferment sugars, isolated from a fuel cell; genus Prolixibacter denitrificans is iron-corroding, facultative aerobic, nitrate-reducing isolated from crude oil.	(Huang et al., 2014; Iino et al., 2015)
NN	Otu0042	Ignavibacteriales order (unclassified)	Type genus is Ignavibacterium, a strictly anaerobic, moderately thermophilic, neutrophilic and obligately heterotrophic bacteria. Can grow fermentatively, cannot grow phototrophically	(Iino et al., 2010; Podosokorskaya et al., 2013)
NN	Otu0043	Comamonadaceae family (unclassified)	Comamonadaceae family includes common soil and water microorganisms. Some genera in this family: Comamonas, Rhodoferax, Acidovorax and Hydrogenophaga. Chemoorganotrophic or chemolithotrophic with H_2, or CO_2 oxidation. Oxidative metabolism, using O_2 as a terminal electron acceptor; some species can also use nitrates. They use few carbohydrates, but can use a wide variety of organic acids, including amino acids as carbon source.	(Willems et al., 1991)
NN	Otu0023	Candidatus Paracaedibacter	Obligate intracellular bacteria that colonize a wide range of eukaryotic hosts	(Hess et al., 2016)
NN	Otu0036	Brevundimonas	Aerobic with a respiratory type of metabolism; never fermentative	(Abraham et al., 1999; Segers et al., 1994)
NN	Otu0066	Gammaproteobacteria (genus Ga0077536)	unclassified genus	
NN	Otu0063	Methylopilaceae MM2	Methylopila genus is an aerobic chemoorganotrophic and facultatively methylotrophicc bacteria. Methylopila capsulata type genus uses methanol, me th ylated amines, but anol, ethanol, glycerol, maltose, sucrose, L-arabinose, D-fructose, D-glucose, succinate, fumarate, pyruvate as carbon sources	(Doronina et al., 1998)
NN	Otu0038	Ferrovibrio	Facultatively anaerobic, neutrophilic Fe(II)-oxidizing bacterium, capable of organotrophic, lithoheterotrophic and mixotrophic growth with Fe(II) as electron donor. Can couple oxidation of Fe(II) to reduction of nitrate, or of N2O to N2, as well as with O2 as an electron acceptor under microaerobic conditions.	(Dahal & Kim, 2018; Sorokina et al., 2012)
NN	Otu0088	Bacteroidota phylum (unclassified)	Unclassified genus within Bacteroidota phylum	

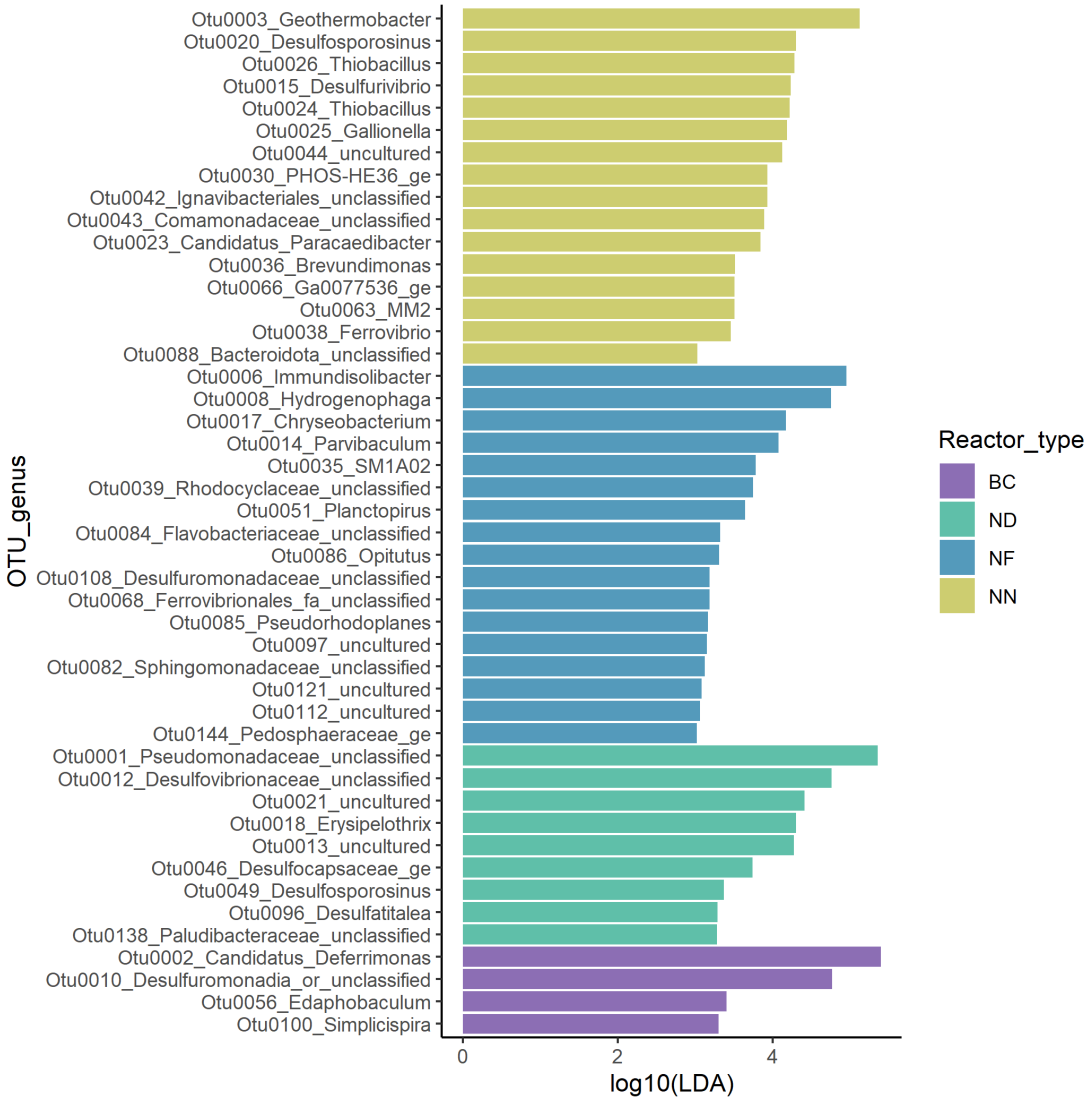

Figure A.5.2. Effect size (LDA) for the significant taxa per group (reactor type) from LEfSe analysis**.**

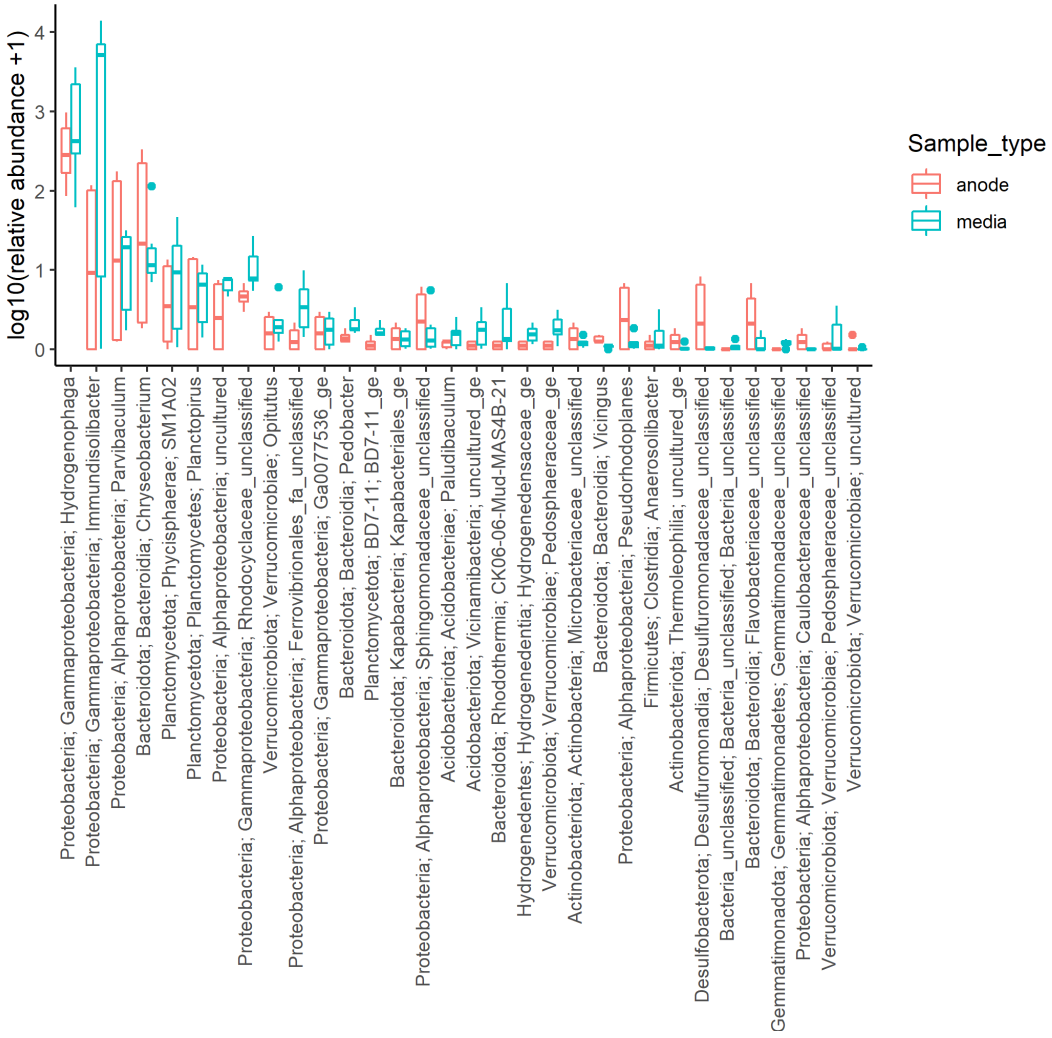

Figure A.5.3. Relative abundance of OTUs differentially represented in NF reactors according to LEfSe analysis.

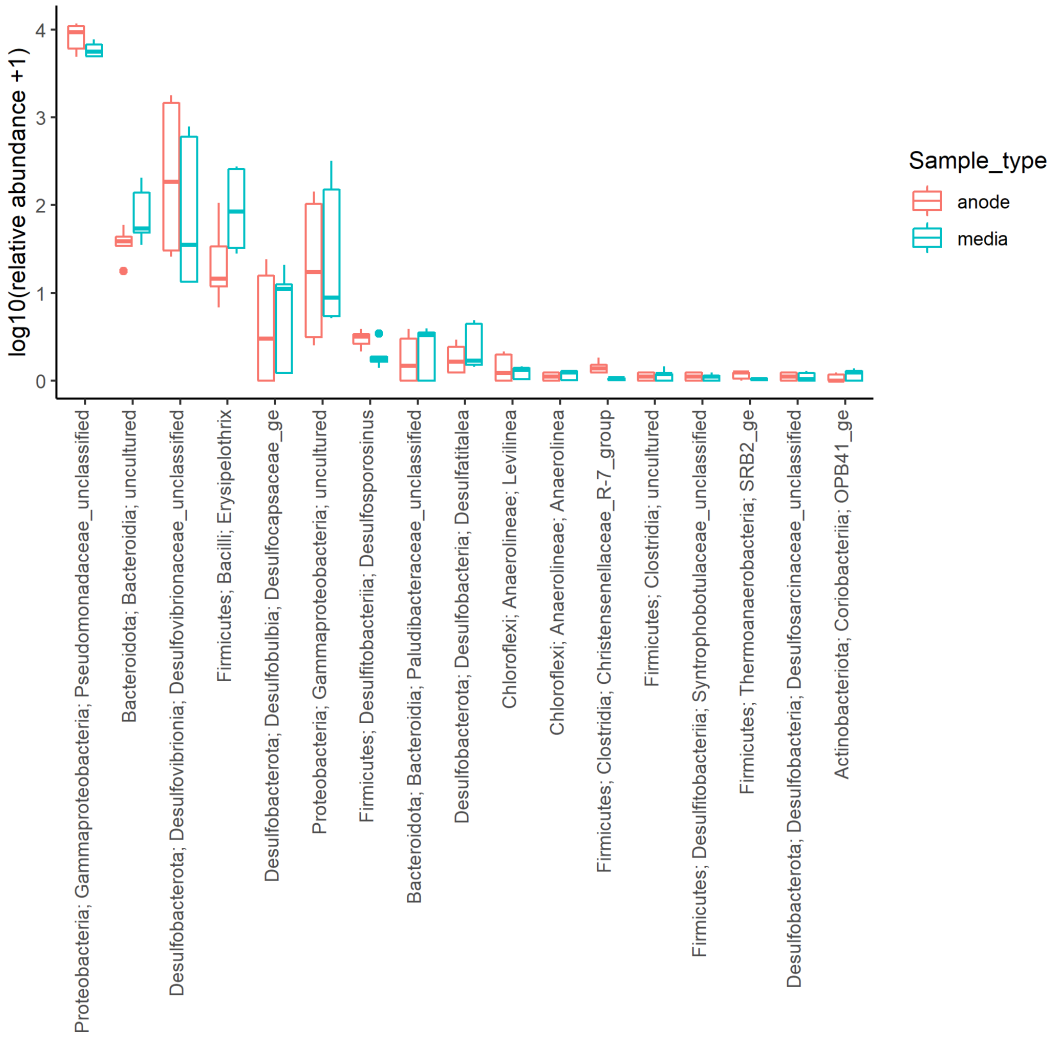

Figure A.5.4. Relative abundance of OTUs differentially represented in ND reactors according to LEfSe analysis.

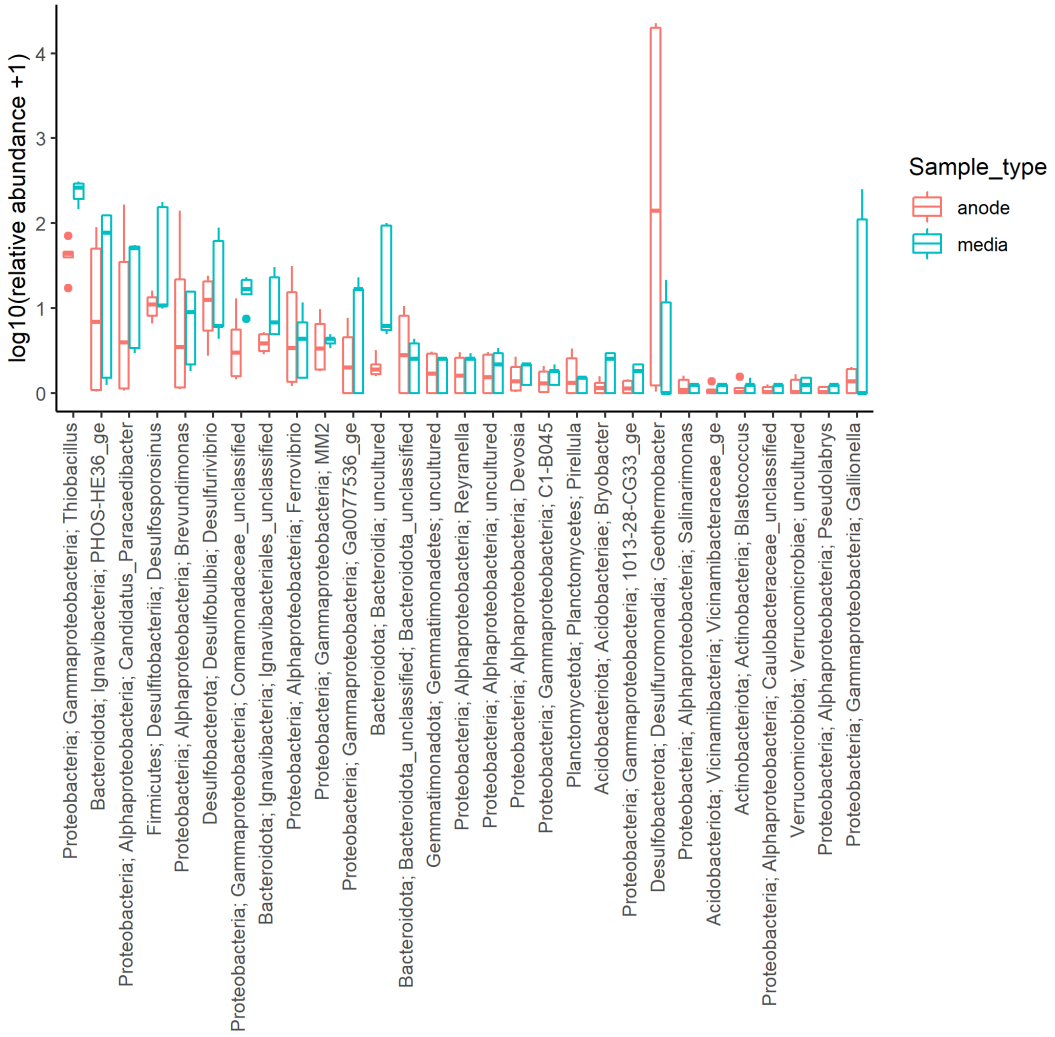

Figure A.5.5. Relative abundance of OTUs differentially represented in NN reactors according to LEfSe analysis.

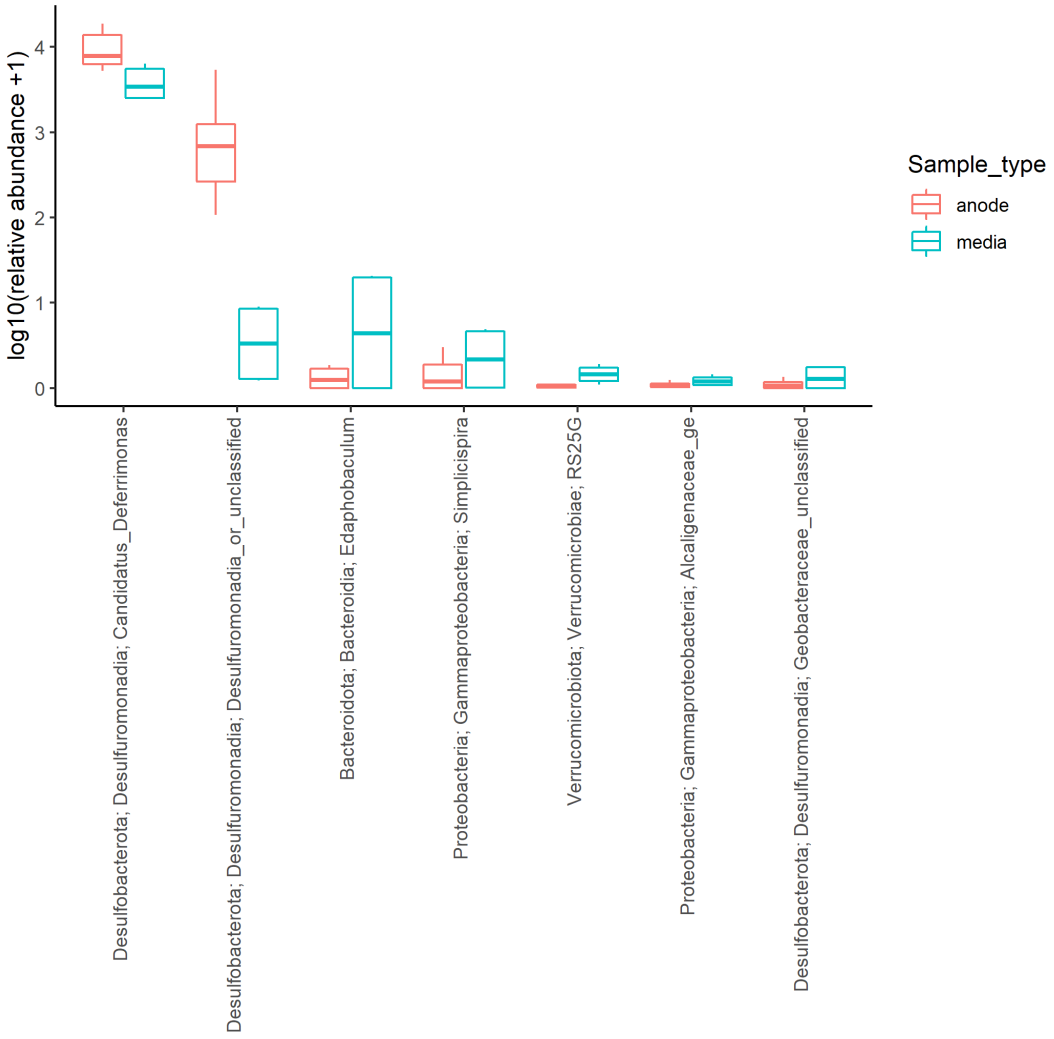

Figure A.5.6. Relative abundance of OTUs differentially represented in BC reactors according to LEfSe analysis.

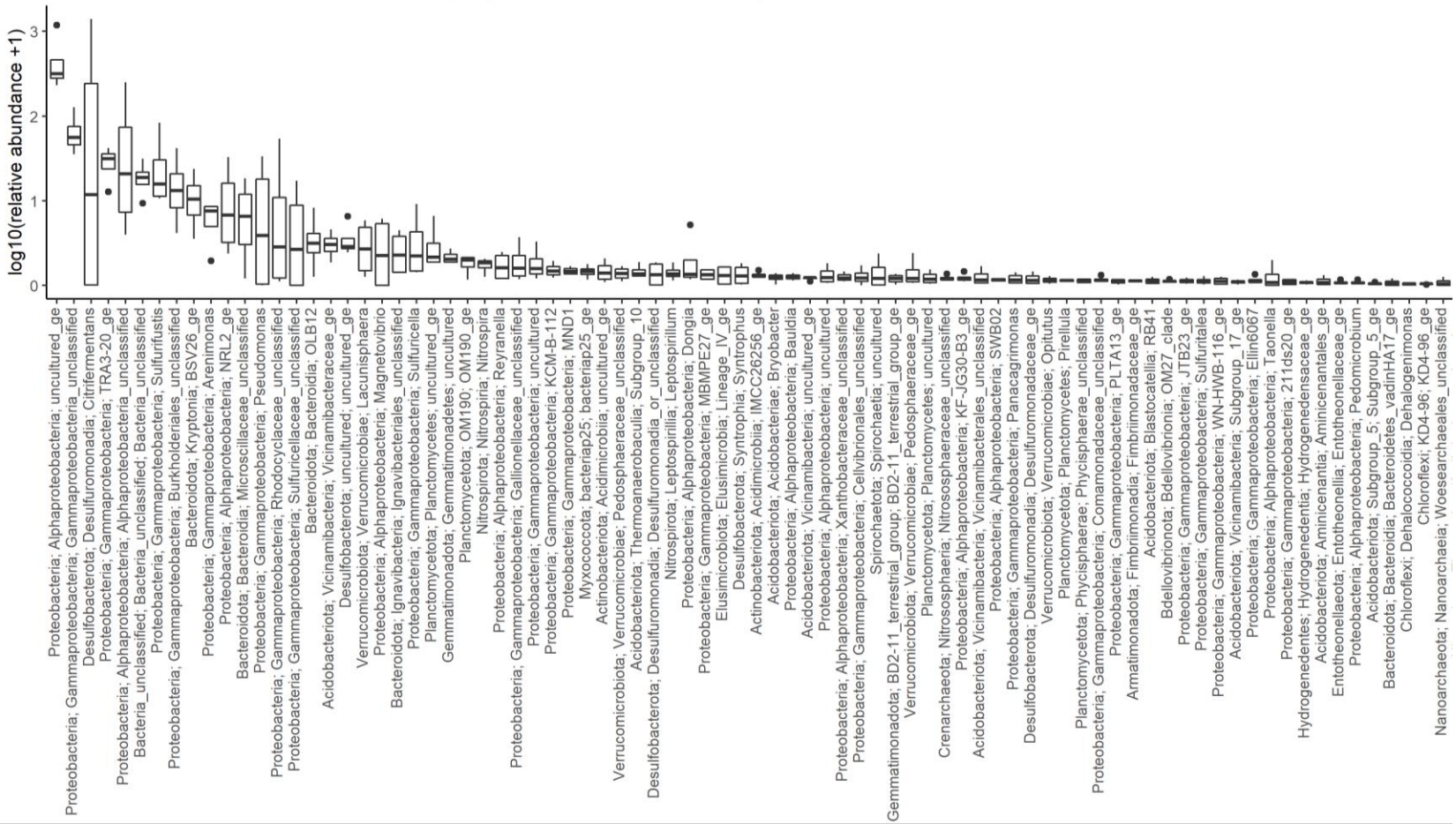

Figure A.5.7. Relative abundance of OTUs differentially represented in the inoculum according to LEfSe analysis**.**

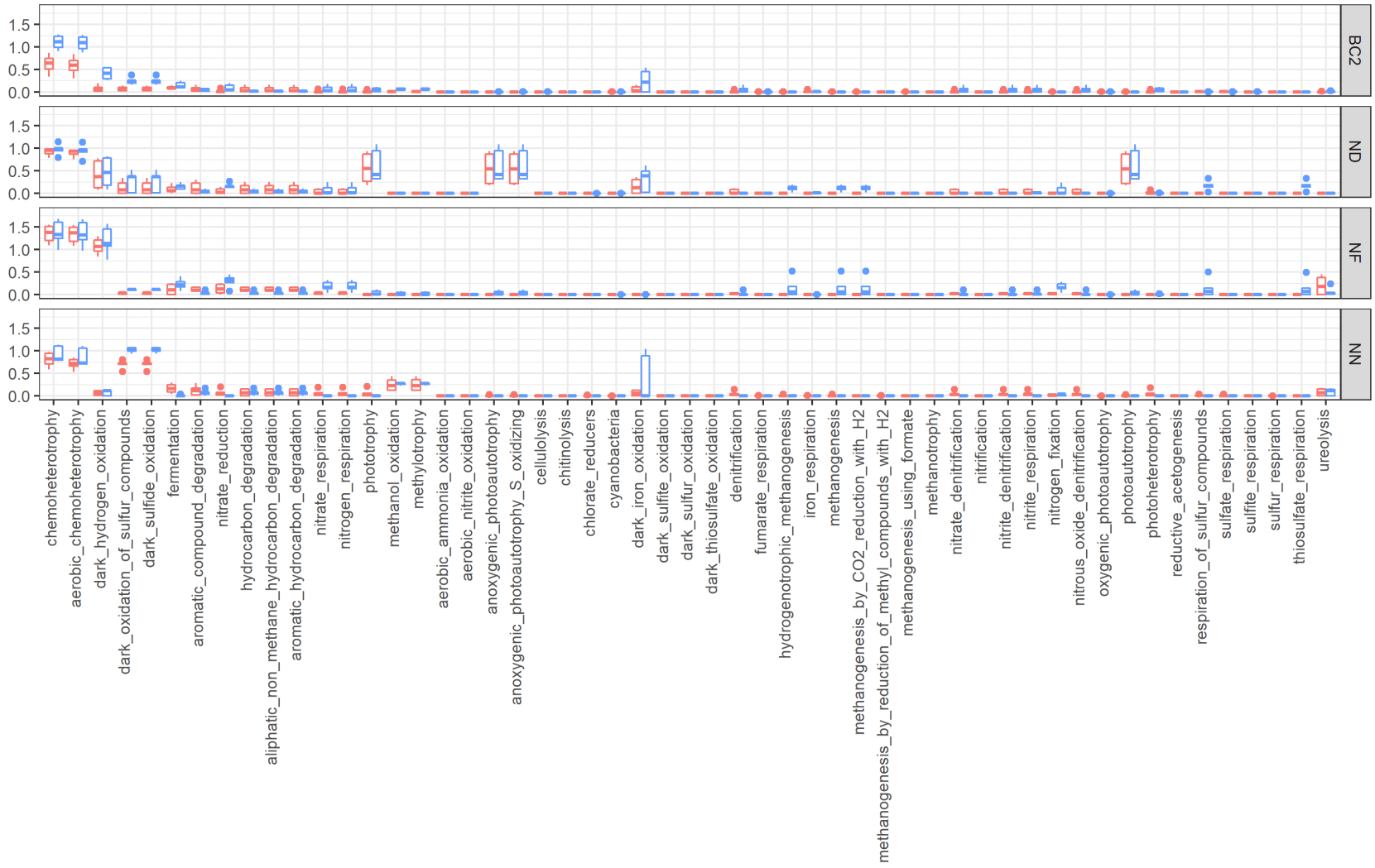

Figure A.5.8. Average relative abundance [log(relative abundance +1)] of bacteria with known metabolic potential according to FAPROTAX database. Blue boxes represent media samples and red boxes represent anode samples

Appendix B – **Sorption Experiment Supplementary Information**

Appendix B includes additional experimental data and analysis from the naphthalene sorption experiment presented in Chapter2.

B.1 Sorption experiment protocol

1. Prepare materials for sorption tests
   - Outside the anaerobic chamber, add 3x 21 mg of dry quartz sand to 3x glass serum vials. Record sand weight and label them “S_S1-3”.
   - Outside the anaerobic chamber, add a 1x1 cm^2 pieces of carbon cloth to each one of (3) 60 mL glass serum vials. Record cloth weight and label them “S_C1-3”.
   - Label vials “S_Fe1-3” and measure tare weight
   - Prepare 3x empty glass serum vials for blanks. Label “S_B1-3”. Measure tare weight.
2. Prepare basal media (as in MFC experiments)
   - Dissolve salts one by one in 970 mL of MQ.
   - Prepare 100 mL of sodium bicarbonate solution 1 mM.
   - Autoclave bicarbonate buffer and media and replace headspace in bottles with N_2 and N_2/CO_2 respectively.
3. Bring media to anaerobic chamber and dissolve naphthalene.
   - Add 15 mg of naphthalene to media and leave stirring for 2-3 days on a hot plate set to warm.
   - Leave stirring for 2-3 days until crystals are no longer visible
4. Prepare $FeCl_2$ solution
   - Bring 50 mL DI to de-air inside the anaerobic chamber. Leave the bottle in for 2-3 days.
   - Add 2.2815 g of dry $FeCl_2$ to the 50 ml de aired water, crimp seal.
5. Finalize preparing the media
   - Add 30 mL of sodium bicarbonate buffer 1 mM to the naphthalene-spiked media inside the anaerobic chamber
   - Take a sample for pH, close sample with parafilm

6. Before starting the experiments
   - Take a first set of samples from the media for naphthalene analysis (initial naphthalene)
   - Using a 1000 μL pipette with a glass tip, sample 2 mL into an Agilent amber glass vial. Take duplicate samples and fill with no headspace.
7. Add naphthalene-spiked media to sorption test vials.
   - Add 55 mL of naphthalene-spiked media to blank vials. Crimp seal with Teflon septa.
   - Add 45 mL of naphthalene-spiked media to vials with sand. Crimp seal with Teflon septa.
   - Add 55 mL of naphthalene-spiked media to vials with cloth. Crimp seal with Teflon septa.
   - Add 55 mL of naphthalene-spiked media to $FeCl_2$ vials, add 280 ul of 360 mM $FeCl_2$ solution using a 1 mL syringe. Crimp seal with Teflon septa.
   - Leave all experiments for 3 hrs, shake every 15 min.
8. Take a set of samples for naphthalene analysis after 3 hrs (average time from set up to sampling in the MFC experiments)
   - Bring out experiments 1 and 2
   - Weight experiments and record weights
   - Sample experiments: using a de-crimper, open the experiment vials, sample 500 μL from the experiment vial using a glass pipette tip. When sampling Fe experiment sample supernatant avoiding the decanted precipitate.
   - Pour sample into amber glass vial (pre-filled with 500 μL of hexane). Vortex sample vials and store in freezer.
9. Take a sample from the third experiment after 7 days
   - Bring experiments out of the anaerobic chamber
   - Weight experiments and record weight.
   - Using a 1000 μL pipette with a glass tip, sample 500 μL from the remaining experiment vials for into an Agilent amber glass vial.
   - Add 500 μL of hexane, vortex and store in the freezer.

B.2 Naphthalene sorption for individual MFC reactors – calculations

Because the actual initial naphthalene concentration and quartz sand height was slightly different for each reactor, the determination of the amount of naphthalene adsorbed into reactor materials involved individual measurements.

The amount of naphthalene adsorbed to each material Q_e (mg/g) depends on: C_i the initial naphthalene concentration (mg/L) in the media (variable between reactors), m the mass of sorbent (g, with variable values for each material), V the volume of media (L, constant), and K_d the distribution coefficient obtained from the sorption experiment (L/g; a different value for each material).

First, the mass of sorbent was calculated for each material in the reactor, and because the mass is different in the anode chamber and cathode chamber, different values for the mass was considered in each case.

The mass of glass in both the anode and the cathode chamber were:

$$m_{glass\ anode}\ [g] = 362\ g$$

$$m_{glass\ cathode}\ [g] = 272\ g$$

The mass of the carbon cloth of both anode and cathode was the same and was calculated based on the average mass, m_{ave}, measured for the 1 cm^2 pieces tested in the sorption experiment and considering the area of the electrodes used in the MFC reactors, a.

$$m_{ave} = 0.034\ \left[\frac{g}{cm^2}\right]$$

$$a = 5 \times 5\ [cm^2].$$

$$m_{electrodes}\ [g] = a\ [cm^2]\ \times m_{ave}\ \left[\frac{g}{cm^2}\right]$$

The mass of iron precipitate was estimated assuming all the iron present in the media precipitated. The iron concentration in the MFC reactors was $[Fe]$ = 1.8 mM, the molecular weight of iron is MW_{Fe} = 55.85 g/mol, and the volume of media corresponds to $V_{chamber}$. The volume of media is $V_{anode} = 1\ L$ for the anode chamber, and $V_{cathode} = 0.45\ L$ for the cathode chamber. The mass of iron precipitate was calculated using:

$$m_{Fe\ pp.}\ [g] = [Fe]\left[\frac{mmol}{L}\right]\left(\frac{1\ mol}{1000\ mmol}\right) V_{chamber}(L) \times\ MW_{Fe}\ \left[\frac{g}{mol}\right]$$

Sand was only present in the cathode chamber, but it varied slightly between reactors. First, the volume occupied by quartz sand was calculated based on the height of the sand column, H, and the vessel radius, r:

$$V_{sand}[cm^3] =\ H[cm] \times\ \pi\ r^2\ [cm^2]$$

Then, the volume of solids was calculated using a measured porosity of θ = 0.22.

$$V_{solids}[cm^3] =\ (1-\theta)\ V_{sand}[cm^3]$$

The mass of sand was calculated using this volume of solids and the density of quartz ρ = 2.65 [g/cm^3].

Table B.2.1 specifies the individual parameter values used for each MFC reactor, and Table B.2.2 shows the calculated naphthalene sorbed to MFC reactor materials per unit gram.

Table B.2.1. Mass of sand calculated for each reactor based on its individual measurements

Reactor ID	Sand height (cm)	Volume filled with sand (cm^3)	Sand mass (g)	Initial naph. (mg/L)
ND_a	11.0	744	1538	15.2
ND_b	11.8	801	1656	15.1
NF_a	12.0	815	1685	14.8
NF_b	11.4	772	1595	14.9
NN_a	11.4	774	1599	0.0
NN_b	11.2	760	1571	0.0
BC_a	11.2	760	1571	15.0
BC_b	11.1	753	1557	14.9

Table B.2.2. Amount of naphthalene sorbed to each material per unit gram*.

Reactor ID	Anode chamber				Cathode chamber			
	K_d glass (L/g)	**K_d sand (L/g)**	**K_d iron pp (L/g)**	**K_d c. cloth (L/g)**	**K_d glass (L/g)**	**K_d sand (L/g)**	**K_d iron pp (L/g)**	**K_d c. cloth (L/g)**
	0.00011	0.00039	0.00253	0.259	0.00011	0.00039	0.00253	0.259
	Q_e glass (mg/g)	**Q_e sand (mg/g)**	**Q_e iron pp (mg/g)**	**Q_e c. cloth (mg/g)**	**Q_e glass (mg/g)**	**Q_e sand (mg/g)**	**Q_e iron pp (mg/g)**	**Q_e c. cloth (mg/g)**
ND_a	0.0016	0	0.038	3.22	0.0016	0.0025	0.038	2.63
ND_b	0.0016	0	0.038	3.21	0.0016	0.0024	0.038	2.63
NF_a	0.0016	0	0.037	3.14	0.0015	0.0023	0.037	2.57
NF_b	0.0016	0	0.038	3.16	0.0015	0.0024	0.038	2.59
BC_a	0.0016	0	0.038	3.18	0.0015	0.0025	0.038	2.60
BC_b	0.0016	0	0.038	3.17	0.0015	0.0025	0.038	2.60

*Top row shows the distribution coefficient for each material (average from sorption experiments).

The amount of naphthalene adsorbed by each material in anode and cathode chamber was determined using:

$$m_{naph\ sorbed}\ [mg] = m_{material}[g] \times Q_{e\ material}\left[\frac{mg}{g}\right]$$

To estimate the variability of the naphthalene sorbed to different materials due to errors in the K_d determination, three values were used: the average experimental K_d, an upper bound of $K_d = K_{d\ ave} + SD$, and a lower bound of $K_d = K_{d\ ave} - SD$, with SD the standard deviation. Table B.2.3 and Table B.2.4 present the naphthalene mass sorbed to each material between all MFCs.

Table B.2.3. Sensitivity analysis of the sorbed naphthalene estimate to K_d variability. Anode chamber.

Average naphthalene (mg) sorbed by material (ave K_d)				
	By glass	**By sand**	**By iron pp**	**By c. cloth**
Average	0.57338	0	0.00381	2.70
SD	4.72E-03	0	3.13E-05	2.22E-02
Lower bound for naphthalene (mg) sorbed by material (K_d - SD)				
	By glass	**By sand**	**By iron pp**	**By c. cloth**
Average	1.01544	0	0.00617	3.48
SD	8.36E-03	0	5.07E-05	2.86E-02
Upper bound naphthalene (mg) sorbed by material (K_d + SD)				
	By glass	**By sand**	**By iron pp**	**By c. cloth**
Average	0.10241	0	0.00145	1.81
SD	8.43E-04	0	1.19E-05	1.49E-02

Table B.2.4. Sensitivity analysis of the sorbed naphthalene estimate to K_d variability. Cathode chamber.

Average naphthalene (mg) sorbed by material (ave K_d)				
	By glass	**By sand**	**By iron pp**	**By c. cloth**
Average	0.420	3.91	0.001713	2.21
SD	3.46E-03	4.82E-02	1.41E-05	1.82E-02
Lower bound for naphthalene (mg) sorbed by material (K_d - SD)				
	By glass	**By sand**	**By iron pp**	**By c. cloth**
Average	0.730	4.58	0.002775	2.71
SD	6.01E-03	4.52E-02	2.28E-05	2.23E-02
Upper bound naphthalene (mg) sorbed by material (K_d + SD)				
	By glass	**By sand**	**By iron pp**	**By c. cloth**
Average	0.077	2.65	0.000652	1.58
SD	6.30E-04	4.70E-02	5.36E-06	1.30E-02

Appendix C – **Details on Analytical Chemistry Methods**

Appendix C includes analytical chemistry method details and data from the MFC experiments.

C.1 Naphthalene measurements from MFC experiments

Naphthalene measurement in MFC samples was performed in the same way as in the sorption experiment. Calibration curves with five points were typically used. Duplicate samples were analyzed to provide an estimate of errors. The average from duplicate samples is reported as the final concentration. See Chapter 2 for an example of calibration curve.

Table C.1.1. Naphthalene data from MFC experiments**.**

Sample ID	Reactor ID	Day	Naph (ppm)	Naph error (ppm)
ND_a 190711	ND_a	0	13.19	NA
ND_b 190711	ND_b	0	10.78	NA
NF_a 190711	NF_a	0	12.51	NA
NF_b 190711	NF_b	0	13.91	NA
ND_a 190718	ND_a	7	4.01	NA
ND_b 190718	ND_b	7	4.66	NA
NF_a 190718	NF_a	7	3.55	NA
NF_b 190718	NF_b	7	3.80	NA
ND_a 190725	ND_a	14	3.52	NA
ND_b 190725	ND_b	14	3.27	NA
NF_a 190725	NF_a	14	2.51	NA
NF_b 190725	NF_b	14	2.99	NA
ND_a 190801	ND_a	21	3.22	NA
ND_b 190801	ND_b	21	2.63	NA
NF_a 190801	NF_a	21	1.52	NA
NF_b 190801	NF_b	21	2.61	NA
ND_a 190808	ND_a	28	3.01	NA
ND_b 190808	ND_b	28	2.20	NA
NF_a 190808	NF_a	28	0.73	NA
NF_b 190808	NF_b	28	2.10	NA
ND_a 190815	ND_a	35	2.90	NA
ND_b 190815	ND_b	35	1.94	NA
NF_a 190815	NF_a	35	0.02	NA
NF_b 190815	NF_b	35	1.64	NA
ND_a 190828	ND_a	48	2.38	0.18
ND_b 190828	ND_b	48	1.02	0.07
NF_a 190828	NF_a	48	0.00	0.0008

Sample ID	Reactor ID	Day	Naph (ppm)	Naph error (ppm)
NF_b 190828	NF_b	48	0.45	0.003
NN_a 191119	NN_a	0	NA	NA
NN_b 191119	NN_b	0	NA	NA
NN_a 191126	NN_a	7	NA	NA
NN_b 191126	NN_b	7	NA	NA
NN_a 191203	NN_a	14	NA	NA
NN_b 191203	NN_b	14	NA	NA
BC_a 191203	BC_a	0	14.42	NA
BC_b 191203	BC_b	0	5.50	NA
NN_a 191210	NN_a	21	NA	NA
NN_b 191210	NN_b	21	NA	NA
BC_a 191210	BC_a	7	7.19	NA
BC_b 191210	BC_b	7	3.65	NA
BC_a 191217	BC_a	14	5.13	0.18
BC_b 191217	BC_b	14	2.93	0.10
NN_a 191217	NN_a	28	NA	NA
NN_b 191217	NN_b	28	NA	NA
NN_a 191224	NN_a	35	NA	NA
NN_b 191224	NN_b	35	NA	NA
BC_a 191224	BC_a	21	3.94	NA
BC_b 191224	BC_b	21	2.15	NA
BC_a 191231	BC_a	28	3.50	NA
BC_b 191231	BC_b	28	1.78	NA
NN_a 200107	NN_a	49	NA	NA
NN_b 200107	NN_b	49	NA	NA
BC_a 200107	BC_a	35	3.48	NA
BC_b 200107	BC_b	35	1.79	NA
BC_a 200121	BC_a	49	2.91	NA
BC_b 200121	BC_b	49	1.09	NA

C.2 Alkalinity measurement

Alkalinity measurements were done according to the protocols in (Rounds, 2012). Alkalinity was determined by analyzing acidimetric-titration data with the Gran function plot method. Subsamples were filtered and poured into a glass graduated cylinder immediately after collection. Time, initial pH, sample volume and temperature were recorded. Sulfuric acid was added in small increments to the sample, and the pH was measured. Gran function F1 was calculated using $F1 = (V_0 + V_t)(10^{-pH})$, where V_0 is the initial sample volume and V_t the total volume of acid titrant added. Then the bicarbonate equivalence point was determined by extrapolating a straight line through the data in the region beyond the equivalence point.

Alkalinity was calculated using $Alk\left(\frac{meq}{L}\right) = \frac{B(mL)\times C_a\left(\frac{meq}{L}\right)}{V_s(mL)\times\left(\frac{1L}{1000mL}\right)}$, where B is the volume of titrant added from the initial pH to the bicarbonate equivalence point, C_a is the acid normality, and V_s is the volume of the sample.

Titrant used was sulfuric acid approximately 0.18N. The solution was prepared by adding 0.5 mL concentrated H_2SO_4 to approximately 95 mL of fresh distilled deionized water. After mixing thoroughly, the solution was topped up with deionized water to the 100 mL mark. The normality of the titrant was checked before titrating samples, and re-standardized values were used for the alkalinity calculations.

Standardization of sulfuric acid was done by titrating the acid with fresh 0.01639N sodium carbonate solution and determining the equivalence point of the titration using the inflection point method. Standard solution of 0.01639N sodium carbonate (Na_2CO_3) was prepared by drying 1.0 gram (g) of Na_2CO_3 at 150°C for 2 hours, cooling in a desiccator; adding 0.8686 g of dried and cooled Na_2CO_3 to a 1 L volumetric flask and diluting to the 1 L mark with distilled de-ionized water.

Acid normality was calculated using $C_a\left(\frac{eq}{L}\right) = (25\ mL)\left(\frac{0.01639\frac{eq}{L}}{V_a(mL)}\right)$, where 25 mL is the volume of sodium bicarbonate standard solution, and V_a is the volume of sulfuric acid added to reach the

equivalence point. As a check, acid normality was also calculated using the Gran function method.

Sulfuric acid standardization example

Table C.2.1. Sulfuric acid standardization data record sheet example.

Date	19-Dec-19	
Sample vol	5.0698	mL
C_a =	0.1490	
V_a=	0.5575	ml
Na_2CO3 N =	0.01639	
Na_2CO_3 weight =	0.8689	g
Na_2CO_3 MW =	105.989	g/mol

Table C.2.2. Sulfuric acid standardization data, pH, acid added, Gran function F1 and slope values for example.

pH	acid added (uL)	acid added total (uL)	acid added total (mL)	Gran fn. F1	delta pH	delta mL	ΔpH/ΔmL
11.04	0	0	0	0			
9.74	200	200	0.2	3.64E-11	1.3	0.2	6.5
7.31	100	300	0.3	1.47E-08	2.43	0.1	24.3
6.46	100	400	0.4	1.39E-07	0.85	0.1	8.5
6.05	68	468	0.468	4.17E-07	0.41	0.068	6.0
5.77	32	500	0.5	8.49E-07	0.28	0.032	8.8
3.84	50	550	0.55	7.95E-05	1.93	0.05	38.6
3.36	20	570	0.57	0.000249	0.48	0.02	24.0
3.16	20	590	0.59	0.000408	0.2	0.02	10.0
2.95	30	620	0.62	0.000696	0.21	0.03	7.0
2.81	30	650	0.65	0.001007	0.14	0.03	4.7
2.68	30	680	0.68	0.001421	0.13	0.03	4.3
2.57	40	720	0.72	0.001938	0.11	0.04	2.8

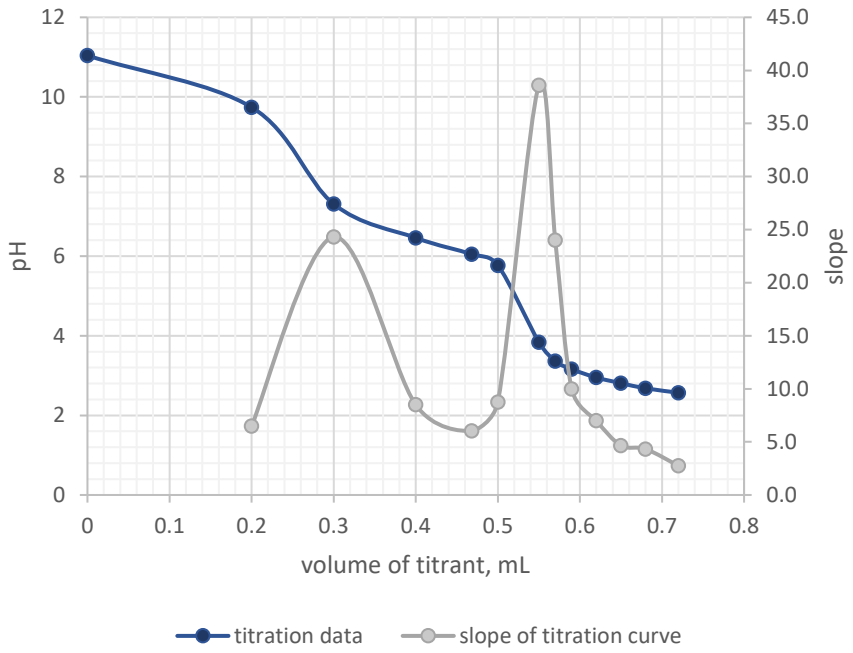

Figure C.2.1. Alkalinity titration plot for sulfuric acid solution standardization example. pH and slope of the pH curve vs total acid added.

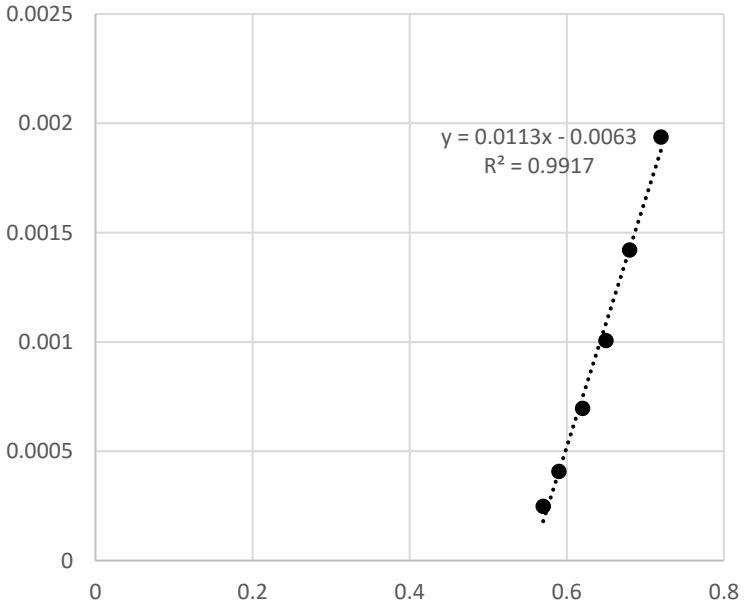

Figure C.2.2. Alkalinity titration Gran function F1 vs total acid added, for sulfuric acid standardization example.

Alkalinity titration example

Table C.2.3. Alkalinity titration data record sheet example.

Sample ID	NN_b 191224	
Date	24-Dec-19	
Start time	9:45	
pH_i	7.46	
Sample vol.	3.2424	mL
Titrant N	0.1490	N
T	22	°C
Alkalinity=	**23.5**	**meq/L**
B=	0.512	
Trend line parameters (y=mx+b)		
m=	0.0973	
b=	-0.0499	

Table C.2.4. Alkalinity titration data record, pH, acid added and Gran function F1 values, for sample NN_b 191224

pH	acid added (µL)	acid added total (µL)	acid added total (mL)	Gran fn F1
7.46	0	0	0	1.12E-07
6.42	200	200	0.2	1.31E-06
6.07	100	300	0.3	3.02E-06
5.92	50	350	0.35	4.32E-06
5.7	50	400	0.4	7.27E-06
5.39	50	450	0.45	1.5E-05
4.69	50	500	0.5	7.64E-05
3.64	20	520	0.52	0.000862
3.18	20	540	0.54	0.002499
2.91	20	560	0.56	0.004678
2.7	30	590	0.59	0.007647
2.53	40	630	0.63	0.011428

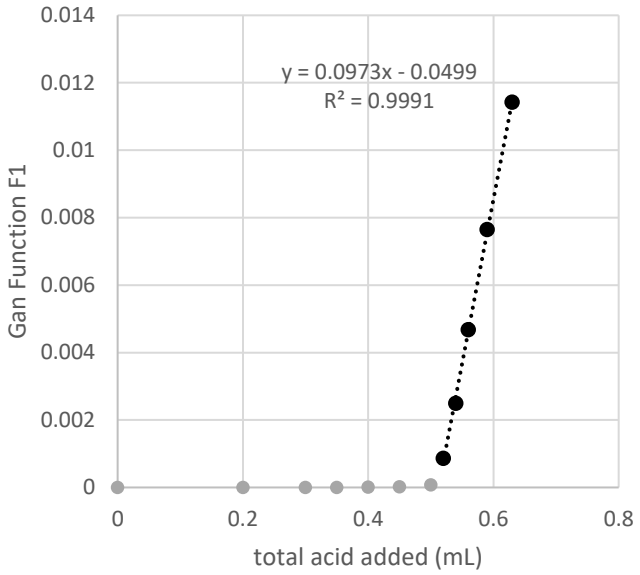

Figure C.2.3. Alkalinity titration Gran function F1 vs total acid added, for sample NN_b 191224.

Alkalinity data for MFC experiments

Table C.2.5. Alkalinity and pH data for all MFC experiment samples.

Sample ID	Reactor ID	pH	Alk (meq/L)
B3 ND_a 190711	ND_a	7.41	25.10
B3 ND_a 190718	ND_a	7.44	25.23
B3 ND_a 190725	ND_a	7.49	24.93
B3 ND_a 190801	ND_a	7.54	25.89
B3 ND_a 190808	ND_a	7.6	25.71
B3 ND_a 190815	ND_a	7.58	25.19
B3 ND_a 190828	ND_a	7.67	25.88
B3 ND_a 190828_d	ND_a	7.65	25.63
B3 ND_a 190828	ND_a	7.66	25.75
B3 ND_b 190711	ND_b	7.48	25.26
B3 ND_b 190718	ND_b	7.48	24.91
B3 ND_b 190725	ND_b	7.53	24.97
B3 ND_b 190801	ND_b	7.59	25.10
B3 ND_b 190808	ND_b	7.62	24.93
B3 ND_b 190815	ND_b	7.66	26.94
B3 ND_b 190828	ND_b	7.65	24.42
B3 ND_b 190828_d	ND_b	7.67	24.47
B3 ND_b 190828	ND_b	7.66	24.45
B3 NF_a 190711	NF_a	7.57	27.61
B3 NF_a 190718	NF_a	7.65	27.83

Sample ID	Reactor ID	pH	Alk (meq/L)
B3 NF_a 190725	NF_a	7.71	28.07
B3 NF_a 190801	NF_a	7.67	27.97
B3 NF_a 190808	NF_a	7.68	27.56
B3 NF_a 190815	NF_a	7.63	28.54
B3 NF_a 190828	NF_a	7.71	27.06
B3 NF_a 190828_d	NF_a	7.69	27.73
B3 NF_a 190828	NF_a	7.7	27.39
B3 NF_b 190711	NF_b	7.64	27.74
B3 NF_b 190718	NF_b	7.65	28.34
B3 NF_b 190725	NF_b	7.66	28.61
B3 NF_b 190801	NF_b	7.6	27.81
B3 NF_b 190808	NF_b	7.69	27.12
B3 NF_b 190815	NF_b	7.68	29.12
B3 NF_b 190828	NF_b	7.72	26.83
B3 NF_b 190828_d	NF_b	7.72	27.80
B3 NF_b 190828	NF_b	7.72	27.31
B3 NN_a 191119	NN_a	7.32	23.58
B3 NN_a 191126	NN_a	7.34	23.34
B3 NN_a 191203	NN_a	7.35	23.99
B3 NN_a 191210	NN_a	7.32	23.84
B3 NN_a 191217	NN_a	7.24	22.98
B3 NN_a 191224	NN_a	7.2	22.31
B3 NN_a 200107	NN_a	7.3	22.40
B3 NN_b 191119	NN_b	7.4	22.36
B3 NN_b 191126	NN_b	7.37	23.28
B3 NN_b 191203	NN_b	7.39	23.94
B3 NN_b 191210	NN_b	7.35	23.50
B3 NN_b 191217	NN_b	7.4	23.48
B3 NN_b 191224	NN_b	7.46	23.55
B3 NN_b 200107	NN_b	7.62	23.31
B3 BC_a 191203	BC_a	7.35	24.02
B3 BC_a 191210	BC_a	7.31	25.50
B3 BC_a 191217	BC_a	7.46	24.60
B3 BC_a 191224	BC_a	7.26	23.73
B3 BC_a 191231	BC_a	7.26	23.77
B3 BC_a 200107	BC_a	7.32	23.52
B3 BC_a 200121	BC_a	7.38	24.86
B3 BC_b 191203	BC_b	7.35	24.02
B3 BC_b 191210	BC_b	7.33	25.15
B3 BC_b 191217	BC_b	7.42	25.25
B3 BC_b 191224	BC_b	7.35	25.95

Sample ID	Reactor ID	pH	Alk (meq/L)
B3 BC_b 191231	BC_b	7.31	24.71
B3 BC_b 200107	BC_b	7.38	24.38
B3 BC_b 200121	BC_b	7.45	27.66

C.3 Cation measurements

Cation data processing method

To determine the Limit of Detection and Limit of Quantitation (LOD and LOQ):

- Calculate the internal standard recovery factor.
  ISTD recovery = ISTD counts in sample/ ISTD counts in blank (internal standard was Sc).

  This is done for the 3 standards of lowest concentration. Sc 335 (nm) was the wavelength used.

  Correct the 3 lower standards intensities by the ISTD recovery factor (recalculate intensities).
- Calculate the sensitivity factor (counts/ppm) using the low concentration standards
  Sensitivity (counts/ppm) = slope(corrected std. intensities, std. known concentrations)
  ** For K, in some analysis rounds, the intensity of the 2 lowest standards was not linear, so standards 3-5 were used to determine the sensitivity.
- Calculate LOD and LOQ for each element and each wavelength
  LOD[counts] = Blank intensity + 3*SD(Blank intensity)

  LOQ[counts] = Blank intensity + 10*SD(Blank intensity)
- Convert the LOD and LOQ from counts to ppm by dividing by the sensitivity

Table C.3.1. Internal standard (ISTD) recovery factor for the three lowest standards. Example from one cation analysis round. Different standards were used for sulfur (S) and all the other elements analyzed (ME, multi element standard)

	Standard 1	Standard 2	Standard 3
ISTD recovery =	0.999430	1.008921	1.021301
	Standard 1	**Standard 2**	**Standard 3**
Conc. ME (ppm)	0.099	0.502	1.01
Conc. S (ppm)	0.095	0.485	0.96

Table C.3.2. Raw and corrected intensity data for cation analysis. Example from one analysis round.

Element	Raw data (intensities)					Intensities corrected by ISTD recovery		
	Blank	Blank (SD)	Standard 1	Standard 2	Standard 3	Standard 1	Standard 2	Standard 3
Al 236.705	9.572	1.46	15.88	43.56	81.36	15.9	43.9	83.1
Al 394.401	33.246	3.23	73.18	277.7	522.2	73.1	280.2	533.3
Al 396.152	21.325	10.92	213	934.5	1836	212.9	942.8	1875.1
Ca 318.127	29.214	2.69	62.49	93.21	145.8	62.5	94.0	148.9
Ca 393.366	1116.269	6.47	15740	63330	121100	15731.0	63895.0	123679.5
Ca 422.673	27.736	12.83	291.4	1152	2223	291.2	1162.3	2270.4
Co 237.863	6.039	1.25	60.4	280.8	562.5	60.4	283.3	574.5
Co 238.892	5.932	2.04	68.2	327	652	68.2	329.9	665.9
Cu 224.700	3.900	2.11	22.27	86.34	164.7	22.3	87.1	168.2
Cu 327.395	9.282	1.47	276.4	1364	2724	276.2	1376.2	2782.0
Fe 238.204	11.568	4.39	156.3	744.3	1490	156.2	750.9	1521.7
Fe 239.563	5.026	2.58	30.16	139.5	282.1	30.1	140.7	288.1
K 769.897	2696.991	40.44	2672	2706	2813	2670.5	2730.1	2872.9
Mg 280.270	10.634	1.44	658	3219	6452	657.6	3247.7	6589.4
Mg 285.213	6.820	0.59	228.9	1087	2174	228.8	1096.7	2220.3
Mn 257.610	8.273	0.74	1018	5076	10150	1017.4	5121.3	10366.2
Mn 293.931	8.769	1.80	226.9	1110	2221	226.8	1119.9	2268.3
Mo 201.512	2.293	2.38	14.38	64.68	120.5	14.4	65.3	123.1
Mo 204.598	2.296	1.16	20.18	83.88	167.9	20.2	84.6	171.5
Na 588.995	2338.745	122.41	3257	5366	7547	3255.1	5413.9	7707.8
Na 589.592	52.886	16.34	644	2331	4290	643.6	2351.8	4381.4
Ni 222.486	6.782	3.44	21.56	98.55	187.3	21.5	99.4	191.3
Ni 230.299	3.116	0.76	47.44	227.5	451.2	47.4	229.5	460.8
S 180.669	4.575	0.74	8.44	20.48	35.79	8.4	20.7	36.6
S 181.972	4.341	2.33	7.953	22.55	39.69	7.9	22.8	40.5
S 182.562	3.211	1.98	4.401	7.71	12.95	4.4	7.8	13.2
Si 250.690	13.940	0.70	28.64	86.92	171.1	28.6	87.7	174.7
Si 251.432	9.696	1.75	16.09	42.3	77.84	16.1	42.7	79.5
Si 288.158	42.700	8.43	79.68	249.3	460.1	79.6	251.5	469.9
Sr 216.596	3.967	1.35	32.29	156	306.6	32.3	157.4	313.1

Element	Raw data (intensities)					Intensities corrected by ISTD recovery		
	Blank	Blank (SD)	Standard 1	Standard 2	Standard 3	Standard 1	Standard 2	Standard 3
Sr 407.771	103.458	8.56	20970	104200	210900	20958.1	105129.6	215392.3
Sr 460.733	479.527	1.63	671.5	1382	2247	671.1	1394.3	2294.9

Table C.3.3. Sensitivity, LOD and LOQ for elements and wavelengths corrected by ISTD recovery factor. Example.

Element	Sensitivity counts/ppm	LOD counts	LOD ppm	LOQ counts	LOQ ppm
Al 236.705	74	14	0.19	24	0.33
Al 394.401	505	43	0.09	66	0.13
Al 396.152	1825	54	0.03	130	0.07
Ca 318.127	95	37	0.39	56	0.59
Ca 393.366	118460	1136	0.01	1181	0.01
Ca 422.673	2173	66	0.03	156	0.07
Co 237.863	565	10	0.02	19	0.03
Co 238.892	656	12	0.02	26	0.04
Cu 224.700	160	10	0.06	25	0.16
Cu 327.395	2751	14	0.00	24	0.01
Fe 238.204	1500	25	0.02	55	0.04
Fe 239.563	283	13	0.05	31	0.11
K 769.897	225	2818	12.54	3101	13.80
Mg 280.270	6514	15	0.00	25	0.00
Mg 285.213	2187	9	0.00	13	0.01
Mn 257.610	10265	11	0.00	16	0.00
Mn 293.931	2242	14	0.01	27	0.01
Mo 201.512	119	9	0.08	26	0.22
Mo 204.598	166	6	0.03	14	0.08
Na 588.995	4872	2706	0.56	3563	0.73
Na 589.592	4098	102	0.02	216	0.05
Ni 222.486	186	17	0.09	41	0.22
Ni 230.299	454	5	0.01	11	0.02
S 180.669	31	7	0.22	12	0.39
S 181.972	36	11	0.32	28	0.77
S 182.562	10	9	0.94	23	2.37
Si 250.690	161	16	0.10	21	0.13
Si 251.432	70	15	0.21	27	0.39
Si 288.158	428	68	0.16	127	0.30
Sr 216.596	308	8	0.03	18	0.06
Sr 407.771	213584	129	0.00	189	0.00
Sr 460.733	1782	484	0.27	496	0.28

To calculate final concentrations, data below the LOD were removed, and %RSD was calculated between all wavelengths for each element. The average concentration value between all element wavelengths was used as the final concentration, providing RSD < 5%. After checking %RSD for Na wavelengths it was decided that the 589 Na wavelength had interferences and Na 588 was used for the final concentration. Measurements were corrected for dilution using the dilution factor (DF) determined at the time of sampling or diluting samples prior to analysis.

Table C.3.4. Concentrations of standards used in the example analysis round.

Sample ID	Ca	Fe	K	Mg	Na	S	Si
Blank	<0.4	<0.05	<12.5	<0.004	<0.6	<0.94	<0.2
Standard 1	<0.4	<0.11	<12.5	0.1	<0.6	<0.94	<0.2
Standard 2	<0.6	0.5	<12.5	0.5	<0.6	<0.94	0.5
Standard 3	1.0	1.0	<12.5	1.0	1.0	<2.37	1.0
Standard 4	2.5	2.5	<12.5	2.5	2.5	2.5	2.5
Standard 5	5.0	5.0	<12.5	5.0	5.0	4.9	5.0
Standard 6	10.2	10.2	<12.5	10.2	10.2	9.7	10.2
Standard 7	25.4	25.4	25.4	25.4	25.4	24.6	25.4
Standard 8	50.6	50.6	50.6	50.6	50.6	48.9	50.6
Standard 9	75.3	75.3	75.3	75.3	75.3		75.3
Standard 10	100.0	100.0	100.0	100.0	100.0		100.0

Table C.3.5. Final cation concentrations for samples analyzed in the example round.

Sample ID	Ca	Fe	K	Mg	Na	S	Si
ND_a 190815	29.5	1.2	344.3	47.6	1220.8	134.3	2.1
ND_b 190815	28.8	1.3	341.3	46.8	1228.6	136.3	2.1
NF_a 190815	30.3	<0.05	340.5	51.2	1230.3	138.7	2.6
NF_b 190815	30.5	<0.05	345.1	51.8	1237.1	141.1	2.3
ND_a 190828_dup1	29.4	0.9	342.0	47.7	1228.5	135.1	2.7
ND_a 190828_dup2	30.2	1.0	346.3	48.4	1240.2	137.2	2.8
ND_b 190828_dup1	28.2	1.2	340.9	46.9	1224.2	137.0	2.6
ND_b 190828_dup2	28.1	1.2	336.9	46.7	1215.6	136.9	2.7
NF_a 190828_dup1	30.5	<0.05	339.3	51.7	1237.2	140.7	3.4
NF_a 190828_dup2	30.3	<0.05	337.6	51.3	1238.1	139.6	3.4
NF_b 190828_dup1	29.6	<0.05	339.3	50.6	1212.2	138.1	2.9
NF_b 190828_dup2	30.7	<0.05	350.0	51.9	1249.3	141.6	2.9
ND_a 190815_d10	26.6	<0.11	299.4	42.1	1156.9	118.3	<0.4
ND_b 190815_d10	26.1	<0.11	292.7	41.4	1157.6	120.4	<0.4
NF_a 190815_d10	27.5	<0.05	292.6	45.3	1167.0	122.8	<0.4
NF_b 190815_d10	27.0	<0.05	299.6	45.4	1169.4	123.5	<0.4
ND_a 190828_dup1_d10	27.0	<0.11	299.8	42.8	1176.4	119.4	<0.4
ND_a 190828_dup2_d10	27.0	<0.11	306.7	42.8	1173.5	120.9	<0.4
ND_b 190828_dup1_d10	25.3	<0.11	294.2	41.3	1152.0	119.6	<0.4
ND_b 190828_dup2_d10	25.7	<0.11	300.1	41.4	1154.0	120.8	<0.4
NF_a 190828_dup1_d10	27.1	<0.05	294.4	45.4	1173.5	123.6	<0.4
NF_a 190828_dup2_d10	27.3	<0.05	292.7	45.5	1171.6	123.0	<0.4
NF_b 190828_dup1_d10	27.2	<0.05	298.4	45.6	1170.3	123.1	<0.4
NF_b 190828_dup2_d10	27.2	<0.05	303.6	45.7	1173.1	124.3	<0.4

"_dup" samples correspond to duplicates.
"_d10" denotes diluted samples; concentrations reported incorporate dilution factor correction.

C.4 Anion measurements

Seven standard solutions were prepared from a 1 mM multi-anion stock solution (F^-, Cl^-, NO^{2-}, NO_3^-, SO_4^{2-}, $S_2O_3^{2-}$, PO_4^{3-}) for each analysis round (0, 3, 10, 30, 100, 300, 1000 µmol/L standards were used). Check samples (50 µmol/L) were used to determine measurement errors. Samples were diluted 1:100 to match the range of standard solutions. The analysis batch included three blanks, an initial calibration check (set of standards), the sample batch with a 50 check µmol/L sample somewhere in the middle, a rinse, a blank, and a final calibration check (set of standards). Errors were calculated using duplicate samples. Values blow LOD and LOQ were removed, and data was corrected for dilution before reporting final concentrations.

Table C.4.1. Raw concentration data for anion samples. Example.

Sample #	DF	Cl^- µmol/L	NO_3^- µmol/L	SO_4^{2-} µmol/L	PO_4^{3-} µmol/L
Standard 0		n.a.	165.5712	10385.5228	8023.5261
Standard 0		n.a.	n.a.	n.a.	5.8134
Standard 0		n.a.	8.208	2.0656	n.a.
Standard 3 µmol/L		3.388	10.0137	7.981	2.2672
Standard 10 µmol/L		9.7843	10.295	14.5712	11.0794
Standard 30 µmol/L		30.3514	24.1669	31.2486	28.6037
Standard 100 µmol/L		95.743	97.5109	96.6929	93.0635
Standard 300 µmol/L		298.6334	289.7692	293.8354	293.992
Standard 1000 µmol/L		999.7624	992.9721	991.7885	991.6845
Standard 0		n.a.	n.a.	0.7526	1.8915
Standard 0		n.a.	n.a.	n.a.	2.2125
NN_a 191126	0.00877	316.3174	n.a.	33.9375	3.7245
NN_a 191203	0.00872	319.7811	n.a.	33.9259	3.4103
NN_a 191210	0.00901	324.0115	n.a.	34.0032	3.3054
NN_a 191217	0.009	335.5678	n.a.	34.7012	3.2623
NN_a 191217_d	0.00899	331.6662	n.a.	34.131	2.7995
NN_a 191224	0.00898	331.85	n.a.	33.1446	2.9031
NN_a 200107	0.00903	328.177	0.0671	33.9823	2.4895
NN_b 191126	0.00879	319.7279	0.7149	33.6375	2.515
NN_b 191203	0.00872	325.6958	0.3217	33.0575	2.2771
NN_b 191210	0.009	328.5587	0.3455	33.5617	2.7742
NN_b 191217	0.00898	319.3934	0.5737	33.1556	2.0912
NN_b 191217_d	0.00897	328.7835	n.a.	33.3264	2.542
NN_b 191224	0.009	328.0886	n.a.	32.3139	2.5329
NN_b 200107	0.00899	324.6703	0.316	32.9384	2.033
Check sample 50 µM	1	48.2188	47.1434	46.8163	42.496

Sample #	DF	Cl^- µmol/L	NO_3^- µmol/L	SO_4^{2-} µmol/L	PO_4^{3-} µmol/L
BC_c 191203	0.00858	295.3146	0.5042	29.9798	2.07
BC_c 191210	0.00879	316.1648	1.5825	31.9683	1.7729
BC_c 191217	0.00898	324.6764	2.1642	32.5985	2.1509
BC_c 191217_d	0.00902	328.2569	0.8533	32.7154	2.1843
BC_c 191224	0.00897	322.6857	1.208	32.5672	2.3146
BC_c 191231	0.009	327.7243	0.8989	32.6181	2.2512
BC_c 200107	0.00897	321.1046	0.3376	32.0498	2.302
BC_c 200121	0.00899	344.9966	n.a.	34.9108	2.3815
BC_d 191203	0.00873	310.0337	n.a.	32.038	2.3698
BC_d 191210	0.00899	319.3429	n.a.	33.109	2.4302
BC_d 191217	0.00897	319.3972	n.a.	31.861	2.3169
BC_d 191217_d	0.009	320.3944	n.a.	31.8463	2.458
BC_d 191224	0.009	323.3337	n.a.	32.8811	2.349
BC_d 191231	0.00898	320.2429	n.a.	33.5749	2.3917
BC_d 200107	0.00898	323.0921	n.a.	33.8353	2.4017
BC_d 200121	0.00897	339.2131	n.a.	34.9243	2.2512
NN_a 191119	0.01	352.0749	n.a.	35.0392	4.3593
NN_b 191119	0.01	352.3204	n.a.	35.7546	4.2359
rinse		n.a.	n.a.	n.a.	n.a.
Blank		0.9965	0.9395	n.a.	2.4038
Standard 0		0.9972	0.4387	n.a.	2.398
Standard 3 µmol/L		3.5054	3.8698	1.0671	4.2701
Standard 10 µmol/L		11.2592	10.2933	13.8509	10.4807
Standard 30 µmol/L		30.9409	30.0104	32.0099	27.1314
Standard 100 µmol/L		97.6852	99.6485	98.8544	96.2657
Standard 300 µmol/L		299.7476	301.5009	303.9215	303.7792
Standard 1000 µmol/L		1001.3286	1010.0761	1009.1386	1010.1619
Standard 0		1.5961	n.a.	n.a.	3.8846
Standard 0		1.2771	n.a.	n.a.	2.8339

Appendix D **– MFC Experiments Set-up Protocol**

Appendix D includes additional methods for MFC experiments: media preparation details, media compositions, and reactor set-up instructions.

D.1 MFC microbial media preparation

1. Prepare basal media according to recipe

Modified Basal Media	**1 L media***	
Distilled water	1	L
NaCl	1	g
$MgCl_2 \cdot 6H_2O$	0.4	g
$CaCI_2 \cdot 2H_2O$	0.1	g
Na_2SO_4**	0.6	g**
NH_4Cl	0.25	g
KH_2PO_4	0.2	g
KCI	0.5	g

**Sulfate content was modified from original recipe to resemble Kidd 2 site (using less than Widdel and Bak)

- Add salts one by one to less than 1 L water, top up to 967 mL (*) to have space for 30 mL of bicarbonate buffer and 3 mL of vitamins and trace elements.

2. Prepare trace element mixture and selenite-tungstate solution

Non-chelated trace element mixture				
Distilled water	987	ml		
HCI (25% = 7.7 M)	12.5	ml	100	mM
$FeSO_4 \cdot 7H_2O$*	2100	mg	7.5	mM
H_3BO_3	30	mg	0.5	mM
$MnCl_2 \cdot 4H_2O$	100	mg	0.5	mM
$CoCl_2 \cdot 6H_2O$	190	mg	0.8	mM
$NiCl_2 \cdot 6H_2O$	24	mg	0.1	mM
$CuCl_2 \cdot 2H2O$	2	mg	0.01	mM
$ZnSO_4 \cdot 7H_2O$*	144	mg	0.5	mM
$Na_2MoO_4 \cdot 2H_2O$	36	mg	0.15	mM

3. Prepare bicarbonate buffer 1 M in a 500 mL bottle with rubber stoppers

Bicarbonate buffer solution				
Distilled water	250	ml		
$NaHCO_3$	21000	mg	999.9	mM

   – Measure and add $NaHCO_3$ to the bottle, then add DI water. Do not mix. Seal with rubber stopper and crimp seal and flush the headspace with N_2/CO_2 gas mix (this is to prevent water with bicarbonate to equilibrate with atmospheric CO_2).

4. Autoclave media, bicarbonate buffer solution and glass wool filter for gas station.
   – Use Liquid 3 cycle. While autoclaving, flush gas lines in gas station with N_2 and turn on the heat in the graphite O_2 scrubber.

5. Replace headspace in media bottles with N_2 gas (CO_2/N_2 for bicarbonate solution) and let cool.
   – Put media bottles on stir plates at about 1000 rpm.
   – First, pierce septa with a 22-gauge needle (black) to evacuate steam.
   – Then pierce septa with an 18-gauge (pink) needle attached to an Acrodisk to flush with N_2 gas. Flush with gas for 5 min.
   – 20 seconds before the time is over remove black needle to over pressurize the headspace in the bottle a little to help prevent atmospheric oxygen ingress after the bottle cools down completely.
   – Let media cool down completely before doing the additions
   – Close gas tanks.

6. Prepare vitamin mixture (1mL per L)

Vitamin mixture			
Sodium phosphate buffer	(10 mM; pH 7.1)	100	ml
4-Aminobenzoic acid		4	mg
D(+)-Biotin		1	mg
Nicotinic acid		10	mg
Calcium D(+)-panthothenate		5	mg
Pyridoxine dihydrochloride		15	mg

7. Prepare B12 vitamin solution (1mL per L)

Vitamin B12 solution		
Distilled water	100	mL
Cyanocobalamin	5	mg

8. Additions

Put bottles on stir plates and pierce septa with a black and pink needle (out and in lines). While flushing with N_2/CO_2 gas mix (through Acrodisk), add:

- Add 1 mL of vitamin mix (through Acrodisk)
- Add 1 mL of vitamin B12 solution (t through Acrodisk)
- Add 1 mL of trace element mix solution (through Acrodisk)
- Add 1 mL of selenite-tungstate solution (through Acrodisk)
- Add 30 mL of bicarbonate buffer 1 M (sterile)

Note: for additions through Acrodisk, draw 2.5 ml into syringe, put Acrodisk on, flush Acrodisk with 0.5 ml of solution, then add 1 ml to each of the stirring flushing bottles.

9. Sub sample 10 mL and check pH in all bottles
   - Set up a small flushing station with a bottle connected to a back flow catcher and the oxygen scrubber connected to the N_2/CO_2 gas line
   - Flush syringe 3 times with N_2/CO_2
   - The fourth time, draw 10 mL of gas, put on a 22-gauge black needle, and flush it with the gas
   - Puncture the media bottle stopper, inject the gas
   - Invert the bottle and draw 10 ml of sample
   - Pour sample into small beaker and read pH
10. Prepare $FeCl_2$ solution

$FeCl_2$ solution 360 mM		
De-aired distilled water	100	mL
$FeCl_2$	4563	mg

This is done inside the anaerobic chamber, check chamber status O_2 = 0 ppm.

11. Add 5 ml of 360 mM Fe2Cl solution through an Acrodisk to each 1L media bottle inside the anaerobic chamber
12. Sample bottles and adjust pH
13. Add naphthalene to media bottles.
14. Remove rubber septa from bottles, add 15 mg of naphthalene and re-cap with a purple plastic cap
15. Stir bottles for 2-3 days to allow low-solubility naphthalene to dissolve
16. Prepare inoculum
    - Flush a rubber stoppered media bottle with N_2 gas
    - Add 200 cc sediments to it and re-flush it (record the mass of sediments added for reference)
    - Bring inside the anaerobic chamber
    - Aseptically add 200 cc of prepared media (from the extra one prepared) to the bottle with sediments (with a sterile syringe and needles through the stoppers in each bottle)
    - Shake water and sediments, and let settle horizontally
    - Take a 15 ml sample of the inoculum for DNA analysis, centrifuge this sample at 10000 rcf (= 8819 rpm) for 20 min, decant water and store pellet at -20°C.
17. Draw 10 cc of supernatant and inoculate media bottles

D.2 Reactor set up instructions

1. Assemble reactors.
2. Autoclave the sand (Dry30 cycle) and bring into the anaerobic chamber for 2-3 days to de-air
3. Bring inside the chamber: Reactor vessels, glass rod, parafilm
4. Check chamber status
5. Add 1L media to reactor, use glass rod to help get the water to the anode chamber
6. Add 400 ml more of media and let the sand settle through the water in the cathode chamber
7. Seal top of reactor with parafilm and bring outside the anaerobic chamber
8. Sample anode chamber water initial conditions
9. Put in the cathode, and solder resistance to the wire
10. Connect wire to datalogger

D.3 Microbial media composition

Table D.3.1 shows the chemical composition of the media used in the MFCs, calculated based on the salt additions specified in Chapter 3.

Table D.3.1. MFC microbial media composition.

Element or compound	Concentration	
	mM	mg/L
Naphthalene	0.1	15
Na	55.6	1279
Cl	37.4	1327
Mg	2.0	48
Ca	0.7	27
SO_4^{-2}	4.2	406
NH_4^{+}	4.7	84
K	8.2	327
PO_4^{-2}	1.5	141
Fe	1.8	101

Appendix E – **Naphthalene Mass Distribution in MFC Reactors**

Appendix E includes data associated with Figure 3.11, and the determination of the mass distribution of naphthalene in anode chamber of the MFC experiments. Aqueous naphthalene corresponds to dissolved naphthalene, from weekly samples measured via GC-MS. The mass sorbed to the carbon cloth anode was determined based on the aqueous concentration and the experimental K_d of the carbon cloth, obtained from the sorption experiment. Degraded naphthalene was determined based on a mass balance and considering diffusion between anode and cathode chambers.

Table E.1. Naphthalene concentration or mass sorbed to MFC components according to calculations or measurements**.** BC experiments.

Reactor ID	Day	anode chamber (mg/L)	anode chamber (mM)	sorbed anode (mg)	sorbed anode (mmol)	sorbed sand (mg)	sorbed sand (mmol)	sorbed cathode (mg)	sorbed cathode (mmol)	cathode chamber (mg/L)
BC_a	0	14.97	1.17E-01	2.70	2.11E-02	1.10	8.56E-03	2.13	1.66E-02	6.91
BC_a	0.1	14.42	1.12E-01	3.17	2.48E-02	0.62	4.85E-03	1.53	1.19E-02	6.93
BC_a	6.9	7.19	5.61E-02	1.58	1.24E-02	0.71	5.54E-03	1.74	1.36E-02	7.92
BC_a	13.9	5.31	4.14E-02	1.17	9.12E-03	0.70	5.47E-03	1.72	1.34E-02	7.82
BC_a	20.7	3.94	3.07E-02	0.87	6.77E-03	0.67	5.24E-03	1.65	1.29E-02	7.48
BC_a	27.7	3.50	2.73E-02	0.77	6.01E-03	0.63	4.90E-03	1.54	1.20E-02	7.00
BC_a	34.9	3.48	2.72E-02	0.77	5.98E-03	0.58	4.56E-03	1.43	1.12E-02	6.51
BC_a	48.8	2.91	2.27E-02	0.64	5.00E-03	0.51	3.99E-03	1.25	9.78E-03	5.70
BC_b	0.0	14.95	1.17E-01	2.70	2.10E-02	1.10	8.55E-03	2.12	1.66E-02	6.90
BC_b	0.1	5.50	4.29E-02	1.21	9.45E-03	0.62	4.85E-03	1.52	1.19E-02	6.92
BC_b	6.9	3.65	2.85E-02	0.80	6.27E-03	0.60	4.71E-03	1.48	1.16E-02	6.74
BC_b	13.9	2.84	2.21E-02	0.62	4.87E-03	0.57	4.42E-03	1.39	1.08E-02	6.32
BC_b	20.8	2.15	1.68E-02	0.47	3.70E-03	0.52	4.10E-03	1.29	1.01E-02	5.85
BC_b	27.7	1.78	1.39E-02	0.39	3.06E-03	0.48	3.74E-03	1.18	9.19E-03	5.35
BC_b	34.9	1.79	1.39E-02	0.39	3.07E-03	0.44	3.39E-03	1.07	8.33E-03	4.85
BC_b	48.8	1.09	8.53E-03	0.24	1.88E-03	0.36	2.82E-03	0.89	6.91E-03	4.03

Table E.2. Naphthalene concentration or mass sorbed to MFC components according to calculations or measurements. ND experiments.

Reactor ID	Day	anode chamber (mg/L)	anode chamber (mM)	sorbed anode (mg)	sorbed anode (mmol)	sorbed sand (mg)	sorbed sand (mmol)	sorbed cathode (mg)	sorbed cathode (mmol)	cathode chamber (mg/L)
ND_a	0.0	15.15	1.18E-01	2.73	2.13E-02	1.11	8.66E-03	2.15	1.68E-02	7.00
ND_a	0.1	13.19	1.03E-01	2.90	2.26E-02	0.63	4.91E-03	1.54	1.21E-02	7.02
ND_a	6.8	4.01	3.13E-02	0.88	6.88E-03	0.70	5.47E-03	1.72	1.34E-02	7.82
ND_a	13.7	3.52	2.74E-02	0.77	6.04E-03	0.66	5.11E-03	1.61	1.25E-02	7.31
ND_a	20.8	3.22	2.51E-02	0.71	5.53E-03	0.61	4.75E-03	1.49	1.17E-02	6.78
ND_a	27.7	3.01	2.35E-02	0.66	5.18E-03	0.57	4.41E-03	1.39	1.08E-02	6.31
ND_a	34.7	2.90	2.27E-02	0.64	4.99E-03	0.53	4.10E-03	1.29	1.01E-02	5.86
ND_a	47.7	2.38	1.86E-02	0.52	4.09E-03	0.46	3.58E-03	1.13	8.78E-03	5.11
ND_b	0.1	10.78	8.41E-02	2.37	1.85E-02	0.63	4.89E-03	1.54	1.20E-02	6.99
ND_b	6.8	4.66	3.64E-02	1.03	8.01E-03	0.67	5.24E-03	1.65	1.29E-02	7.49
ND_b	13.7	3.27	2.55E-02	0.72	5.61E-03	0.64	4.97E-03	1.56	1.22E-02	7.11
ND_b	20.8	2.63	2.05E-02	0.58	4.52E-03	0.59	4.60E-03	1.45	1.13E-02	6.58
ND_b	27.7	2.20	1.72E-02	0.48	3.78E-03	0.54	4.23E-03	1.33	1.04E-02	6.05
ND_b	34.8	1.94	1.51E-02	0.43	3.33E-03	0.50	3.86E-03	1.22	9.48E-03	5.52
ND_b	47.7	1.02	7.93E-03	0.22	1.75E-03	0.41	3.23E-03	1.02	7.94E-03	4.62

Table E.3. Naphtalene concentration or mass sorbed to MFC components according to calculations or measurements. NF experiments

Reactor ID	Day	anode chamber (mg/L)	anode chamber (mM)	sorbed anode (mg)	sorbed anode (mmol)	sorbed sand (mg)	sorbed sand (mmol)	sorbed cathode (mg)	sorbed cathode (mmol)	cathode chamber (mg/L)
NF_a	0.0	14.78	1.15E-01	2.67	2.08E-02	1.08	8.45E-03	2.10	1.64E-02	6.83
NF_a	0.1	12.51	9.76E-02	2.75	2.15E-02	0.61	4.79E-03	1.51	1.18E-02	6.85
NF_a	6.8	3.55	2.77E-02	0.78	6.10E-03	0.68	5.31E-03	1.67	1.30E-02	7.58
NF_a	13.8	2.51	1.96E-02	0.55	4.32E-03	0.63	4.92E-03	1.55	1.21E-02	7.03
NF_a	20.8	1.52	1.19E-02	0.34	2.62E-03	0.58	4.50E-03	1.41	1.10E-02	6.42
NF_a	27.7	0.73	5.73E-03	0.16	1.26E-03	0.52	4.03E-03	1.27	9.90E-03	5.76
NF_a	34.8	0.02	1.85E-04	0.01	4.07E-05	0.46	3.55E-03	1.12	8.71E-03	5.07
NF_a	47.7	0.00	3.38E-05	0.00	7.44E-06	0.34	2.66E-03	0.84	6.53E-03	3.80
NF_b	0.0	14.89	1.16E-01	2.69	2.10E-02	1.09	8.51E-03	2.11	1.65E-02	6.88
NF_b	0.1	13.91	1.09E-01	3.06	2.39E-02	0.62	4.83E-03	1.52	1.18E-02	6.90
NF_b	6.8	3.80	2.96E-02	0.84	6.52E-03	0.70	5.46E-03	1.72	1.34E-02	7.81
NF_b	13.7	2.99	2.34E-02	0.66	5.14E-03	0.65	5.09E-03	1.60	1.25E-02	7.27
NF_b	20.7	2.61	2.03E-02	0.57	4.48E-03	0.60	4.68E-03	1.47	1.15E-02	6.69
NF_b	27.7	2.10	1.64E-02	0.46	3.60E-03	0.55	4.29E-03	1.35	1.05E-02	6.13
NF_b	34.8	1.64	1.28E-02	0.36	2.82E-03	0.50	3.91E-03	1.23	9.59E-03	5.58
NF_b	47.8	0.45	3.48E-03	0.10	7.66E-04	0.41	3.21E-03	1.01	7.88E-03	4.59

Table E.4. Naphthalene mass diffused, degraded and removed from MFC according to calculations. BC experiments**.**

Reactor ID	Day	diffused (mg)	diffused (mmol)	removed (mmol)	removed (%)	degraded (mmol)	degraded (%)
BC_a	0.1	0.008	6.11E-05	4.28E-03	3.7%		
BC_a	6.9	0.394	3.07E-03	6.07E-02	51.9%	4.52E-02	38.7%
BC_a	13.9	-0.039	-3.06E-04	7.53E-02	64.5%	6.65E-02	57.0%
BC_a	20.7	-0.134	-1.04E-03	8.60E-02	73.7%	8.03E-02	68.8%
BC_a	27.7	-0.192	-1.50E-03	8.94E-02	76.6%	8.49E-02	72.7%
BC_a	34.9	-0.196	-1.53E-03	8.96E-02	76.7%	8.51E-02	72.9%
BC_a	48.8	-0.326	-2.54E-03	9.40E-02	80.5%	9.16E-02	78.4%
BC_b	0.1	0.008	6.10E-05	7.37E-02	63.2%	6.42E-02	55.0%
BC_b	6.9	-0.075	-5.84E-04	8.81E-02	75.6%	8.24E-02	70.7%
BC_b	13.9	-0.168	-1.31E-03	9.45E-02	81.0%	9.09E-02	78.0%
BC_b	20.8	-0.186	-1.45E-03	9.98E-02	85.6%	9.76E-02	83.7%
BC_b	27.7	-0.200	-1.56E-03	1.03E-01	88.1%	1.01E-01	86.8%
BC_b	34.9	-0.200	-1.56E-03	1.03E-01	88.0%	1.01E-01	86.7%
BC_b	48.8	-0.330	-2.57E-03	1.08E-01	92.7%	1.09E-01	93.3%

Table E.5. Naphthalene mass diffused, degraded and removed from MFC according to calculations. ND experiments.

Reactor ID	Day	diffused (mg)	diffused (mmol)	removed (mmol)	removed (%)	degraded (mmol)	degraded (%)
ND_a	0.1	0.008	6.18E-05	1.53E-02	13.0%		
ND_a	6.8	0.321	2.51E-03	8.69E-02	73.5%	7.75E-02	65.6%
ND_a	13.7	-0.205	-1.60E-03	9.08E-02	76.8%	8.63E-02	73.0%
ND_a	20.8	-0.209	-1.63E-03	9.31E-02	78.8%	8.92E-02	75.5%
ND_a	27.7	-0.191	-1.49E-03	9.47E-02	80.1%	9.10E-02	77.0%
ND_a	34.7	-0.180	-1.41E-03	9.55E-02	80.8%	9.20E-02	77.8%
ND_a	47.7	-0.298	-2.32E-03	9.96E-02	84.3%	9.79E-02	82.8%
ND_b	0.1	0.008	6.16E-05	3.37E-02	28.6%	1.51E-02	12.8%
ND_b	6.8	0.197	1.54E-03	8.14E-02	69.1%	7.19E-02	61.0%
ND_b	13.7	-0.152	-1.19E-03	9.23E-02	78.4%	8.79E-02	74.6%
ND_b	20.8	-0.211	-1.64E-03	9.73E-02	82.6%	9.44E-02	80.2%
ND_b	27.7	-0.212	-1.66E-03	1.01E-01	85.4%	9.85E-02	83.6%
ND_b	34.8	-0.211	-1.65E-03	1.03E-01	87.2%	1.01E-01	85.7%
ND_b	47.7	-0.360	-2.81E-03	1.10E-01	93.3%	1.11E-01	94.2%

Table E.6. Naphthalene mass diffused, degraded and removed from MFC according to calculations. NF experiments.

Reactor ID	Day	diffused (mg)	diffused (mmol)	removed (mmol)	removed (%)	degraded (mmol)	degraded (%)
NF_a	0.1	0.008	6.03E-05	1.77E-02	15.4%		
NF_a	6.8	0.295	2.30E-03	8.77E-02	76.0%	7.93E-02	68.7%
NF_a	13.8	-0.220	-1.71E-03	9.57E-02	83.0%	9.31E-02	80.7%
NF_a	20.8	-0.244	-1.90E-03	1.03E-01	89.7%	1.03E-01	89.1%
NF_a	27.7	-0.265	-2.07E-03	1.10E-01	95.0%	1.10E-01	95.7%
NF_a	34.8	-0.276	-2.15E-03	1.15E-01	99.8%	1.17E-01	101.7%
NF_a	47.7	-0.509	-3.98E-03	1.15E-01	100.0%	1.19E-01	103.4%
NF_b	0.1	0.008	6.08E-05	7.65E-03	6.6%		
NF_b	6.8	0.365	2.85E-03	8.65E-02	74.5%	7.72E-02	66.4%
NF_b	13.7	-0.216	-1.69E-03	9.28E-02	79.9%	8.93E-02	76.9%
NF_b	20.7	-0.232	-1.81E-03	9.58E-02	82.5%	9.32E-02	80.2%
NF_b	27.7	-0.222	-1.73E-03	9.98E-02	85.9%	9.79E-02	84.3%
NF_b	34.8	-0.221	-1.73E-03	1.03E-01	89.0%	1.02E-01	88.0%
NF_b	47.8	-0.398	-3.11E-03	1.13E-01	97.0%	1.15E-01	99.0%